Journal of Clinical and Translational Research

ACCSCIENCE PUBLISHING
Volume 10 Issue 5, October 2024
ISSN: 2424-810X (online) ISSN: 2382-6533 (print)

ABOUT JCTR

Aims and scope

The Journal of Clinical and Translational Research (JCTR) is an open access, peer-reviewed, multidisciplinary scientific journal that publishes studies with at least an ex vivo, in vivo, or clinical component. The published research is centered on any clearly defined clinical problem, which may comprise a disease or the basis of disease, a form of therapy or intervention, and clinical diagnostics or prognostics. Articles (original research, reviews, technical reports, medical hypotheses, commissioned articles, special issue articles, and editorials) are published continuously online and bimonthly in print. Studies performed in cells only will generally not be accepted unless they contain critical data that are in line with the scope of the journal. Some examples of such studies include molecular pathways that lie at the basis of a disease, novel biotechnological approaches for e.g., the production of drugs, or new techniques that improve clinical diagnostics and prognostics. Articles that combine preclinical and clinical data are given priority. Contributions from academic institutions and industry are welcome.

The research areas that JCTR covers include but are not limited to:

Internal medicine (all branches)
Vascular medicine and phlebology
Oncology
Cardiology
Intensive care medicine
Ophthalmology
Neurology and neurosciences
Anatomy, physiology, and embryology
Pathology
Clinical physics
Epidemiology
Medical devices
Pharmacology
Microbiology
Parasitology
Biomedical spectroscopy and spectrometry
Gastroenterology and hepatology
Surgery and transplantation
Hematology
Nephrology
Dermatology
Endocrinology and metabolism
Anesthesiology
Radiology and nuclear medicine
Clinical chemistry
Genetics and epigenetics
Global health
Nutrition
Immunology
Virology
Biomedical engineering

Key features

- Open access
- Reputable international editorial board
- Easy and fast submissions - no formatting rules (“your paper, your way”)
- No word count or reference restrictions
- Double blind review process to minimize bias
- Rapid online publication of articles upon acceptance
- Outlet for academic institutions and industry

Indexing

The Journal of Clinical and Translational Research is currently indexed by Chemical Abstract Service, Google Scholar, CNKI, and Peking University Library, and is currently working towards being indexed (PubMed, Science Citation Index Expanded, BIOSIS, Scopus, etc.).

Volume 10 • Issue 5 • October 2024
ISSN 2382-6533 (print) ISSN 2424-810X (online)

JOURNAL OF CLINICAL AND TRANSLATIONAL RESEARCH

ACCSCIENCE PUBLISHING

Journal of Clinical and Translational Research

Editorial Board

ACCSCIENCE PUBLISHING

Volume 10 | Issue 5 | October 2024 | Page 269 – 316 |

Journal of Clinical and Translational Research

https://www.jctres.com/en/home/

CONTENTS

CONTACTS

For general inquiries about the journal
y.liu@jctres.com (Dr. Yao Liu)

For ethical/legal inquiries
y.liu@jctres.com (Dr. Yao Liu)

For translation and proofreading services (English)
y.liu@jctres.com (Dr. Yao Liu)

For manuscript production inquiries
production@jctres.com

For advertisement inquiries
y.liu@jctres.com (Dr. Yao Liu)

Other Journal Published by AccScience Publishing

International Journal of Bioprinting is an international journal covering the technology, science and clinical application of the broadly defined field of bioprinting. Bioprinting is defined as the use of 3D printing technology with materials that incorporate viable living cells or biological elements to produce tissue or biotechnological products.

We are interested in the scientific topics spanning all stages of bioprinting process from concept creation to fabrication and beyond. Knowledge generated in these researches must be related to bioprinting.

The journal publishes original research articles on basic and applied research as well as associated social implications of this research. The journal also publishes brief commentaries and reviews. Articles focusing on the practical applications of 3D-printed products are similarly welcome.

Journal of Clinical and Translational Research 2024; 10(5): 269-282

Journal of Clinical and Translational Research

Journal homepage: http://www.jctres.com/en/home

ORIGINAL ARTICLE

A broad appraisal of decompression-induced physiological stress in different simulated dive profiles

Sergio Rhein Schirato[1]*, Ingrid El-Dash[1], Vivian El-Dash[1], Bruna Bizzarro[2], Alessandro Marroni[3], Massimo Pieri[3], Danilo Cialoni[3,4], Jose Guilherme Chaui-Berlinck[1]

[1]Department of Physiology, Biosciences Institute, University of São Paulo, São Paulo, Brazil, [2]Peter Murányi Experimental Research Center, Albert Einstein Hospital, São Paulo, Brazil, [3]DAN Europe Research Division, Roseto Degli Abruzzi, Italy, [4]Environmental Physiology and Medicine Laboratory, Department of Biomedical Sciences, University of Padova, Padova, Italy

ARTICLE INFO

Article history:
Received: May 30, 2024
Accepted: August 26, 2024
Published Online: October 3, 2024

Keywords:
Decompression
Decompression sickness
Immune system activation
Microparticles
Decompression profiles

**Corresponding author:*
Sergio Rhein Schirato
Department of Physiology, Biosciences Institute, University of São Paulo, São Paulo, Brazil. Email: sergio.schirato@gmail.com

ABSTRACT

Background: The present study was designed to observe if different decompression profiles, calculated as a function of tissue supersaturation during ascent, would result in significantly different outcomes, measured through different physiological stress indicators, even in the absence of symptoms of decompression sickness.
Aim: The aim of this study was to evaluate if simulated decompression profiles would affect the immune system, oxidative stress indicators, and heart rate variability.
Methods: A total of 23 volunteers participated in two different experimental protocols in a dry hyperbaric chamber. These simulated dives comprised two different compression–decompression arrangements with the same maximum pressure and duration but different decompression profiles.
Results: The shallow decompression profile with shorter deeper stops and longer shallow stops presented an increase in the standard deviation of the normal-to-normal R-R interval (a wide indicator of overall variability); the deep decompression profile with longer deeper stops and shorter shallow stops did not exhibit such increase. The shallow decompression profile resulted in an increase in neutrophil count and its microparticles (MPs), but no changes were observed for platelet count and its MPs, as well as for endothelial-derived MPs. In contrast, the deep decompression profile resulted in no changes in neutrophil count and its MPs, but a decrease in platelet count along with an increase in MPs from both platelets and endothelial cells. The observed difference might be related to different levels of decompression-related activation of immune system responses and oxidative processes triggered by different levels of inert gas supersaturation upon surfacing.
Conclusion: From previous results and literature data, we present a tentative schematic of how the velocity of ascent would trigger (or not) pro-inflammatory and immune system responses that could ultimately lead to the development of decompression sickness.
Relevance for patients: Increasing safety in exposure to hyperbaric environments and subsequent decompression by evaluating individual physiological responses to the process.

1. Introduction

Exposure to hyperbaric environments and subsequent decompression has been associated with many physiological alterations, which may culminate in decompression sickness. This condition can manifest itself through a variety of symptoms [1], ranging from joint and/or musculoskeletal pain [2], to cardiovascular and neurological impairment and, ultimately, death. Historically, studies related to decompression have adopted a binary approach in regard to decompression sickness [3], separating symptomatic and asymptomatic events. There is, however, a huge spectrum of possible physiological alterations between these two extremes, to which probabilities of decompression sickness

DOI: https://doi.org/10.36922/jctr.24.00021

occurrence are likely to be associated, based on individual responses.

The present study was designed to observe if different decompression techniques would result in significantly different outcomes, measured through different physiological stress indicators, even in the absence of decompression sickness symptoms. For decades, there has been an ongoing debate about how ambient pressure reduction should be conducted in non-saturation dives [4], i.e., whether the reduction of the ambient pressure should start earlier or later in the decompression phase. Dissolved gas models, based on John S. Haldane's tables [1] and later developed by many others, were, over time, partially replaced by decompression algorithms based on the control of bubble formation and growth, including, among others, the varying permeability model developed by Yount [5], causing the speed in ambient pressure reduction, to start earlier in the decompression phase of the dive, i.e., requiring divers to start decompression stops deeper in the water column.

Given the low overall incidence of decompression sickness, there are little scientific data available to support or reject any decompression algorithm. However, there is a widespread belief that including deeper stops in decompression schedules reduces the physiological stress during ascent and the risk of decompression sickness. Conversely, some studies suggest that slower ascents are related to higher counts of bubbles upon surfacing [6]. Nevertheless, whether these counts translate to a higher probability of decompression sickness remains debated [7]. In one of the largest studies comparing the incidence of decompression sickness in bubble-based models versus dissolved gas-based models (derived from Haldane's work), the United States Navy Experimental Diving Unit [4] concluded that decompression schedules with deep stops had a higher incidence of decompression sickness than those with shallower decompression stops.

These findings could be attributed to the different supersaturation observed in the tissues with slower gas kinetics upon surfacing [4]. During deeper decompression stops, these tissues are not yet saturated and continue to absorb gas from the blood [8]. This opposes the purposes of these stops and may aggravate the stress caused by decompression [4].

Besides the well-documented appearance of bubbles, activation of the immune system and small particle (microparticles [MPs] or microvesicles) formation have been suggested to play an important role in decompression sickness [9-11]. Hence, decompression sickness is not merely a physical or mechanical problem, but instead the result of a complex biochemical process. MPs, shed by different cells in a regulated manner and carrying various nuclear components of their originating cells, such as RNA and DNA, are involved in cell signaling and communication [12]. Different studies have identified them as markers of inflammatory diseases [12], and variations in their levels and their cells of origin have been linked to a range of diseases and inflammatory processes [13,14]. During decompression, or probably even earlier, immune system activation and oxidative stress occur. A recent study found that exposure to high-pressure environments, even in the absence of decompression, is sufficient to increase the production of MPs carrying interleukin-1β [15], a cytokine involved in inflammatory responses. The mechanism behind MP formation has been linked to high inert gas pressure, which induces singlet oxygen formation. This toxic free radical is generated through a cycle involving actin S-nitrosylation, nitric oxide (NO) synthase-2, and nicotinamide adenine dinucleotide phosphate (NADPH) oxidase activation [16]. NADPH oxidase, activated by neutrophils, generates reactive oxygen species (ROS) through its heme enzyme, myeloperoxidase (MPO) [17]. ROS production by activated granulocytes and potentially by other cells is part of an orchestrated physiological first response of the immune system to potential aggressors. Therefore, it is expected that higher expressions of MPO are linked to the generation of ROS, leading to MP production.

Another expected physiological alteration related to decompression is heart rate variability (HRV). Recently published studies reported changes in HRV after exposure to hyperbaric environments [18,19]. HRV is defined as the undirected changes in the interval between successive normal-to-normal heartbeats (triggered by the sinus node, excluding extrasystoles) [20], which results from the balanced action of the sympathetic and the parasympathetic branches of the autonomic nervous system (ANS) [20] as well as other non-neural sources of variation.

HRV is commonly studied in the time and frequency domains, and occasionally through the application of non-linear methods [20]. Different HRV indicators have been associated with sympathetic or parasympathetic activity. For many years, it was believed that the low frequency (LF) bandwidth of the HRV spectrogram (a frequency domain indicator) was associated with sympathetic activity, while the high frequency (HF) band was related to the parasympathetic branch of the ANS [20]. In reality, the association between a given bandwidth and one specific branch of the ANS is not so well-defined, and there are probably other factors contributing to the process. HF is highly impacted by respiratory pattern [20], with a response time akin to the parasympathetic response time of the sinoatrial node. The LF band is associated with blood pressure control loops, supporting an association with sympathetic activity [20]. However, experimental evidence indicates that both branches of the ANS play a role in both LF and HF power. A reduction in HRV has been reported in several cardiological and non-cardiological diseases, ranging from diabetes to renal failure [21]. A reduction in HRV, when analyzed in the frequency domain, has also been associated with inflammatory processes in multiple studies [21,22].

Given the clear role of inflammatory processes and immune responses in compression and subsequent decompression processes, studying HRV in this context could provide important insights into the underlying physiological processes and potential outcomes of hyperbaric exposure. As different decompression protocols alter the dynamics of gas absorption and release by tissues and, consequently, the physiological stress sustained by divers, we hypothesized that profiles with deep stops and those with shallow stops would result in distinct changes in HRV.

DOI: https://doi.org/10.36922/jctr.24.00021

2. Methods

2.1. Study participants

The present study was undertaken in healthy individuals, all trained divers, experienced in the experimental profiles utilized. The volunteers provided written informed consent. The ethical committee of the Biosciences Institute of the University of Sao Paulo approved the experimental protocol (CAAE #91231618.6.0000.5464), and all experiments were performed in accordance with relevant guidelines and regulations.

Briefly, a total of 23 male divers participated in this study. Female volunteers were not accepted to avoid the potential effects of neurovegetative changes due to the menstrual cycle [23]. Two volunteers participated in only one experiment and were released from the second due to medical conditions not related to diving. No decompression sickness symptoms were observed during the experimental dives. Table 1 summarizes the anthropometric data of the study population.

2.2. Simulated dives

Experiments involving exposure compression and subsequent decompression were conducted at the Centro Hiperbárico Paulista (São Paulo Hyperbaric Center), Indaiatuba, São Paulo, Brazil, under the supervision of a trained physician. Each volunteer underwent two different trials, each one with the same maximum depth and bottom time. Decompression schedules were created to simulate different decompression profiles with similar total decompression times. Each trial was performed in the morning, at the same time of the day. Divers were requested to rest for at least 30 min before the start of the experiment, and the interval between the experiments was at least 7 days for each volunteer to minimize any carry-over effect [24]. The experiments executed were performed using electronically controlled closed-circuit rebreathers.

2.3. Simulated dive profiles

The diluent gas mix consisted of 18% oxygen, 45% helium, and 37% nitrogen. Rebreathers were set to keep the oxygen pressure at 121 kPa (1.2 ATA; total pressure: Gauge plus 0.93 atm of surface pressure) throughout the dive, raising the oxygen pressure to 141 kPa (1.4 ATA) at 162 kPa (6 meters of seawater [msw]). The bottom pressure was 638 kPa (53 msw) and the time required to reach this pressure was 20 min. The divers were kept at the simulated bottom for an additional 15 min. Subjects were decompressed at a rate of 9 msw/min until the first decompression stop was reached. The dive profiles are detailed in Table 2.

2.4. Electrocardiographic (ECG) data

ECG records were obtained using superficial electrodes in a modified CM5 thoracic positioning. Data were collected while the subjects were seated in a comfortable position using the MP36 system (BIOPAC Systems, Inc., United States of America [USA]), set up at AHA configuration, with 0.05 and 100 Hz as low and high pass filters, respectively, and a sampling rate of 1000 Hz.

Table 1. Study population characteristics

Parameter	Value
Age (years)	44.18±6.77
Weight (kg)	87.82±13.47
Height (cm)	180.32±8.27
Body mass index	27.03±3.90

Note: Data are presented as the mean±standard deviation.

Table 2. Simulated dive profiles

Decompression profile	Depth (msw)	Time (min)	Breathing loop, PO_2 (ATA)
Deep	53	15	1.2
	27	1	1.2
	24	1	1.2
	21	2	1.2
	18	2	1.2
	15	3	1.2
	12	4	1.2
	9	5	1.2
	6	22	1.4
Shallow	53	15	1.2
	21	2	1.2
	18	2	1.2
	15	3	1.2
	12	4	1.2
	9	6	1.2
	6	26	1.4

Abbreviation: msw: Meters of seawater; PO_2: Partial pressure of oxygen.

There were two phases of continuous data collection: (i) a 30-min pre-dive period to establish the baseline condition for each volunteer; and (ii) a 30-min post-dive reading that was initiated 30 min after the end of the dive. This protocol was adopted due to previous observations that the magnitude of HRV changes tends to be higher in the 2nd half-hour post-decompression. Interestingly, it is well-documented that venous gas bubble counts tend to take approximately the same amount of time to reach a peak [24].

ECG recordings were converted into R-R intervals. The R-R time series was then subdivided into non-overlapping windows of 256 consecutive R-R intervals. Subsequently, the following estimators of HRV were obtained from each window (as detailed by the task force of the European Society of Cardiology and the North American Society of Pacing and Electrophysiology [20]):

(i) Time domain:
- R–R interval
- Standard deviation of the normal-to-normal R-R interval (SDNN)
- The square root of the mean squared differences of successive R-R intervals (RMSSD).

(ii) Frequency domain:
- Fast Fourier transform, to obtain the power spectrum density [20], which was subsequently divided into:
  1. Ultra-LF: 0.01 – 0.04 Hz (not relevant to this study due to the relatively short ECG recording intervals)

DOI: https://doi.org/10.36922/jctr.24.00021

2. LF: 0.04 – 0.15 Hz
3. HF: 0.15 – 0.4 Hz

As the size of the time series tends to infinity, the variance and the total power of the spectrum converge to each other, for this reason, in the present study, the power of a given power spectrum density was approximated by SDNN squared.

2.5. Blood samples

Venous blood was collected from an antecubital arm vein by a trained phlebotomist before and after each (simulated) dive. The following variables were measured: red blood cells, hemoglobin, hematocrit, neutrophils, platelets, immunophenotyping, and MPs for quantification through flow cytometry. The samples were collected using Cyto-Chex BCT tubes (Streck, INC, USA).

Blood samples were drawn immediately before the experiment and 1 h after the end of decompression. Hemograms were performed immediately after collection at the hyperbaric center. Immunophenotyping was performed up to 3 days after the blood collection.

2.6. Flow cytometry

Immunophenotyping was performed using 16-color FACSFortessa™ (Becton & Dickinson Company©, BD, USA) and the manufacturer's acquisition software.

Annexin binding buffer and the following antibodies were purchased from Biolegend (United States of America [USA]): fluorescein isothiocyanate (FITC)-conjugated anti-annexin V, FITC-conjugated anti-human MPO, allophycocyanin (APC)-conjugated anti-human CD41, PerCF594-conjugated anti-human CD14, PerCP-conjugated anti-human CD235, Pacific Blue-conjugated anti-human CD31, AF700-conjugated anti-human CD66b, and APC-conjugated anti-human CD19. In addition, live/dead V-500-conjugated anti-human was used to identify the dead cell population. Immunophenotyping was conducted using flow cytometry to evaluate the population of granulocytes (CD 16+/CD66b+) among live cells. This included evaluating the percentage of granulocytes expressing MPOs on its surface (MPO%) and mean fluorescence intensity of MPO (MPO MFI) as indicators of neutrophil activation. The strategy used in this analysis and the hierarchy of the gates are described in [19].

For MP acquisition and processing, blood was centrifuged at 1500 g for 5 min [25]. The supernatant was centrifuged at 15,000 g for 30 min to pellet the few remaining platelets and cell debris. These samples were then frozen at −80°C, allowing all samples to be analyzed on the same day. MPs were stained with annexin V and analyzed as described in [26]. We define MPs as annexin V-positive particles with diameters up to 1.0 µm. Gates were set to include particles with 0.3 – 1.0 µm diameters, with the exclusion of background corresponding to debris, which is usually present in buffers. Detergent Triton X (Sigma-Aldrich, USA) was used as a control, as MPs are expected to disintegrate in its presence.

Each sample analysis was performed using the software FlowJo Treestar© (FlowJo, Becton & Dickinson Company©, BD, USA) at the Center for Experimental Research of the Hospital Albert Einstein.

2.7. Decompression schedules

All decompression schedules were defined using the ZHL-16b algorithm, calculated through a script written in R language. The compartment half-time for nitrogen and helium was set to the original values published by Bühlmann [2]. At the end of the experiment, maximum supersaturation pressures for each compartment were adjusted by multiplying the intercept a of the linear equations to limit the compartment j supersaturation for a given ambient pressure P_{amb} (in the format $P_{\max j} = \frac{P_{amb}}{bj} + a_j$) by 0.85 and 0.65. The factor b_j was adjusted to calculate stops at 0.20 and 0.45 of the original pressure limits provided by Bühlmann's values for the deep and shallow decompression profiles, respectively,

Compartment on-gassing and off-gassing were calculated through the application of the following differential equation:

$$\frac{dP_j}{dt} = k_j \left(P_A - P_j\right) \quad \text{(I)}$$

where P_j is the pressure of inert gas in compartment j, P_A is the alveolar (inspired) pressure of inert gas, and k_j is the inverse of the half-time of the compartment multiplied by the natural logarithm of 2 ($k_j = ln2\ t_{\frac{1}{2}j}^{-1}$). Solving Equation I would yield:

$$P_j(t) = P_{0,j}\ e^{-k_j\ t} + P_A\ \left(1 - e^{-k_j\ t}\right) \quad \text{(II)}$$

where $P_{0,j}$ is the initial pressure of inert gas in compartment j at the time of a change in the inspired gas and/or hydrostatic pressure [23].

2.8. Statistical analysis

Differences between pre- and post-dive data were determined using Student's t-test, provided that the data followed a normal distribution, as confirmed by the Shapiro–Wilk test. When normal distribution was not confirmed, a non-parametric permutation test with 10,000 simulation rounds was performed to determine the p-value [27]. The limit of significance was set at 0.05 (i.e., $p < 0.05$). Data provided in this study are presented as the mean ± standard error or mean ± standard deviation, as specified accordingly. All data analyses were conducted using scripts implemented in MATLAB (MathWorks Inc., USA) and R.

2.9. Clustering analysis

An unsupervised algorithm for clustering was used to identify subgroups within the dataset. The K-means algorithm with K = 2 (i.e., two different decompression profiles used in the study) was applied to each set of training data, minimizing the distance J, defined by:

$$J = \sum_{i=1}^{k} \sum_{j=1}^{s} \| x_{k,h} - M_j\ ^2 \| \quad \text{(III)}$$

Data were normalized according to Equation IV and then used to create the normalized matrix:

DOI: https://doi.org/10.36922/jctr.24.00021

$$x_{k,h} = \frac{x'_{k,h} - \min(x'_h)}{max(x'_h) - \min(x'_h)} \quad \text{(IV)}$$

Where $x_{k,h}$ is the normalized variable.

A confusion matrix was computed to assess the accuracy of the algorithm in attributing the results observed for each volunteer to the respective decompression profile.

3. Results

3.1. HRV

An overall increase in variability was observed for both profiles. For the deep decompression profile, the frequency domain indicators LF, total LFs (very LF + LF), and HF increased but were not statistically significant. LF as a fraction of HF and total variability, respectively, and HF as a fraction of total variability did not exhibit significant changes. In the time domain, RMSSD was significantly increased in post-dive values. SDNN also displayed a tendency to increase, though not statistically significant (Table 3).

The shallow decompression profiles also displayed an overall increase in variability. In the frequency domain, HF and LF as a fraction of HF demonstrated a significant increase. In the time domain, SDNN and RMSSD post-dive values significantly increased (Table 4).

The shallow decompression profile resulted in an increase in post-dive variability, observed from SDNN (i.e., from 42.66 ± 2.35 to 49.43 ± 4.02; p = 0.039), while the deep decompression profile did not exhibit a significant change (i.e., SDNN: 43.39 ± 2.29 – 46.3 ± 3.84; p = 0.21). Both profiles displayed a significant increase in the RMSSD index, i.e., from 19.09 ± 1.43 to 25.4 ± 3.19 (p = 0.014) in the shallow decompression profile and from 20.62 ± 1.73 to 24.7 ± 2.61 (p = 0.003) in the deep decompression profile (Figure 1). Both pre-dive baseline SDNN and RMSSD values were not statistically different between profiles (Figure 2).

In addition, a comparison between post-dive SDNN and RMSSD divided by their pre-dive values (respectively, defined as SDNN and RMSSD ratios) is displayed in Figure 3. Notably, the shallow decompression profile generated higher values, though the difference was not statistically significant.

Table 3. Heart rate variability for the deep decompression profile

Parameter	Pre-dive	Post-dive	p
LF (ms^2)	418.00±77.37	545.01±89.09	0.071
Total LFs (ms^2)	176.18±96.73	151.51±132.61	0.060
HF (ms^2)	77.93±15.74	124.50±21.59	0.696
LF/HF ratio	7.31±1.16	8.79±2.00	0.145
LF as a ratio of total variability	0.20±0.02	0.24±0.03	0.059
HF as a ratio of total variability	0.03±0.00	0.04±0.01	0.097
RMSSD	20.62±1.73	24.76±2.61	0.003
SDNN (ms)	43.39±2.29	46.31±3.84	0.217

Note: Data arepresented as mean±standard error.
Abbreviations: LF: Low frequency; HF: High frequency; SDNN: Standard deviation of the normal-to-normal R-R interval; RMSSD: Root mean squared differences of successive R-R intervals.

Table 4. Heart rate variability for the shallow decompression profile

Parameter	Pre-dive	Post-dive	p
LF (ms^2)	468.04±67.46	647.86±133.48	0.057
Total LFs (ms^2)	663.60±88.75	555.03±171.94	0.050
HF (ms^2)	61.99±9.46	96.15±19.51	0.025
LF/HF ratio	8.97±1.03	9.59±1.43	0.031
LF as a ratio of total variability	0.25±0.03	0.23±0.03	0.138
HF as a ratio of total variability	0.03±0.00	0.03±0.01	0.232
RMSSD	19.09±1.43	25.43±3.19	0.014
SDNN (ms)	42.66±2.35	49.43±4.02	0.039

Note: Data arepresented as mean±standard error.
Abbreviations: LF: Low frequency; HF: High frequency; SDNN: Standard deviation of the normal-to-normal R-R interval; RMSSD: Root mean squared differences of successive R-R intervals.

3.2. Blood assay

Red blood cells, hematocrit, hemoglobin, neutrophils, and platelet counts were different between pre- and post-dive measurements. A statistically significant reduction in red blood cells was observed in the deep decompression profile, while the reduction observed in the shallow decompression profile was not significant (Figure 4).

Similarly, a statistically significant reduction in hemoglobin was observed in the deep decompression profile, while the reduction in hemoglobin in the shallow decompression profile was not significant (Figure 5).

Both profiles reported platelet count reduction post-dive, but the reduction was only statistically significant for the deep decompression profile (Figure 6).

Meanwhile, the neutrophil count increased post-dive in both profiles but was only significant in the shallow decompression profile (Figure 7).

Finally, post-dive hematocrit values were slightly lower than pre-dive values in both decompression profiles, but no statistically significant differences between pre- and post-dive values or between profiles were observed.

3.3. Flow cytometry

Pre- and post-dive neutrophil-, endothelium-, and platelet-derived MP counts in the deep and shallow decompression profiles are displayed in Figures 8 and 9, respectively, and detailed in Tables 5 and 6, respectively. These results are consistent with the increased post-dive neutrophil count (Figure 7).

3.4. Clustering analysis

The clustering algorithm was able to distinguish between the decompression profiles using values from the pre- and post-dive ratios of HRV indicators, blood assay, and MP production with an accuracy of 0.68 (confidence interval [CI]: 0.4817 – 0.8204; p = 0.07). Figure 10 presents the two clusters of results created by the algorithm.

4. Discussion

In recent years, numerous studies have demonstrated that decompression sickness is a multifactorial condition that involves the activation of many biochemical pathways, and its mechanisms

DOI: https://doi.org/10.36922/jctr.24.00021

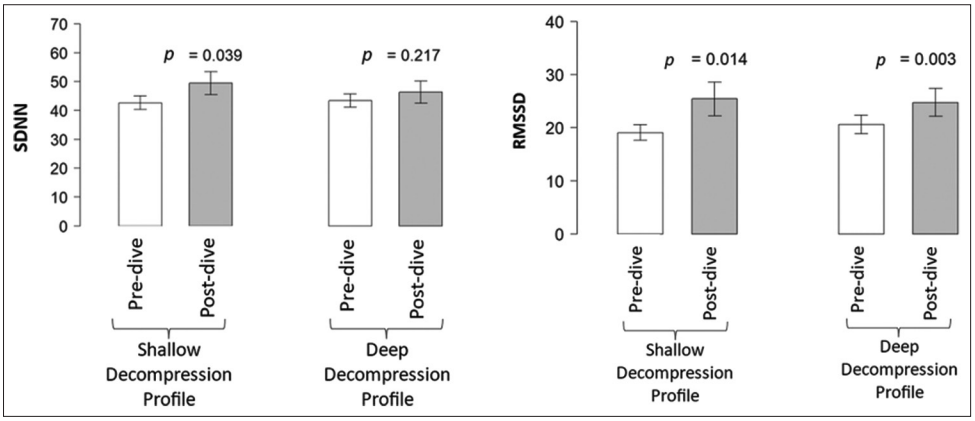

Figure 1. Mean SDNN (left) and RMSSD (right) of pre- and post-dive data for each decompression profile (n = 23)
Abbreviations: SDNN: Standard deviation of the normal-to-normal R-R interval; RMSSD: Square root of the mean squared differences of successive R-R intervals

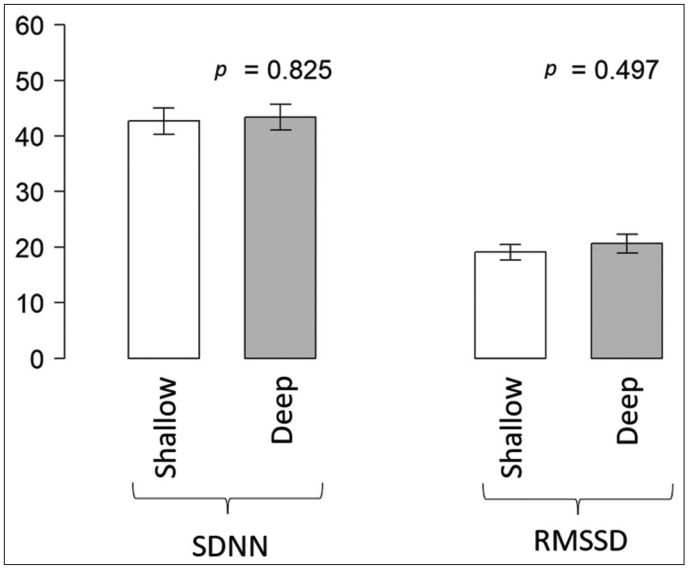

Figure 2. SDNN and RMSSD pre-dive data comparison between the shallow and deep decompression profiles (n = 23)
Abbreviations: SDNN: Standard deviation of the normal-to-normal R-R interval; RMSSD: Square root of the mean squared differences of successive R-R intervals

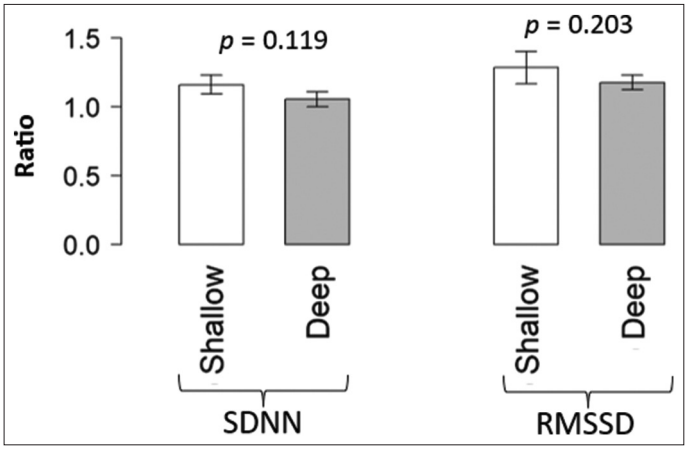

Figure 3. Comparison of SDNN and RMSSD ratios for both shallow and deep decompression profiles (n = 23)
Abbreviations: SDNN: Standard deviation of the normal-to-normal R-R interval; RMSSD: Square root of the mean squared differences of successive R-R intervals

remain not fully understood [28,29]. The present study aims to evaluate possible associations between different levels of inert gas supersaturation in different theoretical compartments and their respective outcomes, in terms of HRV alterations, inflammation, and oxidative processes. Clustering analysis demonstrated that the outcomes of the different profiles can be differentiated with reasonable accuracy, despite the relatively small sample size, supporting the notion that they are distinct. The utilization of HRV is based on its well-established negative correlation with inflammation and immune system activation [30]. Recent studies have reported that hyperbaric exposure and subsequent decompression are associated with HRV changes [31,32]. In a previous work [18], we observed an increase in the LF band post-decompression from 45 msw-simulated dives. Here, a similar pattern is observed (Tables 5 and 6), indicating that decompression generally increases HF, SDNN, and LF.

Other studies also reported that immersion and inspiration of higher partial pressures of oxygen are associated with HRV changes [33], occurring even before ambient pressure reduction, during decompression, or ascent in self-contained breathing apparatus diving. It is plausible that the general post-dive increase in HRV observed in this and other studies is related to hyperoxia, which is commonly linked to exposure to hyperbaric environments where inspired oxygen pressures are typically at 1.0 – 1.2 ATA.

The observed changes in the total LF band could be associated with changes in the baroreceptor activity. LF is linked to baroreflex function, as previous studies demonstrated that carotid sinus stimulation increases LF power in individuals with normal baroreflex function, but not in those with impaired baroreflex sensitivity [34,35]. In addition, LF has been negatively correlated with endothelial function [22]. The ANS and the endothelium work together to maintain vascular tone. There is a tonic balance between the release of vasodilating factors from the endothelium and vasoconstricting factors

DOI: https://doi.org/10.36922/jctr.24.00021

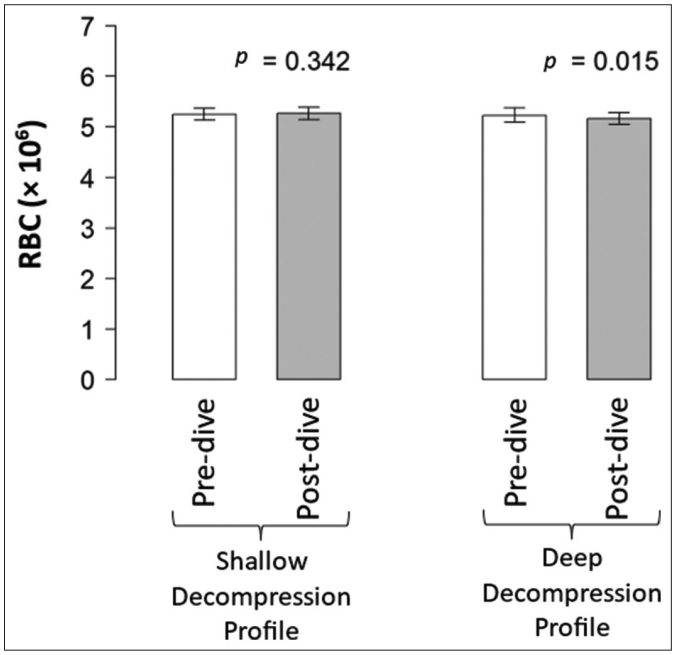

Figure 4. Red blood cell count (mean ± standard deviation) for both shallow and deep decompression profiles (n = 17). In the shallow decompression profile, the pre-dive mean count was $5.25 \times 10^6 \pm 0.48 \times 10^6$, while the post-dive mean count was $5.23 \times 10^6 \pm 0.57 \times 10^6$. In the Deep Decompression Profile, the pre-dive mean count was $5.26 \times 10^6 \pm 0.48 \times 10^6$, while the post-dive mean count was $5.16 \times 10^6 \pm 0.45 \times 10^6$

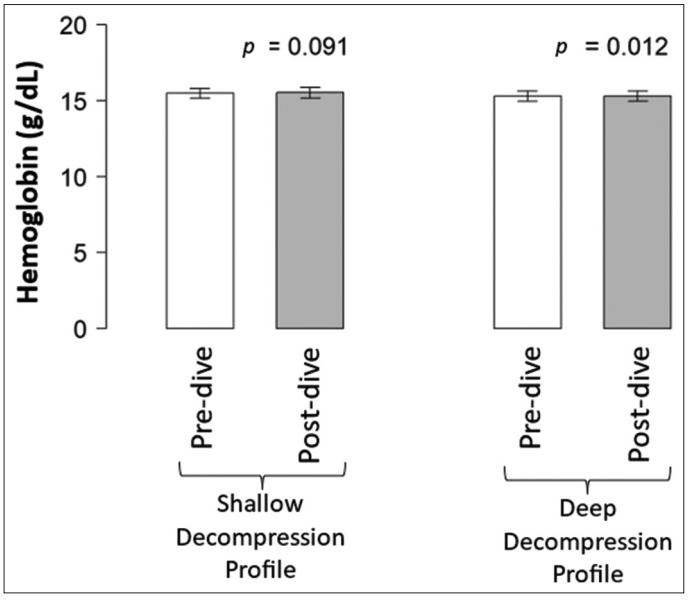

Figure 5. Hemoglobin levels for the shallow and deep decompression profiles (n = 17). Both profiles have a pre-dive mean hemoglobin level of 15.5 g/dL and a post-dive mean hemoglobin level of 15.3 g/dL. The difference in standard deviation for both profiles resulted in statistically significant differences. For the shallow decompression profile, the pre-dive standard deviation was 1.34 g/dL and the post-dive standard deviation was 1.42 g/dL; for the deep decompression profile, the pre- and post-dive standard deviations were 1.40 g/dL

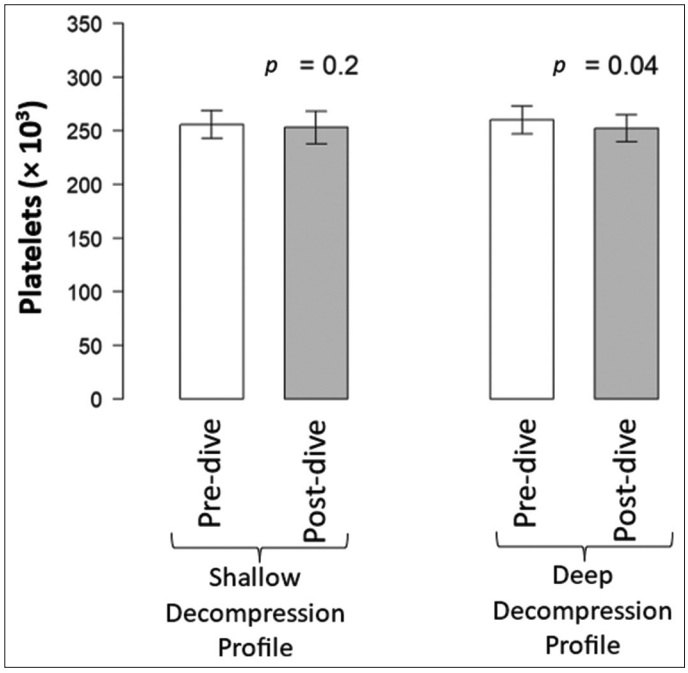

Figure 6. Platelet count (mean ± standard deviation) for the shallow and deep decompression profiles (n = 17). In the shallow decompression profile, the pre-dive mean count was $255 \times 10^3 \pm 54.1 \times 10^3$, and the post-dive mean count was $253 \times 10^3 \pm 52.8 \times 10^3$. In the deep decompression profile, the pre-dive mean count was $260 \times 10^3 \pm 61.5 \times 10^3$, and the post-dive mean count was $252 \times 10^3 \pm 54.4 \times 10^3$

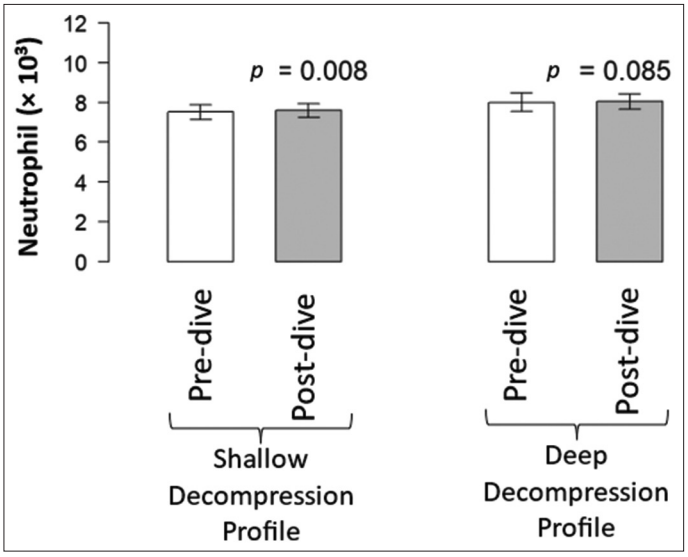

Figure 7. Neutrophil count (mean ± standard deviation) for the shallow and deep decompression profiles (n = 17). In the shallow decompression profile, the pre-dive mean count was $7.512 \times 10^3 \pm 1.56 \times 10^3$, and the post-dive mean count was $8 \times 10^3 \pm 1.90 \times 10^3$. In the Deep Decompression Profile, the pre-dive mean count was $7.594 \times 10^3 \pm 1.36 \times 10^3$, and the post-dive mean count was $8 \times 10^3 \pm 1.55 \times 10^3$

triggered by the sympathetic branch of the ANS. The balance between these opposing forces acts on the vascular smooth muscle cells to maintain vessel tone [36]. The disturbance of

DOI: https://doi.org/10.36922/jctr.24.00021

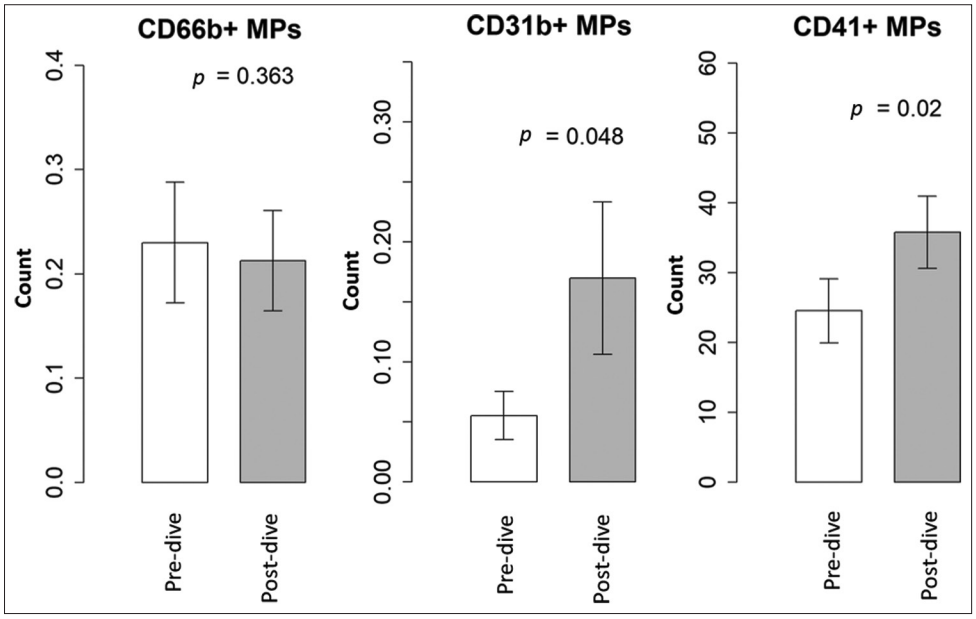

Figure 8. MP count for the deep decompression profile: CD31+ MPs presented a pre-dive mean count of 5.52×10^{-2} and a post-dive mean count of 16.99×10^{-2}; CD41+ MPs presented a pre-dive mean count of 24.5 and a post-dive mean count of 35.8; no significant changes were observed for CD66b+ MPs
Abbreviation: MPs: Microparticles

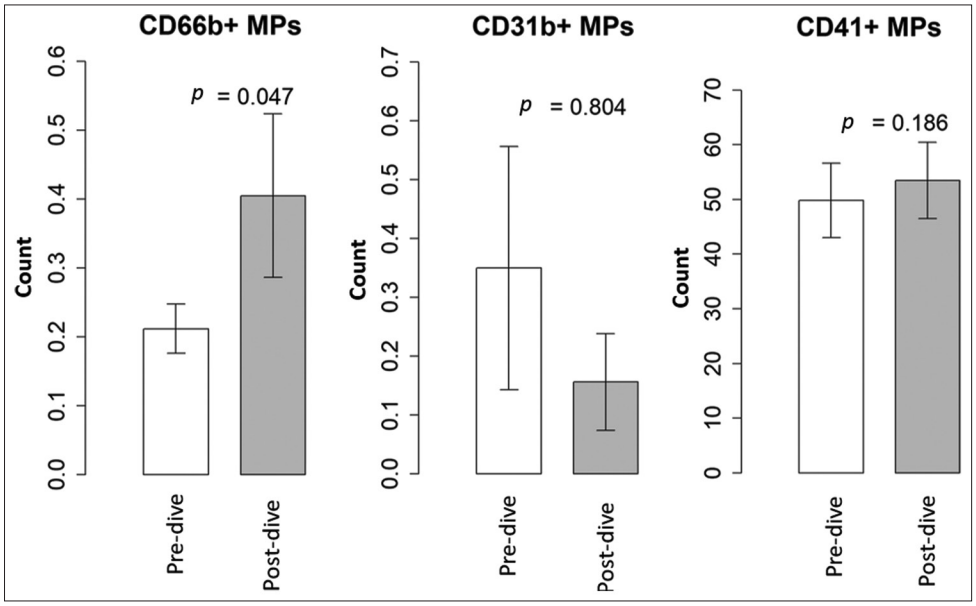

Figure 9. MP count for the shallow decompression profile: CD66b+ MPs presented a pre-dive mean count of 21×10^{-2} and a post-dive mean count of 40×10^{-2}; CD31+ MPs presented a pre-dive mean count of 35×10^{-2} and a post-dive mean count of 15×10^{-2}; CD41+ MPs presented a pre-dive mean count of 49.8 and a post-dive mean count of 53.5
Abbreviation: MPs: Microparticles

this tonic balance, due to the reduced NO availability, maybe the reason why sympathetic activity is associated with loss of endothelial function in some circumstances. Such disturbance of the tonic balance mentioned above is compatible with changes possibly caused by oxidative processes observed in the present study, including the increased numbers of CD31+ MPs [37].

There are also significant increases in HF and RMSSD, variability markers indicating more cardiac control activity. SDNN increased only in the shallow decompression profile. In previous studies, we observed a significant increase in overall HRV in control groups exposed to gases with higher oxygen fractions but not to increased ambient pressure [18].

The results obtained in the present study indicate that different decompression profiles may affect HRV differently, potentially influencing neutrophil count, platelet activation, and MP production. A reduction in circulating platelet counts

DOI: https://doi.org/10.36922/jctr.24.00021

Table 5. MPO and microparticle levels for the deep decompression profile

Parameter	Pre-dive	Post-dive	P
MPO+ (%)	2.448±0.830	2.549±0.888	0.758
MPO (MFI)	576.796±171.399	526.565±137.525	0.472
CD66b+	0.28±0.07	0.27±0.06	0.207
CD31+	0.06±0.03	0.17±0.08	0.022
CD41+	24.50±5.64	35.80±4.92	0.027

Note: Data are presented as mean±standard error.
Abbreviation: MFI: Mean fluorescence intensity; MPO: Myeloperoxidase.

Table 6. MPO and microparticle levels for the shallow decompression profile

Parameter	Pre-dive	Post-dive	P
MPO+ (%)	2.61±1.17	2.32±1.16	0.15
MPO (MFI)	314.95±31.93	291.05±28.29	0.07
CD66b+	0.21±0.04	0.40±0.12	0.000
CD31+	0.35±0.21	0.16±0.08	0.199
CD41+	49.80±6.80	53.46±6.96	0.186

Note: Data are presented as mean±standard error.
Abbreviation: MFI: Mean fluorescence intensity; MPO: Myeloperoxidase.

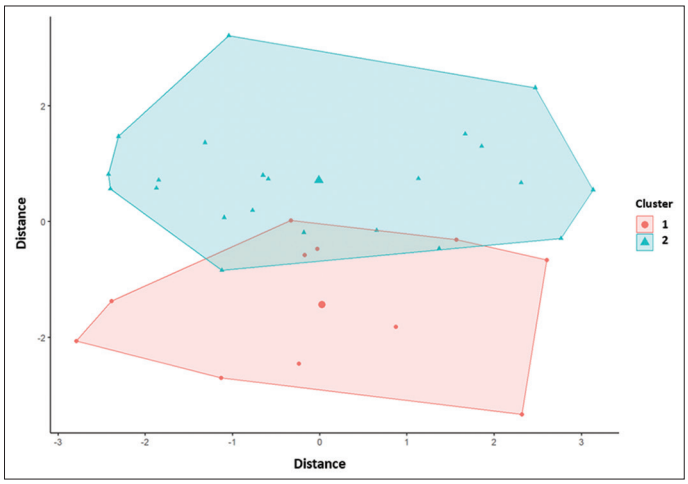

Figure 10. Clusters identified by the clustering algorithm. Cluster 1: Shallow decompression profile; Cluster 2: Deep decompression profile

was observed in the deep decompression profile. Platelets are regarded as effectors of hemostasis, essential for vascular integrity [38,39]. Recent understanding has clarified that they are key effectors in inflammation, immune responses, and signaling, with the potential to orchestrate complex immune and inflammatory events [39,40]. Three different studies by the same research team investigated platelet count and its association with decompression sickness in mice models and with bubble formation in humans [41-43]. Their results indicate that higher bubble counts in humans correlate with a greater reduction in platelet count, even in the absence of decompression sickness after decompression. Conversely, in mice suffering from decompression sickness after provocative decompression, a regression model linked platelet reduction to symptom severity. In both cases, they speculated that such reduction was due to platelet activation and aggregation.

Activated platelets release MPs (CD41 + MPs) that are involved in intercellular (endogenous) signaling by inducing immune responses in distant sites [44]. *In vitro* studies revealed that CD41 + MPs facilitate leukocyte–leukocyte interactions and the binding of P-selectin/P-selectin glycoprotein ligand-1 [45], increasing leukocyte accumulation at injury sites and on activated endothelium. In addition, platelet shedding of MPs positively correlates with increased vascular permeability [46]. The results obtained in this study suggest an increase in circulating CD41+ MPs after decompression in the deep decompression profile, which aligns with the observed reduction in circulating platelets. This is likely due to platelet activation and recruitment to inflammation sites. The release of platelet, endothelial, and leukocyte MPs is increased during inflammatory conditions [13]. Oxidative stress is known to induce the release of CD31+ MPs, which attract leukocytes to the inflammatory site by adhesion molecules, such as vascular cell adhesion molecule-1, a key factor endothelial dysfunction [28,37].

Our results demonstrated a post-dive increase in platelet- and endothelial-derived MPs (CD41+ and CD31+ MPs, respectively) in the deep decompression profile (Figure 9). Similarly, the shallow decompression profile displayed a marked increase in neutrophil-derived MPs (Figure 9).

A decrease in red blood cells and hemoglobin was observed in the deep decompression profile (Figures 4 and 5, respectively), likely due to eryptosis [47,48], a form of programmed cell death in erythrocytes. Eryptosis, triggered by oxidative stress, involves the activation of caspases expressed by erythrocytes, resulting in their recognition and engulfment by circulating macrophages. Since erythrocyte membranes are highly vulnerable to oxidative damage and cannot repair damaged proteins by re-synthesis, they are particularly sensitive to oxidative stress [49]. Eryptosis of young red blood cells is often reported in subjects returning from high altitudes or space flights [47], and its putative mechanism is related to changes in the erythropoietin sensitivity of the cells. Therefore, the observed change in red blood cell and hemoglobin counts might be related to a stressful decompression profile.

The shallow and deep decompression profiles can also be distinguished by indicators of immune system activation and inflammation. The shallow decompression profile increases peripheral blood neutrophil count and its corresponding MPs, without affecting platelet count and its MPs, as well as in endothelial MPs. Conversely, the deep decompression profile exhibited an increase in the platelet- and endothelial-derived MPs and a decrease in platelet count, with no variations in neutrophil count and its MPs.

Neutrophils are widely recognized for their role in promoting inflammatory responses at the initial stages of these processes. Increased neutrophil count is associated with various pathologies (e.g., bacterial infections, hypertension, and certain types of cancer [50-54]) and non-pathological conditions (e.g., after exercising) [55]. Their activation might also promote platelet activation [13,44] and even endothelial damage [13,56], then

DOI: https://doi.org/10.36922/jctr.24.00021

enhancing the inflammatory process. From this more orthodox standpoint, increased neutrophil count and activation would act as pro-inflammatory agents.

However, neutrophils play an anti-inflammatory role in many instances. Neutrophil-derived MPs are potential inhibitors of macrophage activation [57]. For instance, annexin-1-rich neutrophil-derived MPs inhibit neutrophil activation [58], downregulating an inflammatory response. The production of platelet activation factors depends on the neutrophils' state; it occurs when neutrophils are adherent (i.e., under a stimulated condition) but not when they are in suspension [44]. Neutrophil-derived MPs are not a homogeneous set, and they can induce or inhibit inflammation [59]. Besides this functional diversity, variations in neutrophil counts might lead to different outcomes. For instance, an increase in neutrophil count seems to be associated with benign prostate enlargement, whereas a decrease might indicate a malignant case [60]. Exercise-induced neutrophilia illustrates the challenge of defining a consistent pattern in response to physical effort, as reports of neutrophil counts in peripheral blood vary widely. In our previous study [19], the MPO MFI, an important marker of neutrophil activation, demonstrated a negative correlation with the number of circulating neutrophils (−0.55), and a significant positive correlation with the percentage of granulocytes expressing MPO on the membrane surface (0.7). A negative correlation between neutrophil-derived MPs (CD66b+) and MPO MFI was also observed (−0.32). These results suggest that increased circulating neutrophil counts are not necessarily indicative of their activation or associated inflammatory processes.

It is also important to consider the role of platelet- and endothelial-derived MPs and their interactions with neutrophils. Platelets, once regarded as a thrombus-forming agent, are now recognized as primary players in inflammatory processes. Activated platelets produce platelet-derived MPs that induce neutrophil clustering and further activation [45,61]. Similarly, endothelial-derived MPs induce neutrophil adhesion and activation [62]. Therefore, an inflammatory process can become self-sustaining, as the activation of one cell type leads to the activation of another, which in turn further activates the original cell type. In such a setting, an intriguing phenomenon may occur: Despite being activated and having a tendency for neutrophilia, the neutrophil count might decrease due to migration/sequestration in damaged tissues [63,64]. In other words, the inflammatory condition might appear, without changes in neutrophil count.

Considering HRV as an index of physiological stress from various sources, our results, along with other reports [18,32], suggest the putative illustration depicted in Figure 10. The initial phase of decompression leads to a certain degree of bubble formation and inflammatory response activation [65]. Subsequently, depending on the decompression rate, one of three outcomes may occur, as modeled in a dynamical system by Schirato *et al.* [65], which represent the interactions of supersaturation, bubble production, inflammation, and their respective feedbacks.

In the case of elevated overall supersaturation, increased tissue damage and bubble formation occur, resulting in positive inflammatory feedback [66,67]. At the end of the decompression process, a state of high physiological stress with an important inflammatory process in progress is likely to be observed. In this case, subjects will most probably develop decompression sickness [68].

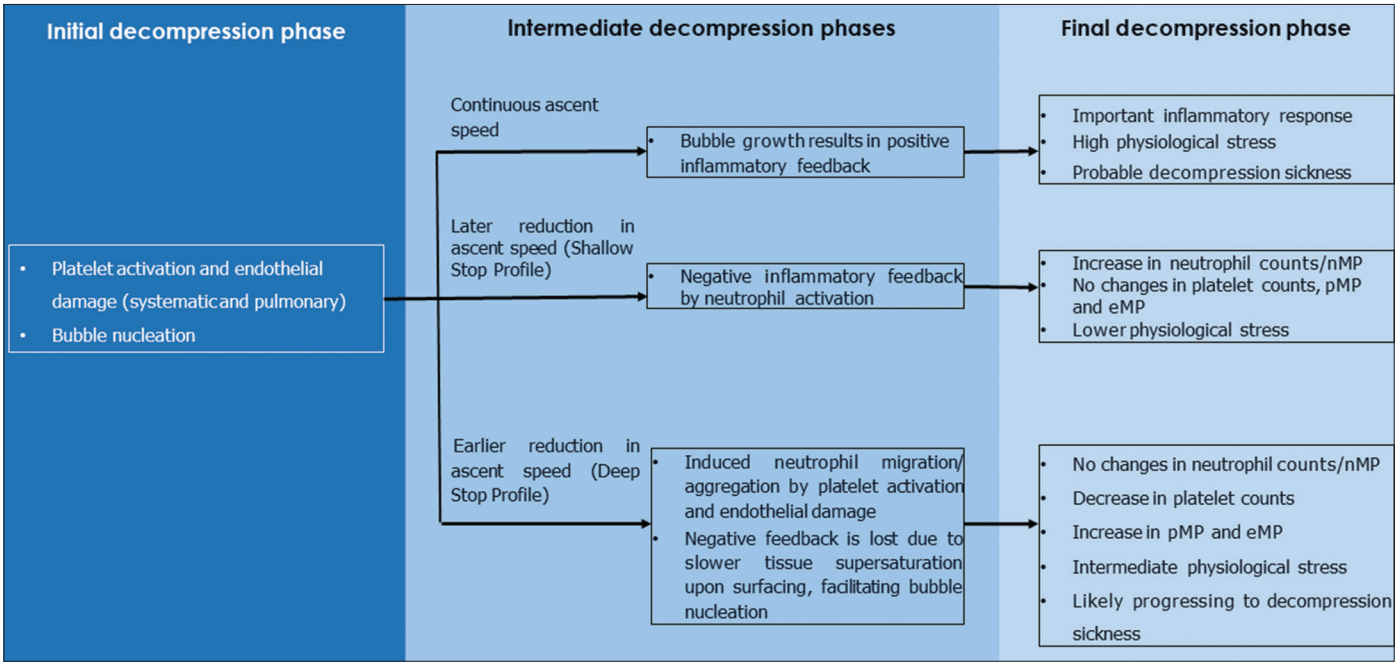

Figure 11. Possible schematics of the immune system response to decompression, with platelet- and endothelial-derived MPs are referred to as pMPs and eMPs, respectively
Abbreviation: MP: Microparticle; pMPs: Platelet microparticles; eMPs: Endothelial microparticles

DOI: https://doi.org/10.36922/jctr.24.00021

Finally, if the decompression proceeds at a pace that allows neutrophils to become active but not activated by platelet- and endothelial-derived MPs, they will inhibit the ongoing inflammatory process initiated earlier. Bubble formation would likely be minimal due to the absence of nucleation sources, resulting in the individual surfacing with low physiological stress.

The levels of supersaturation required to trigger the processes depend on individual responses, i.e., activation of the person's inflammatory processes. Moreover, the correlation between HRV and the degree of stress (sympathetic tonus) seems to be highly individualized. Notably, different decompression profiles generate different tissue supersaturation upon surfacing. The composition of the breathing gases (i.e., the fraction of oxygen and the presence of helium) causes different physiological responses. It might be possible to speculate the existence of a dose-dependent response, where lower tissue supersaturation would lead to little or no physiological alterations, while higher tissue supersaturations would lead to progressively greater physiological responses and subsequently the development of decompression sickness.

Our proposed schematics presented in Figure 11 highlight two aspects of decompression: (i) the combination of bubble count, inflammatory markers, and HRV can be an important predictor of decompression success on an individual basis; (ii) if a clear relationship between HRV indexes and bubble/inflammation is established post-decompression, HRV could be employed to assess an individual's likelihood of success in a given decompression profile.

Of course, the ideas presented in this study should be interpreted with caution due to the small cohort of investigated divers and the large inter-individual variance observed in the variables analyzed. Besides, it is important to note that the data were obtained through dives simulated in hyperbaric chambers, which might not necessarily reflect the actual conditions encountered when divers are immersed [69], though the data obtained in chamber and swimming pool dives, already presented in other studies, displayed similar patterns.

5. Conclusion

Although no cases of decompression sickness were observed in the experiments described in this manuscript, it has been demonstrated in the present study that different decompression profiles trigger different physiological responses. Whether these physiological responses translate into a higher risk of developing symptoms of decompression sickness is unclear at the present moment, and further research is required. It can be speculated, however, that, according to the scheme described in Figure 11 and further developed by Schirato *et al.* [65], they might play a relevant role in more aggressive exposures.

Acknowledgments

None.

Funding

None.

Conflicts of Interest

The authors have no competing interests.

Ethics Approval and Consent to Participate

The volunteers provided written informed consent. The ethical committee of the Biosciences Institute of the University of Sao Paulo approved the experimental protocol (CAE #91231618.6.0000.5464), and all experiments were performed in accordance with relevant guidelines and regulations.

Consent for Publication

All volunteers signed an informed consent before joining the experiments.

Availability of Data

Data are available from the corresponding author upon reasonable request.

References

[1] Boycott AE, Damant GC, Haldane JS. The Prevention of Compressed-air Illness. J Hyg (Lond) 1908;8:342-443. doi: 10.1017/s0022172400003399

[2] Bühlmann A. Decompression, Decompression Sickness. Berlin: Springer Verlag Heidelberg; 1984. doi: 10.1007/978-3-662-02409-6

[3] Howle LE, Weber PW, Hada EA, Vann RD, Denoble PJ. The Probability and Severity of Decompression Sickness. PLoS One 2017;12(3):1-25. doi: 10.1371/journal.pone.0172665

[4] Doolette D, Gerth W, Gault K. Redistribution of Decompression Stop Time from Shallow to Deep Stops Increases Incidence of Decompression Sickness in Air Decompression Dives. Panama City: Navy Experimental Diving Unit; 2011.

[5] Yount DE, Hoffman DC. On the Use of a Bubble Formation Model to Calculate Diving Tables. Aviat Space Environ Med 1986;57:149-56.

[6] Marroni A, Bennett PB, Cronje FJ, Cali-Corleo R, Germonpre P, Pieri M, *et al*. A Deep Stop during Decompression from 82 fsw (25 m) Significantly Reduces Bubbles and Fast Tissue Gas Tensions. Undersea Hyperb Med 2004;31:233-43.

[7] Doolette DJ. Venous Gas Emboli Detected by Two-Dimensional Echocardiography are an Imperfect Surrogate Endpoint for Decompression Sickness. Diving Hyperb Med 2016;46:4-10.

[8] Doolette DJ, Murphy FG, Gerth WA. Thalmann Algorithm parameter sets for support of constant 1.3 atm PO_2 He-O_2 diving to 300 fsw. Panama City:Navy Experimental Diving Unit; 2018.

[9] Madden LA, Laden G. Gas Bubbles may not be the Underlying cause of Decompression Illness - the at-

Depth Endothelial Dysfunction Hypothesis. Med Hypotheses 2009;72:389-92.
doi: 10.1016/j.mehy.2008.11.022

[10] Thom SR, Bennett M, Banham ND, Chin W, Blake DF, Rosen A, *et al*. Association of Microparticles and Neutrophil Activation with Decompression Sickness. J Appl Physiol 2015;119:427-34.
doi: 10.1152/japplphysiol.00380.2015

[11] Bhullar J, Bhopale VM, Yang M, Sethuraman K, ThomSR. Microparticle Formation by Platelets Exposed to High Gas Pressures - An Oxidative Stress Response. Free Radic Biol Med 2016;101:154-62.
doi: 10.1016/j.freeradbiomed.2016.10.010

[12] Batool S, Abbasian N, Burton JO, Stover C. Microparticles and their Roles in Inflammation: A Review. Open Immunol J 2013;6:1-14.
doi: 10.2174/1874226201306010001

[13] Cognasse F, Hamzeh-Cognasse H, Laradi S, ChouML, Seghatchian J, Burnouf T, *et al*. The Role of Microparticles in Inflammation and Transfusion: A Concise Review. Transfus Apher Sci 2015;53:159-67.
doi: 10.1016/j.transci.2015.10.013

[14] Puddu P, Puddu GM, Cravero E, Muscari S, Muscari A. The Involvement of Circulating Microparticles in Inflammation, Coagulation and Cardiovascular Diseases. Can J Cardiol 2010;26:140-5.
doi: 10.1016/S0828-282X(10)70371-8

[15] Brett KD, Nugent NZ, Fraser NK, Bhopale VM, Yang M, Thom SR. Microparticle and Interleukin-1B Production with Human Simulated Compressed Air Diving. Sci Rep 2019;9:13320.

[16] Thom SR, Bhopale VM, Yang M. Neutrophils Generate Microparticles during Exposure to Inert Gases Due to Cytoskeletal Oxidative Stress. J Biol Chem 2014;289:18831-45.
doi: 10.1074/jbc.M113.543702

[17] Winterbourn CC, Kettle AJ, Hampton MB. Reactive Oxygen Species and Neutrophil Function. Annu Rev Biochem 2016;85:765-92.
doi: 10.1146/annurev-biochem-060815-014442

[18] Schirato SR, El-Dash I, El-Dash V, Natali JE, Starzynski PN, Chaui-Berlinck JG. Heart Rate Variability Changes as an Indicator of Decompression-Related Physiological Stress. Undersea Hyperb Med 2018;45:173-82.

[19. Schirato SR, El-Dash I, El-Dash V, Bizzarro B, Marroni A, Pieri M, *et al*. Association between Heart Rate Variability and Physiological Stress. Front Physiol 2020;11:743.
doi: 10.3389/fphys.2020.00743

[20] The North American, Task Force of the European Society of Cardiology and The North American Society of Pacing and Electrophysiology. Heart Rate Variability: Standards of Measurement, Physiological Interpretation, and Clinical Use. Eur Heart J 1996;17:354-81.
doi: 10.1161/01.CIR.93.5.1043

[21] von Käne R, Nelesen RA, Mills PJ, Ziegler MG, Dimsdale JE. Relationship between Heart Rate Variability, Interleukin-6, and Soluble Tissue Factor in Healthy Subjects. Brain Behav Immun 2008;22:461-8.

[22] Kaufman CL, Kaiser DR, Steinberger J, Dengel DR. Relationships between Heart Rate Variability, Vascular Function, and Adiposity in Children. Clin Auton Res 2007;17:165-71.
doi: 10.1007/s10286-007-0411-6

[23] Haraguchi R, Hoshi H, Ichikawa S, Hanyu M, Nakamura K, Fukasawa K, *et al*. The Menstrual Cycle Alters Resting-State Cortical Activity: A Magnetoencephalography Study. Front Hum Neurosci 2021;15:652789.
doi: 10.3389/fnhum.2021.652789

[24] Cialoni D, Pieri M, Balestra C, Marroni A. Dive Risk Factors, Gas Bubble Formation, and Decompression Illness in Recreational SCUBA Diving: Analysis of DAN Europe DSL Data Base. Front Psychol 2017;8:1587.
doi: 10.3389/fpsyg.2017.01587

[25] Thom SR, Yang M, Bhopale VM, Milovanova TN, Bogush M, Buerk DG. Intramicroparticle Nitrogen Dioxide is a Bubble Nucleation Site Leading to Decompression-Induced Neutrophil Activation and Vascular Injury. J Appl Physiol 2013;114:550-8.
doi: 10.1152/japplphysiol.01386.2012

[26] Thom SR, Milovanova TN, Bogush M, Bhopale VM, Yang M, Bushmann K, *et al*. Microparticle Production, Neutrophil Activation, and Intravascular Bubbles Following Open-Water SCUBA Diving. J Appl Physiol 2012;112:1268-78.
doi: 10.1152/japplphysiol.01305.2011

[27] Ludbrook J, Dudley H. Why Permutation Tests Are Superior to t and F Tests in Biomedical Research. John Ludbrook and Hugh Dudley Source : The American Statistician, 52, 127-132. Am Stat Assoc 2008;52:127-32.

[28] Vince RV, McNaughton LR, Taylor L, Midgley AW, Laden G, Madden LA. Release of VCAM-1 Associated Endothelial Microparticles Following Simulated SCUBA Dives. Eur J Appl Physiol 2009;105:507-13.
doi: 10.1007/s00421-008-0927-z

[29] Madden D, Thom SR, Dujic Z. Exercise Before and After SCUBA Diving and the Role of Cellular Microparticles in Decompression Stress. Med Hypotheses 2016;86:80-4.
doi: 10.1016/j.mehy.2015.12.006

[30] Ernst G. Heart-Rate Variability-More than Heart Beats? Front Public Health 2017;5:240.
doi: 10.3389/fpubh.2017.00240

[31] Noh Y, Posada-Quintero HF, Bai Y, White J, Florian JP,

Brink PR, *et al*. Effect of Shallow and Deep SCUBA Dives on Heart Rate Variability. Front Physiol 2018;9:110.
doi: 10.3389/fphys.2018.00110

[32] Marchitto N, Iannarelli N, Paparello PT, Cioeta E, Parisi F, Pirrone S, *et al*. The Cardiovascular Risk in the Scuba Divers. J Sports Med Phys Fitness 2019;59:1779-82.
doi: 10.23736/S0022-4707.19.09358-7

[33] Lauscher P, Kertscho H, Enselmann P, Lauscher S, Habler O, Meier J. Effects of Alterations of Inspiratory Oxygen Fractions on Heart Rate Variability. Br J Anaesth 2012;108:402-8.
doi: 10.1093/bja/aer404

[34] Chapleau MW, Li Z, Meyrelles SS, Ma X, Abboud FM. Mechanisms Determining Sensitivity of Baroreceptor Afferents in Health and Disease. Ann N Y Acad Sci 2006;940:1-19.
doi: 10.1111/j.1749-6632.2001.tb03662.x

[35] Rahman F, Pechnik S, Gross D, Sewell L, Goldstein DS. Low Frequency Power of Heart Rate Variability Reflects Baroreflex Function, not Cardiac Sympathetic Innervation. Clin Auton Res 2011;21:133-41.
doi: 10.1007/s10286-010-0098-y

[36] Harris KF, Matthews KA. Interactions between Autonomic Nervous System Activity and Endothelial Function: A Model for the Development of Cardiovascular Disease. Psychosom Med 2004;66:153-64.
doi: 10.1097/01.psy.0000116719.95524.e2

[37] Brodsky SV, Zhang F, Nasjletti A, Goligorsky MS. Endothelium-Derived Microparticles Impair Endothelial Function *in Vitro*. Am J Physiol Heart Circ Physiol 2004;286(5):H1910-5.
doi: 10.1152/ajpheart.01172.2003

[38] Cialoni D, Brizzolari A, Barassi A, Bosco G, Pieri M, Lancellotti V, *et al*. White Blood Cells, Platelets, Red Blood Cells and Gas Bubbles in SCUBA Diving: Is there a Relationship? Healthcare (Basel) 2022;10:182.
doi: 10.3390/healthcare10020182

[39] Lindemann S, Tolley ND, Dixon DA, McIntyre TM, Prescott SM, Zimmerman GA, *et al*. Activated Platelets Mediate Inflammatory Signaling by Regulated Interleukin 1β Synthesis. J Cell Biol 2001;154:485-90.
doi: 10.1083/jcb.200105058

[40] Alicia P, Yourish K. Platelets: Versatile Effector Cells in Hemostasis, Inflammation, and the Immune Continuum. Nyt 2018;34:5-30.
doi: 10.1007/s00281-011-0286-4

[41] Pontier JM, Vallée N, Bourdon L. Bubble-Induced Platelet Aggregation in a Rat Model of Decompression Sickness. J Appl Physiol (1985) 2009;107:1825-9.
doi: 10.1152/japplphysiol.91644.2008

[42] Pontier JM, Blatteau JE, Vallée N. Blood Platelet Count and Severity of Decompression Sickness in Rats After a Provocative Dive. Aviat Space Environ Med 2008;79:761-4.
doi: 10.3357/ASEM.2299.2008

[43] Pontier JM, Jimenez C, Blatteau JE. Blood Platelet Count and Bubble Formation After a Dive to 30 msw for 30 Min. Aviat Space Environ Med 2008;79:1096-9.
doi: 10.3357/ASEM.2352.2008

[44] Watanabe J, Marathe GK, Neilsen PO, Weyrich AS, Harrison KA, Murphy RC, *et al*. Endotoxins Stimulate Neutrophil Adhesion Followed by Synthesis and Release of Platelet-Activating Factor in Microparticles. J Biol Chem 2003;278:33161-8.
doi: 10.1074/jbc.M305321200

[45] Jy W, Mao WW, Horstman LL, Tao J, Ahn YS. Platelet Microparticles Bind, Activate and Aggregate Neutrophils *in Vitro*. Blood Cells Mol Dis. 1995;21:217-31.
doi: 10.1006/bcmd.1995.0025

[46] Hottz ED, Lopes JF, Freitas C, Valls-de-Souza R, Oliveira MF, Bozza MT, *et al*. Platelets Mediate Increased Endothelium Permeability in Dengue through NLRP3-Inflammasome Activation. Blood 2013;122:3405-14.
doi: 10.1182/blood-2013-05-504449

[47] Lang F, Lang E, Fller M. Physiology and Pathophysiology of Eryptosis. Transfus Med Hemother 2012;39:308-14.
doi: 10.1159/000342534

[48] Pretorius E, Du Plooy JN, Bester J. A Comprehensive Review on Eryptosis. Cell Physiol Biochem 2016;39:1977-2000.
doi: 10.1159/000447895

[49] Perovic A, Nikolac N, Njire Braticevic M, Milcic A, Sobocanec S, Balog T, *et al*. Does Recreational Scuba Diving have Clinically Significant Effect on Routine Haematological Parameters? Biochem Med (Zagreb) 2017;27:27-38.
doi: 10.11613/BM.2017.035

[50] Al-Gwaiz LA, Babay HH. The Diagnostic Value of Absolute Neutrophil Count, Band Count and Morphologic Changes of Neutrophils in Predicting Bacterial Infections. Med Princ Pract 2007;16:344-7.
doi: 10.1159/000104806

[51] Tatsukawa Y, Hsu WL, Yamada M, Cologne JB, Suzuki G, Yamamoto H, *et al*. White Blood Cell Count, Especially Neutrophil Count, as a Predictor of Hypertension in a Japanese Population. Hypertens Res 2008;31:1391-7.
doi: 10.1291/hypres.31.1391

[52] de Jager CPC, Wever PC, Gemen EFA, Kusters R, van Gageldonk-Lafeber AB, van der Poll T, *et al*. The Neutrophil-Lymphocyte Count Ratio in Patients with Community-Acquired Pneumonia. PLoS One 2012;7:e46561.
doi: 10.1371/journal.pone.0046561

[53] Teramukai S, Kitano T, Kishida Y, Kawahara M,

Kubota K, Komuta K, *et al*. Pretreatment Neutrophil Count as an Independent Prognostic Factor in Advanced Non-Small-Cell Lung Cancer: An Analysis of Japan Multinational Trial Organisation LC00-03. Eur J Cancer 2009;45:1950-8.
doi: 10.1016/j.ejca.2009.01.023

[54] Shafi S, Afsheen M, Reshi F. Total Leucocyte Count, C-Reactive Protein and Neutrophil Count: Diagnostic Aid in Acute Appendicitis. Saudi J Gastroenterol 2009;15:117.
doi: 10.4103/1319-3767.48969

[55] Peake J, Suzuki K. Neutrophil Activation, Antioxidant Supplements and Exercise-Induced Oxidative Stress. Exerc Immunol Rev 2004;10:129-41.

[56] Pitanga TN, de Aragão França L, Rocha VCJ, Meirelles T, Borges VM, Gonçalves MS, *et al*. Neutrophil-Derived Microparticles Induce Myeloperoxidase-Mediated Damage of Vascular Endothelial Cells. BMC Cell Biol 2014;15:21.
doi: 10.1186/1471-2121-15-21

[57] Gasser O, Schifferli JA. Activated Polymorphonuclear Neutrophils Disseminate Anti-Inflammatory Microparticles by Ectocytosis. Blood 2004;104:2543-8.
doi: 10.1182/blood-2004-01-0361

[58] Dalli J, Norling LV, Renshaw D, Cooper D, Leung KY, Perretti M. Annexin 1 Mediates the Rapid Anti-Inflammatory Effects of Neutrophil-Derived Microparticles. Blood 2008;112:2512-9.
doi: 10.1182/blood-2008-02-140533

[59] Dalli J, Montero-Melendez T, Norling LV, Yin X, Hinds C, Haskard D, *et al*. Heterogeneity in Neutrophil Microparticles Reveals Distinct Proteome and Functional Properties. Mol Cell Proteomics 2013;12:2205-19.
doi: 10.1074/mcp.M113.028589

[60] Fujita K, Imamura R, Tanigawa G, Nakagawa M, Hayashi T, Kishimoto N, *et al*. Low Serum Neutrophil Count Predicts a Positive Prostate Biopsy. Prostate Cancer Prostatic Dis 2012;15:386-90.
doi: 10.1038/pcan.2012.27

[61] Maugeri N, Capobianco A, Rovere-Querini P, Ramirez GA, Tombetti E, Valle PD, *et al*. Platelet Microparticles Sustain Autophagy-Associated Activation of Neutrophils in Systemic Sclerosis. Sci Transl Med 2018;10:eaao3089.
doi: 10.1126/scitranslmed.aao3089

[62] Buesing KL, Densmore JC, Kaul S, Pritchard KA Jr., Jarzembowski JA, Gourlay DM, *et al*. Endothelial Microparticles Induce Inflammation in Acute Lung Injury. J Surg Res 2011;166:32-9.
doi: 10.1016/j.jss.2010.05.036

[63] Lee WL, Downey GP. Neutrophil Activation and Acute Lung Injury. Curr Opin Crit Care 2001;7:1-7.
doi: 10.1097/00075198-200102000-00001

[64] Nakagawa M, Toy P. Related Acute Lung Injury : Cases at One Hospital. Transfusion (Paris) 2004;44:1689-94.

[65] Schirato SR, Silva V, Iadocicco K, Maronni A, Pieri M, Cialoni D, *et al*. Post-Decompression Bubble and Inflammation Interactions: A Non-extensive Dynamical System Model. Undersea Hyperb Med 2022;49:207-26.
doi: 10.22462/03.04.2022.6

[66] Thom SR, Milovanova TN, Bogush M, Yang M, Bhopale VM, Pollock NW, *et al*. Bubbles, Microparticles, and Neutrophil Activation: Changes with Exercise Level and Breathing Gas During Open-Water SCUBA Diving. J Appl Physiol 2013;114:1396-405.
doi: 10.1152/japplphysiol.00106.2013

[67] Zhang K, Wang D, Jiang Z, Ning X, Buzzacott P, Xu W. Endothelial Dysfunction Correlates with Decompression Bubbles in Rats. Sci Rep 2016;6:33390.
doi: 10.1038/srep33390

[68] Imbert JP, Egi SM, Germonpré P, Balestra C. Static Metabolic Bubbles as Precursors of Vascular Gas Emboli During Divers' Decompression: A Hypothesis Explaining Bubbling Variability. Front Physiol 2019;10:807.
doi: 10.3389/fphys.2019.00807

[69] Vann RD, Gerth WA, Denoble PJ, Pieper CF, Thalmann ED. Experimental Trials to Assess the Risks of Decompression Sickness in Flying After Diving. UHM 2004;31:431-44.

DOI: https://doi.org/10.36922/jctr.24.00021

Journal of Clinical and Translational Research 2024; 10(5): 283-290

Journal of Clinical and Translational Research

Journal homepage: http://www.jctres.com/en/home

CASE REPORT

Computer-guided implant surgery and tooth-mirroring digital workflow to treat an esthetically compromised clinical case

Claudio Cirrincione*

Department of Experimental and Clinical Medicine, University of Florence, Florence, Italy

ARTICLE INFO

Article history:
Received: July 1, 2024
Accepted: October 8, 2024
Published Online: October 24, 2024

Keywords:
Computer-guided implantology
Surgical diagnosis and design software
Surgical guide
Artificial intelligence
Lithium disilicate veneers

**Corresponding author:*
Claudio Cirrincione
Department of Experimental and Clinical Medicine, University of Florence, Florence, Italy
Email: claudiocirrincione1@gmail.com

ABSTRACT

Background: In multidisciplinary dentistry, it is common to observe clinical cases that present multiple complications at the end of orthodontic therapy, such as differences in gingival height, alterations in size and shape of the teeth, and reduced residual spaces for implant therapies.
Aim: The aim of the study was to solve an esthetic case with the help of digitally assisted prosthetic and surgical design.
Methods: A young patient had been treated orthodontically for the agenesis of tooth 12 and the conoid shape of tooth 22. Previous therapy consisted of opening the space for tooth 12 by positioning a Maryland-type composite bridge, followed by reconstruction with a composite of tooth 22. Various composite reconstructions on teeth 11 and 21 were no longer adequate. Furthermore, both elements had discordant coronal axes, the diastema was observed at the incisal level, and tooth 21 was approximately 1 mm longer than tooth 11. Radiographic analysis revealed that the roots of teeth 11 and 13 converge, providing sufficient space for the insertion of a small-diameter implant. An intraoral scan and cone-beam computed tomography (CBCT) were performed; both data files were merged using surgical design software. A surgical guide was developed for the insertion of an implant in site 12. After insertion, the composite bridge, which was no longer suitable, was removed and a new temporary metal-composite Maryland bridge was positioned. Using an artificial intelligence tool of the design software, tooth 22 was isolated, mirrored, inserted in site 12 to reproduce the gingival profile, and subtracted from the digital impression. A technician then copied this emergence profile to build a zirconia prosthetic crown to be screwed on the implant. Teeth 22, 11, and 21 were restored with a lithium disilicate crown and two veneers, respectively.
Results: The initial digital design and the use of a guided surgery procedure allowed for the insertion of a small diameter implant without damaging the roots of the adjacent teeth. The prosthetic design procedure, using the digital tools of the design program, made it possible to standardize and create symmetrical gingival profiles of teeth 12 and 22. The overall composition was completed by the use of minimally invasive adhesive prosthetic techniques on teeth 11, 21, and 22.
Conclusion: Digital resources have become essential tools for dental professionals. The knowledge and use of technologies like intraoral scanning and CBCT, combined with various innovations such as artificial intelligence in prosthetic and implant design software, enable dentists to manage even the most complex interdisciplinary clinical cases with greater confidence.
Relevance for Patients: Digital techniques are now widely used across all fields of dentistry. This has led to the need for operators of all ages to adjust their decision-making process compared to traditional techniques. These new techniques have also improved communication with patients, allowing the dental team to have a clearer understanding of the clinical path to follow and consequently offer their patients precise dentistry solutions.

1. Introduction

In the 21st century, having a radiant smile has become increasingly important. A smile characterized by white, perfectly aligned teeth that are proportionate in size

DOI: https://doi.org/10.36922/jctr.24.00035

and symmetrically pleasing boosts confidence in social interactions and enhances attractiveness [1]. Dentistry has adapted and improved its techniques to meet these new requirements, strengthening the relationship between various dental disciplines, such as prosthetics, orthodontics, and implantology. This interdisciplinary connection has been facilitated by the impressive development of digital techniques in recent years. This includes the ability to easily manipulate patient impressions obtained with intraoral scanners, such as standard tessellation language (STL) files, and to combine them with 3D visualization of the bone from digital imaging and communications in medicine (DICOM) files generated by cone-beam computed tomography (CBCT) [2]. Therefore, dentists now have the opportunity to create a "virtual patient" on their computers, allowing them to establish adequate diagnostic criteria to obtain excellent results [3]. This strategy becomes particularly important when operators are faced with a reduced buccal bone wall, which can compromise the final long-term esthetic results in immediate [4] and late [5] implant placement. In contrast, adopting this strategy requires operators to improve their skills to become familiar with all the tools necessary to achieve the desired results [6]. Designing esthetically pleasing prosthetic work requires absolute synergy among all dental team members. In the past, this workflow required collaboration between the various operators, which could be complex due to difficulties in visualizing the final result. Conversely, the digital process has greatly simplified communication between dentists, thanks in part to the ability to visualize various steps in 3D, especially in clinical cases where esthetics is critical [7]. The aim of this work was to present an implant-prosthetic clinical case resulting from a previous orthodontic treatment, successfully treated using new digital technologies. This article was prepared following the strengthening the reporting of observational studies in epidemiology guidelines.

2. Methods

This retrospective clinical case was conducted according to the 1964 Helsinki Declaration principles for biomedical research involving human subjects. The patient was informed of the nature of the study, its benefits, risks, and possible alternative treatments, and written consent was also obtained for the use of clinical images. The patient was a 22-year-old man who complained of esthetic problems that arose after a previous orthodontic treatment. The orthodontic therapy involved reopening the space for tooth 12 to resolve agenesis of the related permanent element, along with a temporary composite reconstruction of the conoid tooth 22. The intraoral examination displayed a composite Maryland bridge replacing tooth 22 (Figures 1 and 2), temporarily positioned by the orthodontist, probably in view of the implant therapy. Teeth 11 and 21 featured some old composite reconstructions, discordant coronal axes, and the presence of a diastema at the incisal level; tooth 21 also appeared to be about 1 mm longer than tooth 11 (Figures 3 and 4). In tooth 12, the CBCT (Promax 3D Max; Planmeca, Finland) displayed an adequate vestibulo-palatal bone diameter for the insertion of a small-sized implant (Figures 5-7),

Figure 1. Maryland-type temporary composite bridge in site 12

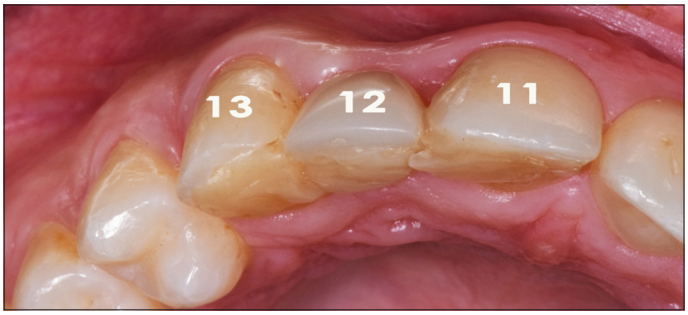

Figure 2. Palatal view detail of the bridge attached to teeth 11 and 13

Figure 3. Frontal view of the smile before treatment

but the root axes of teeth 13 and 11 converged toward the apices, making traditional implant surgery difficult (Figures 8-10). The anteroposterior view of the conoid dental element 22 displayed composite reconstruction with a large horizontal over-contour, most likely to compensate for the vestibulo-palatal inclination of the root axis (Figure 11). The gingival parabolas of the upper anterior group appeared unlevelled. Furthermore, the patient had moderate gingival exposure. Hence, the proposed treatment plan included the insertion of a small diameter implant in site 12 through computer-guided implant surgery, a zirconia crown

DOI: https://doi.org/10.36922/jctr.24.00035

Figure 4. Frontal view with retractor: the interincisive diastema and the different lengths of teeth 11 and 21 can be observed

Figure 5. Frontal view of the large mesial-distal space in site 12

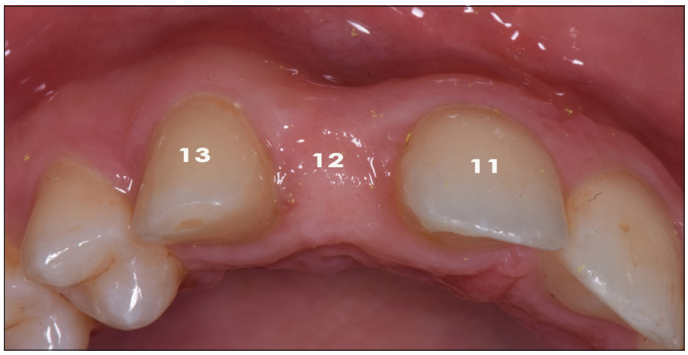

Figure 6. Occlusal view in site 12, which displays an adequate vestibule-palatal space

in site 12, two veneers in sites 11 and 21, and a crown in site 22, all made from lithium disilicate. A first intraoral scan was performed (Medit i500, Medit; MEDIT Co., Korea). The corresponding STL files were merged with the DICOM data derived from the CBCT using surgical diagnosis and planning software (coDiagnostiX; Dental Wings version 10.8, United States of America [USA]). At site 12, a small-diameter dental implant was virtually inserted (3.3 Bone Level Tapered; Straumann, Switzerland), and a surgical guide was designed (Figures 12 and 13). CoDiagnostiX is equipped with an artificial intelligence assistant that can be consulted remotely, making it possible to isolate individual teeth from the jaw bone and obtain individual 3D files. The 3D file of tooth 22 was loaded onto open-source software Meshmixer (Autodesk, USA), mirrored (Figure 14), and inserted where tooth 12 was missing; both were

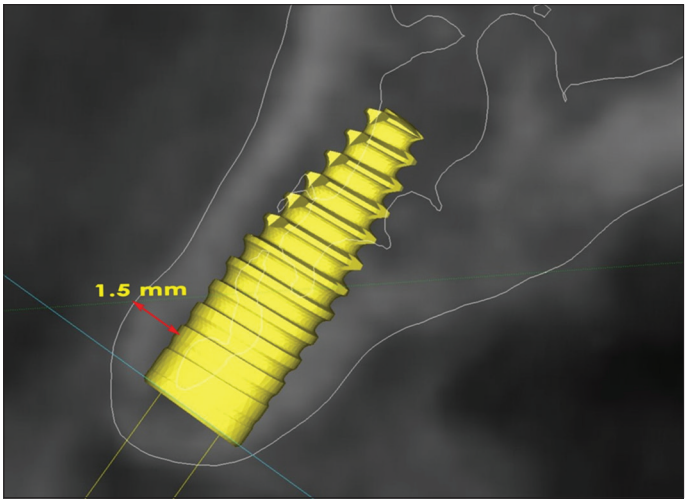

Figure 7. Sagittal view of cone-beam computed tomography with a virtual representation of the implant in site 12, which displays an adequate vestibular bone thickness of 1.5 mm

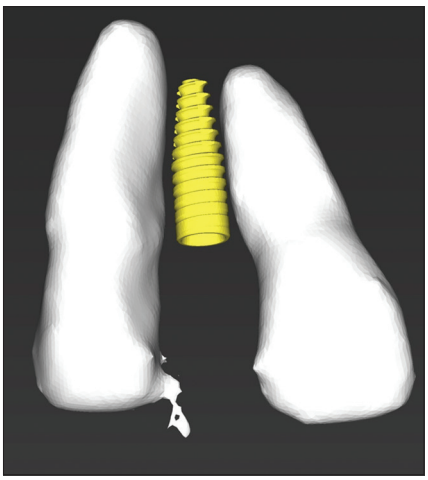

Figure 8. Frontal view of teeth 13 and 11, featuring a convergence of the root apices that reduce the space for the insertion of a standard implant

aligned with the virtual dental implant and gingival level of the contralateral (Figure 15). In Meshmixer, a Boolean procedure was performed on the mirrored tooth 22 by subtracting it from the 3D STL file of the upper jaw and leaving the space corresponding to the emergence profile (Figure 16). The project was then sent to a technician who, using the data related to the virtual emergency profile, created a temporary composite crown to be screwed onto the implant at the time of implant exposure. Using the surgical guide, the implant was inserted at site 12, leaving it submerged (Figures 17 and 18); a metal-composite Maryland bridge was then applied (Figure 19). The decision not to perform an immediate loading procedure was derived from the desire to manage the maturation of the soft tissues at the end of osteointegration. After 3 months of healing, the temporary Maryland in site 12 was removed; the implant was exposed; the previously made composite provisional crown was screwed in. After nearly 60 days of gingival healing, a

DOI: https://doi.org/10.36922/jctr.24.00035

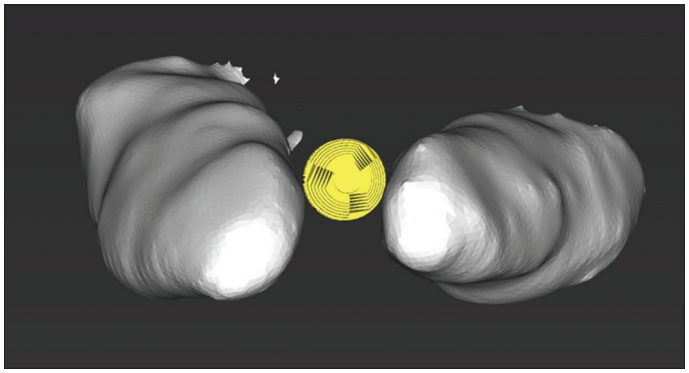

Figure 9. Apical view of teeth 13 and 11 (from Figure 8)

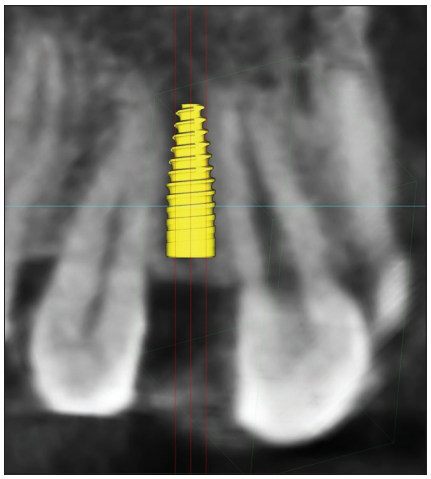

Figure 10. Sagittal cone-beam computed tomography view of the space available for the insertion of the implant in site 12

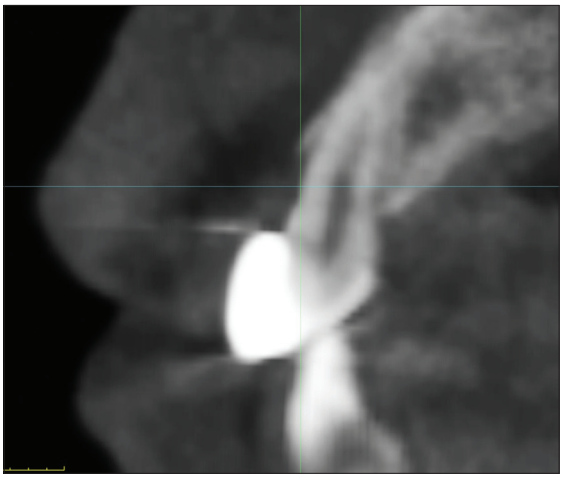

Figure 11. A sagittal view of the cone-beam computed tomography at site 22, displaying the wide horizontal overcontour of the composite reconstruction

digital impression was taken of both the temporary restoration adequately integrated into the soft tissues and the implant, as well as teeth 11, 21, and 22. The final work was then delivered. Both the crown on tooth 22 and the veneers on teeth 11 and 21 were made of pressed lithium disilicate (MT; Ivoclar-Vivadent

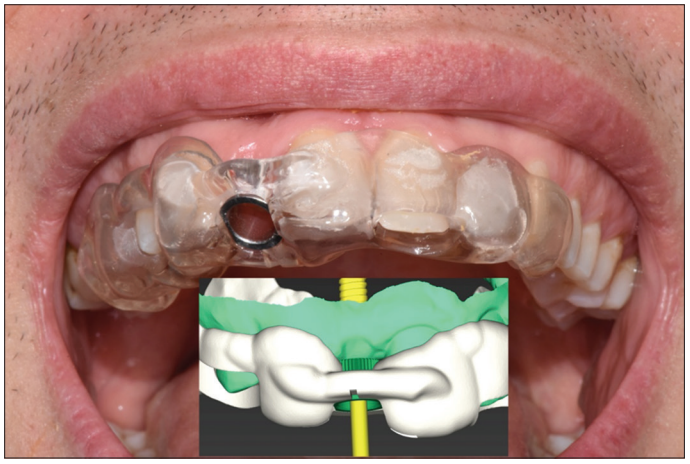

Figure 12. Frontal view of the surgical guide try-in

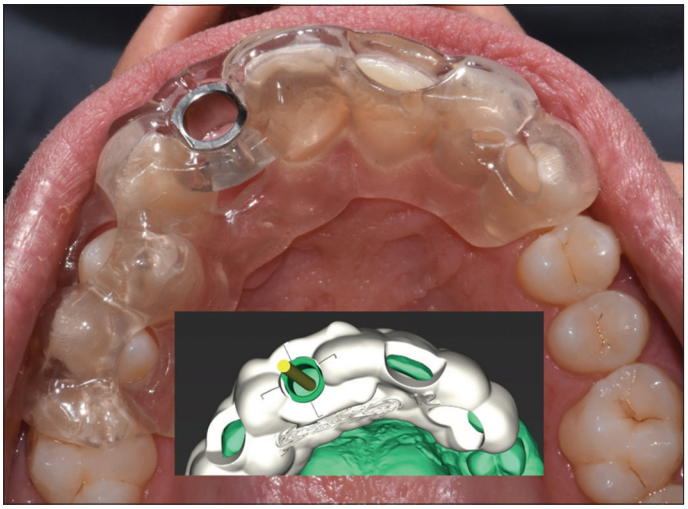

Figure 13. Occlusal view of the surgical guide try-in (from Figure 12)

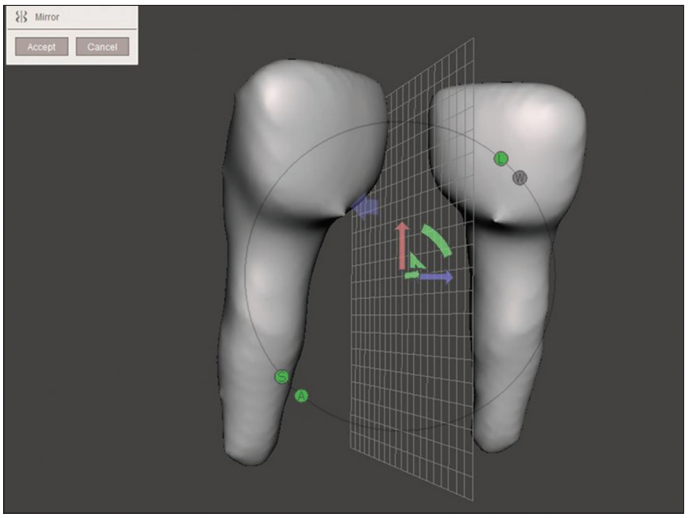

Figure 14. Tooth 22 was extracted from coDiagnostix, imported to Meshmixer (figure above), mirrored, and re-imported into coDiagnostix

AG, Liechtenstein), micro-layered with ceramic (Creation LS, Austria) and colored (Ivocolor; Ivoclar-Vivadent AG,

DOI: https://doi.org/10.36922/jctr.24.00035

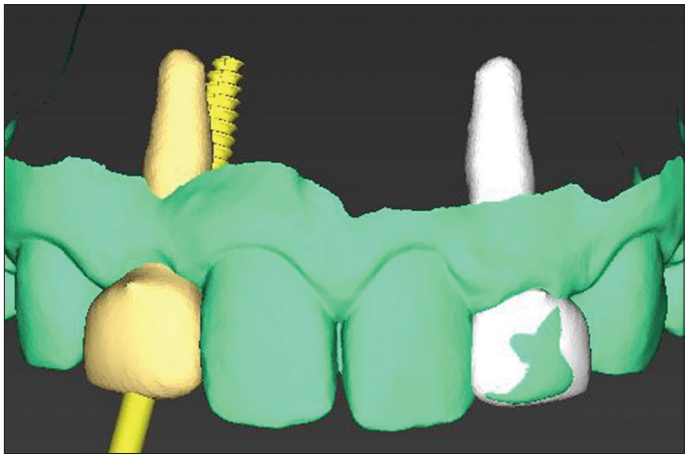

Figure 15. The mirrored tooth 22 was inserted in site 12 and aligned both with the axis of the implant and the gingival margin of tooth 22

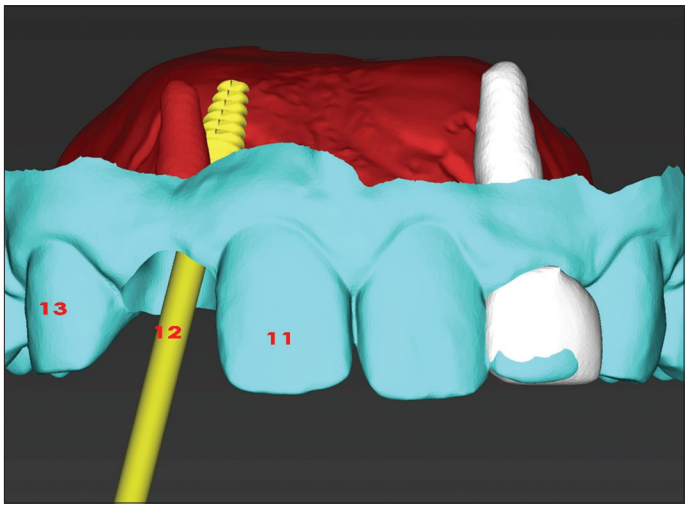

Figure 16. The mirrored tooth 22 was re-imported into Meshmixer along with the digital impression of the upper arch; it was then removed from the zone of tooth 12 using a subtractive Boolean procedure, leaving space for the copy of the emergence profile. Subsequently, it was re-imported into coDiagnostix and sent to the technician through the virtual planning export function.

Liechtenstein). The prosthetic element on the implant in site 12 was made of multilayered Zirconia (Explore Esthetic; Shenzhen Upcera Dental Technology Co. Ltd., China), micro-layered and colored (Figures 20-22).

3. Results

The shaping of the gingival area of tooth 12 with a temporary composite crown screwed on the implant generated an emergence profile identical to tooth 22, ensuring the formation of an optimal gingival profile. In addition to the virtually performed modifications, the provisional crown did not require any further adjustments. This approach minimized the need for its removal and reinsertion, thereby reducing potential damage to the delicate peri-implant epithelium. Likewise, the computer-guided surgery enabled the implant to be inserted in an adequate position to avoid any damage to the roots of the neighboring

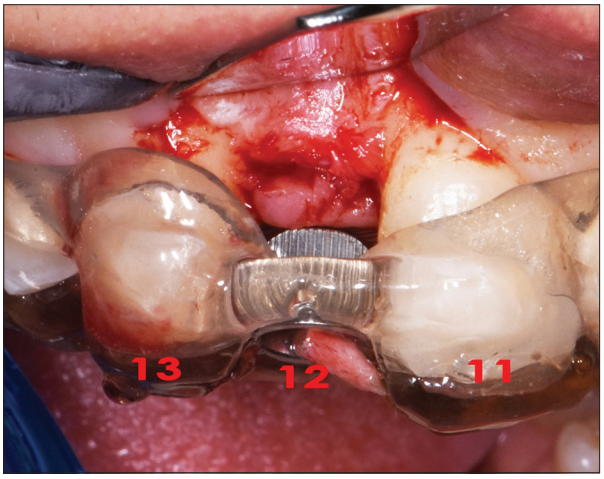

Figure 17. Frontal view of the implant insertion with the guide

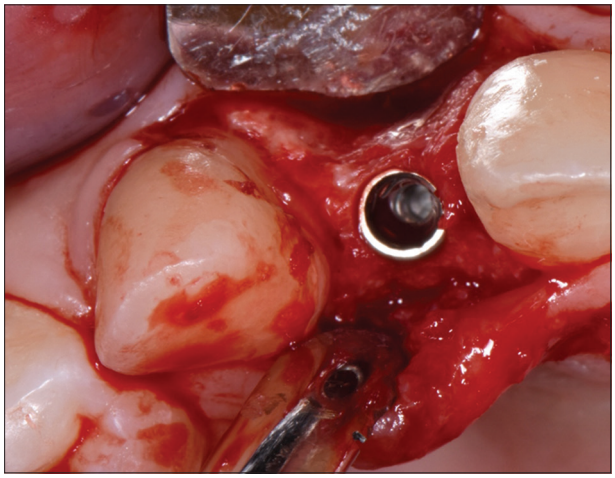

Figure 18. Occlusal view of the implant insertion with the guide (from Figure 17)

teeth. The lithium disilicate veneers in teeth 11 and 21 also improved the length and shape differences of the elements. In general, the ceramic micro-layering technique, while quite sophisticated, has enabled the creation of restorations with optimal esthetics. The use of two modeling and prosthetic design software allowed the workflow to be optimized. In particular, Meshmixer has proven to be an intuitive computer-aided design software, with extremely simplified controls even for prosthetic purposes. To increase the mesiodistal dimensions of tooth 13, a mesial composite reconstruction was also performed.

4. Discussion

This clinical case demonstrates how a precise digital workflow enables efficient treatment of an esthetically compromised clinical case. Mirroring a contralateral tooth has been particularly helpful in developing an adequate emergence profile. Joda *et al.* [8] used the DICOM data of the CBCT to mirror the contralateral tooth. This enabled the creation of a personalized healing abutment, followed by a provisional crown with the same emergency profile. In this clinical case, only the

DOI: https://doi.org/10.36922/jctr.24.00035

Figure 19. Insertion of the temporary metal-composite Maryland bridge

Figure 20. Frontal view of the smile on delivery of the final prosthesis

provisional crown was realized to save time. Similarly, Zeng *et al*. [9] reproduced the emergence profile of a contralateral posterior tooth in an individualized healing abutment, which was then replaced with the provisional crown. Pozza *et al*. [10] proposed a technique to realize a personalized healing abutment based on a failing posterior tooth to be replaced with a dental implant. However, this technique works only if a tooth with an adequately intact emergence profile is present. Both Noharet and Van Dooren [11] and Passos *et al*. [12] proposed an analogical-digital technique, where a fractured anterior tooth was replaced with an implant-supported crown replicating its emergence profile. However, this technique requires the presence of a tooth. From a broader point of view, the aim of all of these digital techniques is to reduce time wastage while improving the clinical performance of the prosthetic workflow [13]. Besides reducing surgical time, digital techniques allow for obtaining a more precise implant insertion, particularly in cases of reduced alveolar spaces. Younes *et al*. [14] reported that guided implant surgery achieves better accuracy compared with free-hand technique in partially edentulous patients. Moreover, a flapless surgical approach appeared to yield better results when combined with guided surgery [15]. However, open-flap surgery is necessary in cases of poor CBCT residual facial bone

Figure 21. Right lateral view of the smile on delivery of the final prosthesis

Figure 22. Left lateral view of the smile on delivery of the final prosthesis

visualization [16]. To achieve an esthetically pleasant final result, adequate prosthetic materials must be used, as well as the right dental technique. 3D printing allows for the realization of highly esthetic restoration [17], particularly when combined with modern dental materials [18].

5. Conclusion

Digital resources have become indispensable tools for dental professionals. The knowledge and use of technologies such as intraoral scanning and CBCT, combined with various innovations such as artificial intelligence offered in prosthetic and implant design software, enable dentists to manage particularly challenging interdisciplinary clinical cases with greater confidence. Computer-guided implant surgery, combined with digital tooth mirroring and appropriate ceramic dental techniques, allowed for the efficient resolution of this clinical case.

DOI: https://doi.org/10.36922/jctr.24.00035

Acknowledgments

The author would like to thank Mr. Alessandro Certini of the Nuova Arte Odontotecnica Laboratory of Florence for providing the prosthetic products and surgical guide.

Funding

None.

Conflicts of Interest

The author declares no competing interests.

Ethics Approval and Consent to Participate

This retrospective clinical case was conducted according to the principles of the Helsinki Declaration of 1964 for biomedical research involving human subjects. The patient was informed of the nature of the study, benefits, risks, and possible alternative treatments, and the patient provided written consent for using the clinical images.

Consent for Publication

The patient was informed of the nature of the study, benefits, risks, and possible alternative treatments, and the patient also provided written consent for using the clinical images.

Availability of Data

Data are available from the corresponding author on reasonable request.

References

[1] Masch L, Gassner A, Rosar U. Can a Beautiful Smile Win the Vote? The Role of Candidates' Physical Attractiveness and Facial Expressions in Elections. Politics Life Sci 2021;40:213-223.
doi: 10.1017/pls.2021.17

[2] Cirrincione C. Digital Workflow Aiming to a Bracketless 37 Distalization and to Implant Insertion. Dent Cad 2023;91:874-80.
doi: 10.19256/d.cadmos.10.2023.09

[3] Wang J, Wang B, Liu YY, Luo YL, Wu YY, Xiang L, *et al*. Recent Advances in Digital Technology in Implant Dentistry. J Dent Res 2024;103787-9.
doi: 10.1177/00220345241253794

[4] Martins SC, Da Costa Marques M, Gomes Vidal M, Tolentino PH, Dinelli RG, De Oliveira Fernandes GV, *et al*. Is the Facial Bone Wall Critical to Achieving Esthetic Outcomes in Immediate Implant Placement with Immediate Restoration? A Systematic Review. Adv Clin Exp Med 2024;33:979-7.
doi: 10.17219/acem/173573

[5] Vignoletti F, Sanz-Esporrin J, Sanz-Martin I, Nuñez J, Luengo F, Sanz M. Ridge Alterations after Implant Placement in Fresh Extraction Sockets or in Healed Crests: An Experimental *in vivo* Investigation. Clin Oral Implants Res 2019;30:353-63.

[6] Donker VJ, Heijs KH, Pol CW, Meijer HJ. Digital Versus Conventional Surgical Guide Fabrication: A Randomized Crossover Study On Operator Preference, Difficulty, Effectiveness, and Operating Time. Clin Exp Dent Res 2024;10:e831.
doi: 10.1002/cre2.831

[7] Ahmed WM, Azhari AA, Sedayo L, Alhaid A, AlhandarR, Almalki A, *et al*. Mapping the Landscape of the Digital Workflow of Esthetic Veneers from Design to Cementation: A Systematic Review. Dent J (Basel) 2024;12:28.
doi: 10.3390/dj12020028

[8] Joda T, Ferrari M, Braegger U. A Digital Approach for One-step Formation of the Supra-Implant Emergence Profile with an Individualized CAD/CAM Healing Abutment. J Prosthodont Res 2016;60:220-223.
doi: 10.1016/j.jpor.2016.01.005

[9] Zeng H, Zhou M, Ge Y, Yao Y, Cai X. Digital Workflow in the Design of Individualized Emergence Profiles of Implant Restorations Based on the Contralateral Tooth. J Prosthodont Res 2024;68:482-6.
doi: 10.2186/jpr.JPR_D_23_00127

[10] Pozza MB, Costa AJ, Burgoa S, Ventura D, Cortes AR. Digital Workflow for Low-cost 3D-Printed Custom Healing Abutment Based on Emergence Profile CBCT Segmentation. J Prosthet Dent 2022;130:155-9.
doi: 10.1016/j.prosdent.2022.10.019

[11] Noharet R, Van Dooren E. Combination of Cone Beam Computed Tomography and CAD-CAM Techniques for Maintaining Natural Emergence Profile in Immediate Extraction and/or Implant Placement and Restoration of a Central Incisor: A Dental Technique. J Prosthet Dent 2019;122:193-7.
doi: 10.1016/j.prosdent.2018.12.003

[12] Passos L, De Vasconcellos AB, Kanashiro L, Kina S. The Natural CAD/CAM Anterior Implant Single Tooth Restoration: A Novel Digital Workflow. J Esthet Restor Dent 2023;35:1194-204.
doi: 10.1111/jerd.13073

[13] Monaco C, Evangelisti E, Scotti R, Mignani G, Zucchelli G. A Fully Digital Approach to Replicate Peri-implant Soft Tissue Contours and Emergence Profile in the Esthetic Zone. Clin Oral Implants Res 2016;27:1511-4.
doi: 10.1111/clr.12599

[14] Younes F, Cosyn J, De Bruyckere T, Cleymaet R, Bouckaert E, Eghbali A. A Randomized Controlled Study on the Accuracy of Free-handed, Pilot-drill Guided and Fully Guided Implant Surgery in Partially Edentulous Patients. J Clin Periodontol 2018;45:721-32.
doi: 10.1111/jcpe.12897

[15] Floriani F, Jurado CA, Cabrera AJ, Duarte W, Porto TS, Afrashtehfar KI. Depth Distortion and Angular Deviation of a Fully Guided Tooth-supported Static Surgical Guide in a Partially Edentulous Patient: A Systematic Review and Meta-analysis. J Prosthodont 2024;33:10-24.
doi: 10.1111/jopr.13893

[16] Gong Z, Li X, Shi M, Cai G, Chen S, Ye Z, *et al*. Measuring the Binary Thickness of Buccal Bone of Anterior Maxilla in Low-Resolution Cone-beam Computed Tomography Via a Bilinear Convolutional Neural Network. Quant Imaging Med Surg 2023;13:8053-8066.
doi: 10.21037/qims-23-744

[17] Schweiger J, Edelhoff D, Schubert O. 3D Printing of Ultra-thin Veneers Made of Lithium Disilicate Using the LCM Method in a Digital Workflow: A Feasibility Study. J Esthet Restor Dent 2024;36:588-94.
doi: 10.1111/jerd.13155

[18] KnezovićZlatarić D, Pongrac R, Soldo M. Shade Management Using a New Zirconia-reinforced Lithium Disilicate Press Ceramic System and Leucite-reinforced Glass-ceramic Veneering System. Int J Esthet Dent 2022;17:324-38.

DOI: https://doi.org/10.36922/jctr.24.00035

Journal of Clinical and Translational Research 2024; 10(5): 291-295

Journal of Clinical and Translational Research

Journal homepage: http://www.jctres.com/en/home

ORIGINAL ARTICLE

Assessment of the humoral immunity against diphtheria, tetanus, and hepatitis B among children with acute lymphocytic leukemia

Sima Omrani[1], Fatemeh Malek[2]*, Shiva Nazari[2]*, Mojhgan Hashemieh[3], Hasan Abolghasemi[2], Mehrnaz Mesdaghi[4], Zahra Khafafpour[2]

[1]Department of Pediatric Medicine, School of Medicine, Shahid Beheshti University of Medical Science, Tehran, Iran, [2]Pediatric Congenital Hematologic Disorders Research Center, Research Institute for Children's Health, Shahid Beheshti University of Medical Sciences, Tehran, Iran, [3]Imam Hossein Medical Center, Shahid Beheshti University of Medical Sciences, Tehran, Iran, [4]Pediatrics and Child Health, Department of Allergy and Clinical Immunology, Mofid Children's Hospital, Shahid Beheshti University of Medical Sciences, Tehran, Iran

ARTICLE INFO

Article history:
Received: August 8, 2024
Accepted: October 15, 2024
Published Online: October 29, 2024

Keywords:
Leukemia
Pediatrics
Immune system
Immunoglobulins
Humoral immune system

**Corresponding author:*
Dr. Shiva Nazari
Pediatric Congenital Hematologic Disorders Research Center, Research Institute for Children's Health, Shahid Beheshti University of Medical Sciences, Tehran, Iran.
Email: shnazari2000@gmail.com

Dr. Fatemeh Malek
Pediatric Congenital Hematologic Disorders Research Center, Research Institute for Children's Health, Shahid Beheshti University of Medical Sciences, Tehran, Iran.
Email: Fmalek7721@gmail.com

ABSTRACT

Background: Approximately all systemic therapies for childhood affect the immune system. The behavior of the immune system in leukemia patients following chemotherapy is not yet clearly defined. The probability of vaccination failure and the need for revaccination remain challenging for these patients.
Aim: To evaluate the humoral immunity against diphtheria, tetanus, and hepatitis B in children with acute lymphocytic leukemia (ALL) immediately and 6 months after chemotherapy.
Materials and Methods: In the present prospective cohort study, 21 patients with ALL referred to Mofid Children's Hospital were studied immediately and 6 months after chemotherapy. Serum samples were collected from patients, and the levels of immunoglobulins (IgG, IgM, IgE, and IgA) antibodies against diphtheria, tetanus, and hepatitis B were determined using specific enzyme-linked immunosorbent assay kits. The obtained data were analyzed using Statistical Package for Social Sciences 21 software.
Results: A total of 13 males and 8 females with an average age of 8.6 ± 2.5 years were included in the present study. Six months after chemotherapy, the mean level of IgG, IgM, IgE, and IgA displayed an increase of 563.1 units in IgG, 11 units in IgM, 11.3 units in IgE, and 5 units in IgA levels. Moreover, data revealed that 6 months after chemotherapy, the mean level of *IgG antibodies* displayed an increase of 7.09, 3.43, and 1.03 units against hepatitis B, diphtheria, and tetanus, respectively. A significant relationship was found between the antibody level against diphtheria and the age group of the patients ($p = 0.003$).
Conclusion: Humoral immune status was boosted after 6 months of chemotherapy, though all patients had some extent of lasting immune dysfunction. We indicate that survivors of childhood cancer have ongoing humoral immunological defects and may remain at risk for infectious complications after completion of therapy.
Relevance for Patients: The present study indicated that systemic therapies for pediatrics with leukemia affect the immune system. Pediatrics with leukemia may remain at risk for infectious complications after completion of therapy.

1. Introduction

Cancer is the second leading cause of death in children under 15, and leukemia is the most common type of cancer in this age group [1,2]. In leukemia patients, the humoral and cellular immune systems are impaired, and the patients are immunocompromised [3,4]. Various types of leukemia affect bone marrow (BM) cells and the immune system. For example, in chronic lymphocytic leukemia, mature B lymphocytes accumulate in

DOI: http://doi.org/10.36922/jctr.24.00050

lymphoid organs, and the BM [5,6]. In addition, immune system dysfunction is an inevitable side effect of chemotherapy, which is used in the treatment of leukemia.

Chemotherapy uses potent cytotoxic and immune-suppressing agents to eliminate cancerous cells, but these drugs also affect normal BM cells, leading to a reduction in blood cells [7] and defects in the humoral immune system. The abnormality in the immune system after chemotherapy in leukemia patients lasts for a general period of 6–12 months after stopping the treatment [8]; however, long-term abnormalities have also been reported [9], and B lymphocytes are mainly sensitive to this side effect of chemotherapy [10,11]. Therefore, these patients appear to be highly susceptible to infection, even diseases they have been vaccinated for, such as diphtheria, tetanus, or hepatitis B.

Post-chemotherapy immune system dysfunction has been reported, but previous findings are not consistent [12,13]. The probability of vaccination failure and the need for revaccination remain challenging for these patients [14]. In this regard, the behavior of the immune system in leukemia patients following chemotherapy is not yet clearly defined. In the present study, we aimed to evaluate the humoral immunity against diphtheria, tetanus, and hepatitis B in pediatrics with leukemia immediately and 6 months after chemotherapy.

2. Materials and Methods

The present prospective cohort study included 21 children (13 males and 8 females) with acute lymphocytic leukemia (ALL). The patients were assessed at 1 and 6 months after therapy termination. The treatment process of all enrolled patients was performed based on the Acute Lymphoblastic Leukaemia: BFM 20001 Schema protocol [15]. Briefly, all patients were treated with a combination of vincristine sulfate, adriamycin, and methotrexate.

Patients with a history of stem cell transplantation or primary immune deficiency disease were excluded from this study. All participants provided written informed consent, and the Institutional Review Board approved the protocol and consent forms at Shahid Beheshti University of Medical Sciences (approval number: IRSBMU.MSP.REC.1399.473).

The following data were collected immediately after and 6 months after the end of the chemotherapy: quantitative level of total immunoglobulins (IgG, IgM, IgE, and IgA), IgG antibody levels against diphtheria, tetanus, and hepatitis B, white blood cell (WBC) number, and neutrophil and lymphocyte percentages.

Serum samples were screened for IgG antibodies against diphtheria and tetanus using the commercial Human Diphtheria Antibody enzyme-linked immunosorbent assay (ELISA) Kit and Tetanus Toxoid IgG ELISA Kit, respectively (MyBioSource, United States of America [USA]). Furthermore, a hepatitis B antibody rapid test kit was used to identify the IgG antibody against the hepatitis B virus. All ELISA reactions were performed according to the manufacturer's instructions.

The patients were categorized into two groups based on age: group 1: ≤8 years old; group 2: >8 years old. The relationship between the immune system-related factors and the age group and gender of the patients was evaluated.

Data were analyzed using Statistical Package for Social Sciences (SPSS) V19 software (SPSS Inc., USA). The Kolmogorov–Smirnov test evaluated the normal distribution of continuous variables. Parametric data are expressed as mean ± standard deviation. The Chi-square test and Spearman correlation were used to analyze data. For all analyses, a $p < 0.05$ is considered significant.

3. Results

3.1. Total IgA, IgE, IgG, and IgM

The mean age of the patients was 8.6 ± 2.5 years old. In general, 6 months after chemotherapy, the mean level of IgG, IgM, IgE, and IgA exhibited an increase of 563.1 units in IgG level, 11 units in IgM, 11.3 units in IgE, and 5 units in IgA levels (Table 1). Changes in study variables 6 months after the completion of chemotherapy are presented in Table 2. Our analyses revealed that the IgM, IgE, and IgA levels were significantly increased after 6 months of chemotherapy compared to the immediate time after chemotherapy ($p = 0.001$), but the increment in IgG level was not significant ($p = 0.336$). Moreover, no statistically significant relationship was observed between the level of these IgG, IgM, IgE, and IgA and gender (Table 3).

3.2. IgG antibody levels against diphtheria, tetanus, and hepatitis B

In total, 6 months after chemotherapy, the mean level of *IgG antibodies* exhibited an increase of 3.43 and 1.03 units

Table 1. Changes in antibody levels

Antibody	Antibody levels (unit)		p-value
	Immediately after chemotherapy	6 months after chemotherapy	
IgG	665.6±509.9	1228.7±1815.2	0.366
IgM	46.9±56.9	57.9±44.3	<0.001
IgE	29.3±80.5	40.6±77.7	<0.001
IgA	84.9±85.4	89.9±69.3	<0.001

Note: Antibody levels are presented by mean±standard deviation.

Table 2. Changes in study variables 6 months after the completion of chemotherapy

Variables	Changes in variables		
	Increase, *n* (%)	Constant, *n* (%)	Decrease, *n* (%)
Serum levels of immunoglobulins			
IgG	10 (47.6)	0 (0)	11 (52.4)
IgM	9 (42.85)	3 (14.3)	9 (42.85)
IgE	12 (57.1)	3 (14.3)	6 (28.6)
IgA	8 (38)	3 (14.3)	10 (47.6)
Antibody titer against diphtheria	11 (52.4)	4 (19)	6 (28.6)
Antibody titer against tetanus	3 (14.3)	5 (23.8)	13 (61.9)
Antibody titer against hepatitis B	1 (4.8)	5 (23.8)	15 (71.4)
WBC count	16 (76.2)	1 (4.8)	4 (19)
Neutrophil count	12 (57.1)	0 (0)	9 (42.8)
Lymphocyte count	10 (47.6)	0 (0)	11 (52.4)

Abbreviations: *n*: Number of patients; WBC: White blood cell.

DOI: http://doi.org/10.36922/jctr.24.00050

against diphtheria and tetanus, respectively. In contrast, results indicated that the mean IgG antibody level against hepatitis B increased by 7.09 units compared to the immediate time after cessation of therapy (Table 3).

Our raw data analyses revealed that 6 months after chemotherapy cessation, one patient had the highest changes in IgG antibody levels against diphtheria (from 0.05 to 71), two patients had the highest changes in IgG antibody levels against tetanus (from 0.35 to 22.9; from 0.27 to >5), and four patients had the highest changes in IgG antibody levels against hepatitis B (from 12 to 6; from 14 to 9.35; from 1 to >200; from 15 to 10).

Our analyses revealed that the changes in antibody levels against diphtheria, tetanus, or hepatitis B were not significant after 6 months compared to the immediate period following chemotherapy cessation (p=0.157, 0.179, and 0.249, respectively; Table 3). No significant relationship was found between the antibody level against diphtheria, tetanus, or hepatitis B and the patient's gender (Table 3). In contrast, a significant relationship was found between the antibody level against diphtheria and the age group of the patients (p = 0.003; Table 3).

3.3. Levels of immune system-related factors

Six months after the completion of chemotherapy, the average levels of WBCs and neutrophils increased by 1121 n/mm^3 and 1.77%, respectively. The average level of lymphocytes decreased by 0.01% after 6 months following chemotherapy cessation. The relationship between the levels of WBCs, neutrophils, and lymphocytes within the age group was not significant (p > 0.05). Changes in WBC number were significant (p = 0.001), but neutrophil (p = 0.516) and lymphocyte (p = 0.262) levels did not change significantly after 6 months compared to the immediate period following chemotherapy cessation (Table 4). Six months following chemotherapy cessation, all patients enrolled in the analysis responded well to the treatment.

Table 3. Changes in antibody levels against diphtheria, tetanus, and hepatitis B

Parameter	Antibody levels		
	Immediately after chemotherapy	6 months after chemotherapy	p-value
Anti-diphtheria (unit)	0.25±0.46	3.68±15.43	0.157
Male	0.22±0.28	6.67±19.62	0.123
Female	0.30±0.68	0.44±0.83	0.358
p	0.383	0.138	
Age (years)			
≤8 (*n*=10)	0.24±0.26	3.65±15.76	0.244
>8 (*n*=11)	0.27±0.35	0.98±0.43	0.003*
Anti-tetanus (unit)	1.15±1.18	2.18±4.94	0.179
Male	1.04±1.08	1.26±1.71	0.349
Female	1.34±1.38	3.37±7.42	0.229
p	0.306	0.234	
Age (years)			
≤8 (*n*=10)	0.98±1.32	1.6±1.43	0.163
>8 (*n*=11)	1.29±1.15	2.98±8.4	0.258
Anti-hepatitis B (unit)	10.76±16.75	17.85±44.61	0.249
Male	12.37±21.09	10.39±19.99	0.404
Female	8.13±5.21	30.10±69.12	0.192
p	0.252	0.239	
Age (years)			
≤8 (*n*=10)	10.87±18.88	13.46±43.61	0.432
>8 (*n*=11)	9.97±7.23	16.64±23.54	0.189

Note: Antibody levels are presented as mean±standard deviation. *p<0.05 indicates statistical significance.

4. Discussion

The present study aimed to investigate the humoral immunity against diphtheria, tetanus, and hepatitis B in children with leukemia both immediately after chemotherapy and 6 months later. The mean of IgM, IgE, and IgA IgG, the total number of WBC significantly increased after 6 months; the mean level of antibodies against diphtheria, tetanus, and hepatitis B, as well as the lymphocyte and neutrophil levels, did not change significantly after 6 months in comparison to the immediate period following chemotherapy cessation.

Immunosuppression is a significant side effect of many antineoplastic drugs. The rebuilding of the immune system can differ depending on the nature of the disease, drug type and dosage, and the patient's age [16]. In a cross-sectional study performed by Ek *et al*. [17], involving 31 children with ALL, it was revealed that the levels of IgG and IgM increased, whereas the level of IgA decreased at 6 months compared to 1 month following treatment cessation; contrary to our findings, these changes were not significant. An increase in IgG, IgM, IgE, and IgA levels after treatment cessation indicates immune system restoration, as demonstrated in various studies [8].

The findings of our study revealed that the levels of antibodies against hepatitis B and tetanus, IgG, IgM, IgE, IgA, and WBCs were not significantly different in the two age groups of patients (≤8 or >8). In line with our findings, Williams *et al*. studied 116 ALL patients with a median age of 6 years (range: 2–17 years) at intervals of 6 months after chemotherapy up to 18 months; no significant relationship was found between age and immune system reconstruction [18]. Our study was limited only to leukemia, and no categorization was performed based on the type of leukemia.

Our study investigated the relationship between gender, antibodies against diphtheria, tetanus, and hepatitis B, and IgG, IgM, IgE, and IgA levels 6 months after treatment cessation. In

Table 4. Changes in white blood cell (WBC), neutrophils, and lymphocyte levels

Parameter	Leukocyte count		p-value
	Immediately after chemotherapy	6 months after chemotherapy	
WBC (*n*/mm^3)	5439±1619	6560±2089	0.001
Neutrophil (%)	49.19±14.93	50.96±8.84	0.516
Lymphocyte (%)	42.07±14.08	42.08±10.50	0.262

Note: WBC, neutrophil, and lymphocyte levels are presented as mean±standard deviation.

DOI: http://doi.org/10.36922/jctr.24.00050

addition, Williams *et al*. revealed that there is no relationship between gender and the recovery rate of the immune system after chemotherapy cessation [18]. They also reported that the WBC level did not change significantly with increased time after treatment cessation.

The present study displayed increased levels of WBC, lymphocytes, and neutrophils 6 months after treatment cessation. Several studies confirmed this finding [8,18]. Perkins *et al*. investigated the immune system status immediately and 6 months after treatment cessation in 20 patients with ALL and acute myeloid leukemia; it was reported that the number of WBCs decreased at both times, but this decrease is compensated to some extent after 6 months following treatment cessation [8]. In a study by Kosmidis *et al*., it was also reported that children experienced significant neutropenia during the first few months of treatment, but this is less common during maintenance chemotherapy [19]. However, lymphopenia with low levels of B and T cells is common and has been reported to persist for up to 6 months after treatment [14,19].

In this study, the average antibody level against diphtheria and tetanus increased 6 months after treatment, whereas the average antibody level against hepatitis B decreased. Although these changes were not significant, the immune system restoration resulted in increases in WBCs and IgG, IgM, IgE, and IgA in this study and previous studies [18,20], and an increase in antibody levels against diphtheria and tetanus was also expected. The decrease in antibodies against hepatitis requires further investigation; it may also return to the average level in a more extended period, as studies have reported that some changes in immune system reconstruction occur in the long term [19]. Collectively, we revealed improvement of the humoral immune system to some extent after 6 months of chemotherapy, but similar to Perkins *et al*., some degree of defects in the immune system were also reported [8].

One of the limitations of this research is that the sample patient population was small, and a study with a more significant population is warranted. In addition, this study did not separate the different types of leukemia, and it is recommended that future studies distinguish between these types for a more detailed investigation.

5. Conclusion

The findings of this study indicate that the status of the humoral immune system exhibits slight improvement 6 months after the end of chemotherapy compared to the initial assessment. In addition, there is no difference between age and the condition of the humoral immune system in the patients 6 months after chemotherapy treatment. We indicated that survivors of childhood cancer have ongoing humoral immunological defects and may remain at risk for infectious complications after completion of therapy.

Acknowledgments

The authors would like to thank the Pediatric Congenital Hematologic Disorders Research Center, Research Institute for Children's Health, Shahid Beheshti University of Medical Sciences, Tehran, Iran for their kind cooperation.

Funding

This research did not receive any specific grant from funding agencies in public, commercial, or not-for-profit sectors.

Conflicts of Interest

The authors declare that they have no competing interests.

Ethics Approval and Consent to Participate

This study was approved by the Ethics Committee of Pediatric Congenital Hematologic Disorders Research Center, Shahid Beheshti University of Medical Sciences, Tehran, Iran (IRSBMU.MSP.REC.1399.473). A questionnaire was designed for each child, and written informed consent was acquired from their parents during the course of sample collection.

Consent for Publication

We explained the aims of the present study to children and their parents. A questionnaire was planned for each of the included children and written informed consent was obtained from all children and their parents during the study.

Availability of Data

All data generated or analyzed during this study are included in this published article.

References

[1] Namayandeh SM, Khazaei Z, Najafi ML, Goodarzi E, Moslem A. Global Leukemia in Children 0-14 Statistics 2018, Incidence and Mortality and Human Development Index (HDI): GLOBOCAN Sources and Methods. Asian Pac J Cancer Prev 2020;21:1487.
doi: 10.31557/APJCP.2020.21.5.1487

[2] Hunger SP, Mullighan CG. Acute Lymphoblastic Leukemia in Children. New Engl J Med 2015;373(16):1541-52.
doi: 10.1056/NEJMra1400972

[3] Steinherz PG, Brown AE, Gross PA, Braun D, Ghavimi F, Wollner N, *et al*. Influenza Immunization of Children with Neoplastic Diseases. Cancer 1980;45:750-6.
doi: 10.1002/1097-0142(19800215)45:4<750::aid-cncr2820450423>3.0.co;2-z

[4] Tavakol M, Delavari S, Salami F, Ansari S, Rasouli SE, Chavoshzadeh Z, *et al*. Diversity of Malignancies in Patients with Different Types of Inborn Errors of Immunity. Allergy Asthma Clin Immunol 2022;18:106.
doi: 10.1186/s13223-022-00747-2

[5] Griggio V, Perutelli F, Salvetti C, Boccellato E, Boccadoro M, Vitale C, *et al*. Immune Dysfunctions and Immune-based Therapeutic Interventions in Chronic Lymphocytic Leukemia. Front Immunol

2020;11:594556.
doi: 10.3389/fimmu.2020.594556

[6] Nazari S. Mechanical Events in Physiopathology of Idiopathic Pulmonary Emphysema: A Theoretical Analysis. Internet J Thorac Cardiovasc Surg 2002;5: 1-17.

[7] Crawford J, Dale DC, Lyman GH. Chemotherapy-induced Neutropenia: Risks, Consequences, and New Directions for Its Management. Cancer 2004;100:228-37.
doi: 10.1002/cncr.11882

[8] Perkins JL, Harris A, Pozos TC. Immune Dysfunction After Completion of Childhood Leukemia Therapy. J Pediatr Hematol Oncol 2017;39:1-5.
doi: 10.1097/MPH.0000000000000697

[9] Layward L, Levinsky RJ, Butler M. Long-term Abnormalities in T and B Lymphocyte Function in Children Following Treatment for Acute Lymphoblastic Leukaemia. Br J Haematol 1981;49:251-8.
doi: 10.1111/j.1365-2141.1981.tb07221.x

[10] Caver TE, Slobod KS, Flynn PM, Behm FG, Hudson MM, Turner EV, *et al*. Profound Abnormality of the B/T Lymphocyte Ratio During Chemotherapy for Pediatric Acute Lymphoblastic Leukemia. Leukemia 1998;12(4):619-22.
doi: 10.1038/sj.leu.2400970

[11] Ito C, Evans WE, McNinch L, Coustan-Smith E, Mahmoud H, Pui CH, *et al*. Comparative Cytotoxicity of Dexamethasone and Prednisolone in Childhood Acute Lymphoblastic Leukemia. J Clin Oncol 1996;14(8):2370-6.
doi: 10.1200/JCO.1996.14.8.2370

[12] Kung FH, Orgel HA, Wallace WW, Hamburger RN. Antibody Production Following Immunization with Diphtheria and Tetanus Toxoids in Children Receiving Chemotherapy During Remission of Malignant Disease. Pediatrics 1984;74(1):86-9.

[13] Rautonen J, Siimes MA, Lundström U, Pettay O, Lanning M, Salmi TT, *et al*. Vaccination of Children During Treatment for Leukemia. Acta Pædiatr Scand 1986;75(4):579-85.
doi: 10.1111/j.1651-2227.1986.tb10254.x

[14] Alanko S, Salmi TT, Pelliniemi TT. Recovery of Blood T-Cell Subsets after Chemotherapy for Childhood Acute Lymphoblastic Leukemia. Pediatr Hematol Oncol 1994;11:281-92.
doi: 10.3109/08880019409141671

[15] Leadman D, Xu Y, Qu S, Zhu Q, editors. Integrative Rare Disease Profile Creation Via NormMap to Advance Rare Disease Research. In: 2022 IEEE International Conference on Bioinformatics and Biomedicine (BIBM). Las Vegas: IEEE; 2022.
doi: 10.1109/BIBM55620.2022.9995172

[16] Lehrnbecher T, Foster C, Vázquez N, Mackall CL, Chanock SJ. Therapy-Induced Alterations in Host Defense in Children Receiving Therapy for Cancer. Journal of Pediatric Hematology Oncology 1997;19(5):399-417.
doi: 10.1097/00043426-199709000-00001

[17] Ek T, Mellander L, Andersson B, Abrahamsson J. Immune Reconstitution after Childhood Acute Lymphoblastic Leukemia is Most Severely Affected in the High Risk Group. Pediatr Blood Cancer 2005;44(5):461-8.
doi: 10.1002/pbc.20255

[18] Williams AP, Bate J, Brooks R, Chisholm J, Clarke SC, Dixon E, *et al*. Immune Reconstitution in Children Following Chemotherapy for Acute Leukemia. EJHaem 2020;1(1):142-51.
doi: 10.1002/jha2.27

[19] Kosmidis S, Baka M, Bouhoutsou D, Doganis D, Kallergi C, Douladiris N, et al. Longitudinal Assessment of Immunological Status and Rate of Immune Recovery Following Treatment in Children with ALL. Pediatr Blood Cancer 2008;50(3):528-32.
doi: 10.1002/pbc.21327

[20] Ibáñez IM, Casas AA, Martinez OC, Aguado JE, Mateos MM. Humoral Immunity in Pediatric Patients with Acute Lymphoblastic Leukaemia. Allergol Immunopathol (Madr) 2003;31(6):303-10.
doi: 10.1016/s0301-0546(03)79203-9

DOI: http://doi.org/10.36922/jctr.24.00050

Journal of Clinical and Translational Research 2024; 10(5): 296-306

Journal of Clinical and Translational Research

Journal homepage: http://www.jctres.com/en/home

ORIGINAL ARTICLE

Immediate inelastic compression garment for swelling management after total knee arthroplasty: a feasibility study

Andrea Marshall[1], Roseann Johnson[2], Jason Jennings[2,3], Douglas Dennis[2,3,4,5], Jennifer Stevens-Lapsley[1,6], Michael Bade[1,6]*

[1]Department of Physical Medicine and Rehabilitation, School of Medicine, University of Colorado Anschutz Medical Campus, Aurora, Colorado, United States of America, [2]Colorado Joint Replacement, AdventHealth Porter, Denver, Colorado, United States of America, [3]Department of Mechanical and Materials Engineering, Ritchie School of Engineering and Computer Science, University of Denver, Denver, Colorado, United States of America, [4]Department of Orthopedics, School of Medicine, University of Colorado Anschutz Medical Campus, Aurora, United States of America, [5]Department of Biomedical Engineering, School of Engineering, University of Tennessee, Knoxville, Tennessee, United States of America, [6]Eastern Colorado Veteran Affairs Geriatric Research Education and Clinical Center, Aurora, Colorado, United States of America

ARTICLE INFO

Article history:
Received: June 6, 2024
Accepted: October 14, 2024
Published Online: November 6, 2024

Keywords:
Feasibility
Inelastic compression garment
Swelling
Total knee arthroplasty

**Corresponding author:*
Michael Bade
Department of Physical Medicine and Rehabilitation, School of Medicine, University of Colorado Anschutz Medical Campus, Aurora, Colorado, United States of America; Eastern Colorado Veteran Affairs Geriatric Research Education and Clinical Center, Aurora, Colorado, United States of America.
Email: michael.bade@cuanschutz.edu

ABSTRACT

Background: Swelling after total knee arthroplasty (TKA) peaks between days 3 and 8. Peak swelling is associated with decreased strength and function.
Aim: The aim of the study was to investigate the feasibility and initial efficacy of an inelastic compression garment on attenuating peak swelling when applied immediately after TKA (immediate compression garment [ICG]).
Methods: The ICG group (n = 14) had the inelastic compression garment applied in the operating room after surgery and wore it for 12 h/day while awake for 21 days. The historical comparison group (n = 16) wore the same garment, which was donned 3 – 4 days after surgery (delayed compression garment). ICG feasibility outcomes at day 21 were safety, satisfaction, and adherence. Initial efficacy outcomes at days 4, 7, 14, 21, and 42 were swelling, quadriceps strength and activation, and pain. Hedges' g effect sizes (ES) were calculated.
Results: One participant was removed from the study on day 7 due to deep vein thrombosis. Median satisfaction with ICG was 5/5, that is, very satisfied. On average, participants wore the garment for 11 h/day. ES favoring ICG were found for: (i) swelling at days 4 (ES = 0.26) and 14 (ES = 0.17) only; (ii) quadriceps activation at days 21 (ES = 0.77) and 42 (ES = 0.72); and (iii) pain at days 14 (ES = 0.43), 21 (ES = 0.57), and 42 (ES = 0.42).
Conclusion: The use of an ICG after TKA appears feasible, though its effect on peak swelling (days 4 and 7) is unclear. All ES should be interpreted with caution due to the small sample size.
Relevance for Patients: Donning the garment immediately in the operating room demonstrates promising trends toward improved quadriceps activation and pain.

1. Introduction

Patients experience significant swelling after total knee arthroplasty (TKA). Swelling increases 10%/day, on average, for the first 3 days after surgery and then peaks at 25 – 47% between post-operative days 3 – 8 [1,2]. Even 90 days after surgery, swelling remains 11% higher than pre-operative values [1]. Swelling after TKA is associated with lower patient satisfaction [3] and is one of the most frequent reasons for emergency department visits shortly after surgery [4,5]. In addition, swelling after TKA is associated with decreased quadriceps strength and functional performance, such as reduced gait speed [1,6,7]. It is thought that the relationship between swelling and functional performance is mediated by quadriceps strength [1,6].

DOI: http://doi.org/10.36922/jctr.24.00026

Quadriceps strength loss after TKA is also significant, with patients experiencing up to a 60% loss in the 1st month after surgery [8-10]. Pre-operative quadriceps strength levels are typically not regained for 6 months [9,10], and, perhaps most concerning, strength may never reach the levels of aged-matched peers without any history of knee pathology [11-15]. Early quadriceps strength loss after TKA is thought to be predominately due to the inability to fully activate the quadriceps muscle voluntarily, also known as arthrogenic muscle inhibition (AMI) [8,16,17]. AMI accounts for 65% of the variance in acute quadriceps strength loss after TKA and is thought to impede the effectiveness of voluntary strengthening during rehabilitation [8,17]. This could explain why even high-intensity, progressive resistance protocols after surgery have failed to mitigate quadriceps strength loss [18,19]. The mechanisms underlying AMI are not fully understood, but joint pain [8,16,20] and swelling [21-24] have been implicated. Pain and swelling may reduce the excitability of the quadriceps by affecting the afferent discharge of the joint sensory receptors [21].

Researchers and clinicians alike have attempted to mitigate swelling after TKA with little success. The use of cryotherapy has mixed findings, which may be due to variations in study methodology [25-29]. Similarly, the effect of kinesiotape [29-33], manual lymphatic drainage [33-36], or a combination of both [37] has been inconclusive. The use of elastic compression bandages, including modified Robert Jones bandages, has also proven ineffective after TKA [38-42]. Conversely, the use of an inelastic compression garment has recently displayed promise [36,43]. Carmichael *et al.* [36] found up to 54% less swelling in the first 21 days after TKA when compared to a control group that wore standard elastic, non-adjustable thromboembolic deterrent (T.E.D.) hose only. In this study, however, the inelastic compression garment was not applied until 3 – 4 days after surgery, potentially limiting its ability to maximally mitigate peak swelling. Peak swelling, not cumulative swelling, has been associated with decreased quadriceps strength and functional performance [7]. Applying the same inelastic garment immediately after surgery could further attenuate peak swelling and consequently improve patient recovery.

Therefore, the purpose of this study was to evaluate the feasibility of an inelastic compression garment donned in the operating room immediately after TKA (i.e., immediate compression garment [ICG]). In addition, we sought to investigate the initial efficacy of ICG on peak swelling, quadriceps activation, strength, and pain as compared to the Carmichael *et al*. [36] study that used the same garment applied 3 – 4 days after surgery (i.e., delayed compression garment [DCG]). We hypothesized that ICG would be feasible, and, when compared to DCG, it would have lower peak swelling, superior quadriceps activation and strength, and reduced pain.

2. Methods

2.1. Study design and participants

This was a prospective feasibility study with a comparison to a historical cohort (DCG). The ICG and DCG cohorts had the same inclusion and exclusion criteria. Participants between the ages of 50 and 85 years, who were undergoing a primary unilateral TKA secondary to end-stage osteoarthritis, were consecutively recruited. They were excluded if they had any of the following: (i) discharge to a location other than home after surgery; (ii) history of heart failure, lymphatic insufficiency, hepatic disease, pre-existing pitting edema, varicose vein ligation, or any other condition associated with chronic swelling of either lower extremity; (iii) uncontrolled diabetes; (iv) body mass index (BMI) >40 kg/m^2; (v) no caregiver or the inability to touch toes, which may affect donning/doffing the compression garment; or (vi) any ongoing neurologic, cardiac, or other unstable orthopedic conditions that limit the function or ability to participate in outcome measures testing. ICG participants were recruited from April 2021 to July 2022 by two orthopedic surgeons from one institution in the Denver metro area.

2.2. Interventions

2.2.1. Inelastic compression garment

Both ICG and DCG cohorts were measured with the inelastic compression garment 1 – 2 weeks before surgery as part of their baseline testing session. The garment (CircAid Juxtafit upper leg and knee garment combined with a lower leg garment; Medi USA, United States of America [USA]) has adjustable straps that enable quick and precise setting of various compression ranges using a standardized garment tensioning tool (Figure 1). Throughout the intervention period, the garment straps were applied using gradient compression to promote venous and lymphatic return using the following pressures: 40 mmHg (lower leg), 30 mmHg (knee), and 20 mmHg (thigh). Participants were trained in garment donning/doffing preoperatively. They were asked to wear the garment for 12 waking hours each day, removing it at night to sleep. They could remove the garment for brief periods throughout the day for hygiene and rehabilitation, as needed. Finally, they were asked to wear the garment until post-operative day 21.

Figure 1. Inelastic compression garment

DOI: http://doi.org/10.36922/jctr.24.00026

2.2.2. Timing of initial garment donning

The DCG group did not don the garment until 3 – 4 days after surgery. The ICG group donned the garment immediately after surgery in the operating room, assisted by an orthopedic physician assistant, a surgical assistant, or a professional research assistant. Approximately 2 h later, a research assistant assessed the participant to ensure proper garment application and to answer any participant questions. The participant was instructed to leave the garment on until the following evening (i.e., bedtime of post-operative day 1) and then to wear it for 12 waking hours per day.

2.2.3. Rehabilitation

Participants in both groups were instructed in a home exercise program designed to promote frequent pumping of calf and thigh musculature to aid in (i) venous and lymphatic return and (ii) knee range of motion (ROM). Participants were asked to perform ankle pumps for 1 min, a minimum of 5 times daily. In addition, they were asked to perform 10 repetitions of a knee flexion exercise, a minimum of 5 times daily. The knee flexion exercise was chosen by the participant from one of the following, with the option to choose a different exercise at any time: heel slides, floor scrubs, or stair stretch (Table S1). These exercises were performed with the garment in place, but the participant could loosen select straps around the knee joint to allow more ROM, if necessary. Finally, all participants also received standard-of-care outpatient rehabilitation separate from this study.

2.3. Outcome measures

Feasibility of ICG was assessed by safety, average daily wear time of the garment, adherence to the prescribed garment wear time of 12 h/day, and participant satisfaction with the garment. To investigate initial efficacy, ICG and DCG were both tested at baseline (1 – 2 weeks preoperatively) and postoperatively on days 4, 7, 14, 21, and 42 (Figure 2).

2.3.1. Safety

Safety was assessed by recording serious adverse events related to the ICG protocol (e.g., deep vein thrombosis, infection, skin necrosis, delayed wound healing, or manipulation under anesthesia to address knee ROM limitations) throughout the study, that is, 42 days.

2.3.2. Daily wear time and adherence

Average daily wear time and adherence were determined by self-report logs that were collected weekly to increase the accuracy of reporting. Average daily wear time was calculated by dividing the sum of the hours the garment was worn each day by the total number of possible days during the intervention period, that is, 21 days. Adherence to the prescribed daily wear time of 12 h was calculated from 0 to 100% by dividing the total number of days the garment was worn for at least 12 h by the total number of possible days during the intervention period. Both were then reported as the mean, standard deviation (SD), and the 95% confidence interval (CI).

2.3.3. Satisfaction

Satisfaction with the garment was measured on completion of the intervention period using a five-point Likert survey, including completely dissatisfied (1), somewhat dissatisfied (2), neither dissatisfied nor satisfied (3), somewhat satisfied (4), and completely satisfied (5). It was then reported as median and range.

2.3.4. Swelling

The swelling was measured at days 4, 7, 14, 21, and 42 days after surgery by a single frequency bioelectrical impedance assessment (SF-BIA) using an RJL Systems Quantum® (USA) device, as further described in the study by Carmichael *et al.* [36] SF-BIA is a reliable and responsive measure of total limb swelling after TKA [44]. The device delivers a 2.5 μA alternating current at a frequency of 50 kHz. The level of impedance met by the current will fluctuate with the presence of swelling in the lower extremity. Lower levels of impedance represent greater levels of swelling. Using a ratio of the impedance of the involved limb to the uninvolved limb accounts for body composition, fluid shifts, and hydration status, allows any changes in impedance between time points to be attributed to changes in limb swelling. Therefore, swelling values at each time point are presented as the percent difference between limbs and calculated as:

$$\text{Swelling} = \left(1 - \frac{\text{involved bioelectrical impedance assessment}}{\text{uninvolved bioelectrical impedance assessment}}\right) \times 100 \quad \text{(I)}$$

Given that swelling is known to peak at 3 – 8 days after surgery, swelling measurements at days 4 and 7 were used to specifically consider ICG's effect on peak swelling.

2.3.5. Quadriceps strength and activation

Quadriceps strength and activation were evaluated on days 21 and 42. Quadriceps strength was assessed by

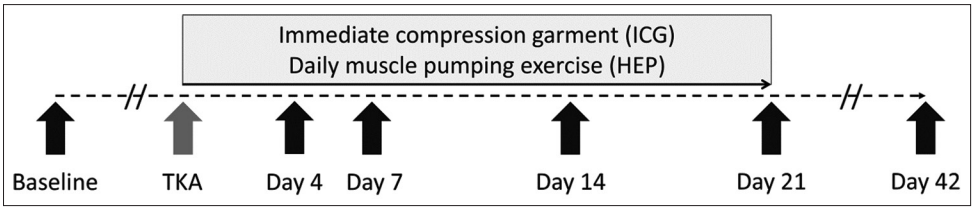

Figure 2. Immediate compression garment intervention and testing timeline
Abbreviations: HEP: Home exercise program; TKA: Total knee arthroplasty

DOI: http://doi.org/10.36922/jctr.24.00026

maximum voluntary isometric contraction (MVIC) using an electromechanical dynamometer (HUMAC NORM; CSMi, USA) at 60° of knee flexion. To ensure maximal strength was recorded, testing was repeated, with 1 min rest between trials, until the readings from two trials were within 5% of each other. The trial with the highest torque was utilized for data analysis, after normalization [45]. Data were collected with a BIOPAC Data Acquisition System (Biodex Medical Systems Inc, USA) at 2000 samples/s and analyzed with Acknowledge software, version 5.0 (Biodex Medical Systems Inc, USA). Voluntary activation of the quadriceps was assessed using the doublet interpolation technique, where a supramaximal stimulus is applied (Grass S48 stimulator and SIU8T stimulus isolation unit, Grass Instruments Co, USA) during quadriceps MVIC testing and again immediately afterward while the muscle is at rest [45]. Stimulus parameters were two pulses, a pulse duration of 600 μs, and a frequency of 100 pulses/s. Full voluntary activation of the quadriceps is 100%, whereas anything less than this represents an activation deficit. As this laboratory assessment of quadriceps activation is not feasible early after surgery, the quadriceps activation battery (QAB) was conducted on day 4 [46]. The QAB consists of the following three clinical tests, each scored from 0 to 2: Isometric quadriceps contraction, straight leg raise, and quadriceps extension lag. Isometric quadriceps contraction was tested with the participant in supine and the surgical knee in full available extension ROM. It was scored as 0 (unable to initiate any contraction), 1 (poor contraction with no superior patellar movement), or 2 (strong contraction with visible superior movement of the patella). Straight leg raise was tested with the participant in supine, the surgical knee in full available extension ROM, and the contralateral knee bent to 90°. It was scored as 0 (unable to lift the heel off the table), 1 (able to lift the heel two feet off the table, but unable to maintain knee in full available extension ROM), or 2 (able to lift the heel off the table and maintain the knee in full available extension ROM). The quadriceps extension lag was tested with the participant sitting upright at the edge of a table. The surgical knee was passively extended by the tester to <5° the available extension ROM. The participant was then instructed to hold this position while the tester withdrew support. It was scored as 0 (unable to keep the surgical knee from bending without tester support), 1 (able to maintain knee extension but for <1 s and able to slow the leg's descent into further flexion without tester support), or 2 (able to maintain knee in extension for >1 s). The total score is the sum of the three tests ranging from 0 to 6. Scoring ≤ 3 on the QAB 4 days after surgery is significantly related to: (i) poorer quadriceps activation 1 month after surgery; and (ii) poorer strength and functional performance 1 – 2 months after surgery [46].

2.3.6. Pain

The Western Ontario and McMaster Universities Osteoarthritis Index (WOMAC) is one of the most commonly utilized patient-reported outcome measures after TKA [47]. It can assess three components of TKA recovery: pain, stiffness, and function. In this study, the self-reported pain of the surgical knee was assessed using the WOMAC pain sub-score on days 14, 21, and 42. The WOMAC pain sub-score includes five questions, each scored as 0 (none), 1 (mild), 2 (moderate), 3 (severe), or 4 (extreme). The total pain sub-score ranges from 0 to 20, with a lower score indicating less pain.

2.4. Power and sample size

A large effect size (ES) (>1.0) was found for DCG on swelling compared to controls without an inelastic compression garment [36]. The anticipated ES of ICG on swelling compared to DCG was unknown, but we believed that it would be at least 0.3. Given this anticipated ES (>0.3), 80% power, and type I error rate of 0.05, Whitehead *et al.* [48] recommended a minimum of 10 participants per cohort in a pilot study to more precisely estimate the variability of a treatment effect. Therefore, we set our minimum sample size for ICG to 10 participants.

2.5. Data analysis

The ICG and DCG groups were compared at baseline for age, BMI, swelling, quadriceps strength and activation, and WOMAC pain using the Wilcoxon rank sum test. The differences between all post-operative time points and baseline were calculated for the same outcomes and assessed for normality statistically using the Shapiro–Wilk test and visually using histograms. Initial efficacy for ICG was assessed with Hedges' g ES for total limb swelling, quadriceps strength, quadriceps activation, and WOMAC pain. ESs were classified as small if $g \leq 0.2$, as medium if $0.21 \leq g \leq 0.79$, or as large if $g \geq 0.8$ [49]. The proportion of participants in each group scoring ≤ 3 and ≥ 4 on the QAB were compared using Fisher's exact test.

3. Results

Participant baseline characteristics can be found in Table 1. A total of 14 participants were enrolled in the ICG protocol (62.3 ± 8.3 years; nine females). One participant self-selected to wear the garment only while sleeping during the third post-operative week due to claustrophobia. An additional participant was instructed by a non-study provider during the third post-operative week to only wear the garment while sleeping due to poor ROM progress. Therefore, the data from days 21 and 42 were not included in the analysis for these two participants. Finally, one participant was removed from the study during the second post-operative week due to deep vein thrombosis (DVT), resulting in no data available for days 14, 21, and 42. There were 16 participants in the DCG group (64.7 ± 7.1; 12 females).

No significant differences were found between groups at baseline for age, BMI, swelling, or quadriceps strength (Table 1). ICG had statistically significantly lower quadriceps activation than DCG at baseline with median values of 57.9% and 84.6%, respectively ($p = 0.01$). The ICG group also had statistically significantly higher WOMAC pain than DCG at baseline with median values of 9.0 and 7.5, respectively ($p = 0.03$).

3.1. Feasibility of ICG

In addition to the DVT reported above, it should be noted that the two participants who wore the garment during sleeping hours

DOI: http://doi.org/10.36922/jctr.24.00026

Table 1. Participant baseline characteristics

Characteristic	ICG		DCG		p-value[a]
	Median (IQR)	Mean (SD)	Median (IQR)	Mean (SD)	
Age, years	64.5 (15.0)	62.3 (8.3)	65.0 (10.0)	64.7 (7.1)	0.40
BMI (kg/m^2)	29.5 (9.4)	28.6 (5.2)	28.9 (7.3)	29.8 (4.9)	0.66
Swelling (%)	0.6 (8.4)	0.3 (8.0)	−1.7 (5.0)	-2.5 (4.9)	0.35
Quadriceps strength (Nm/kg)	0.9 (0.4)	1.1 (0.5)	1.0 (0.6)	1.2 (0.5)	0.72
Quadriceps activation (%)	57.9 (31.9)	61.3 (18.4)	84.6 (14.5)	79.6 (16.4)	0.01[b]
WOMAC pain	9.0 (5.0)	9.6 (3.7)	7.5 (2.5)	7.4 (2.6)	0.04[b]

Note: [a]p-value, Wilcoxon rank sum; [b]statistically significant at $p<0.05$.
Abbreviations: ICG: Immediate compression garment; DCG: Delayed compression garment; IQR: Interquartile range; SD: Standard deviation; BMI: Body mass index; WOMAC: Western Ontario and McMaster Universities osteoarthritis index.

underwent manipulation under anesthesia (MUA) to address knee ROM limitations. On average, participants indicated they wore the garment for 11 ± 2 h/day (95% CI: 10 – 12). They were only adherent to wearing the garment for the prescribed 12-h wear time, on average, 64 ± 37% of the time (95% CI: 43–85%). Median satisfaction with the garment was 5/5 (i.e., very satisfied) on the five-point Likert scale (range: 4 – 5).

3.2. Initial efficacy

The mean and SD for all outcomes at all-time points are listed in Table S2. A summary of ES at all-time points can be found in Table 2**.** For swelling, a medium and a small ES were found in favor of ICG at days 4 and 14, respectively. Conversely, ES for swelling at days 7, 21, and 42 were found in favor of DCG. ES for all other outcomes and time points favored ICG. Small ES were found for quadriceps strength and medium ES for quadriceps activation at days 21 and 42. Medium ES was found for WOMAC pain on days 14, 21, and 42. A significantly greater proportion of ICG scored ≥ 4 on the QAB compared to DCG (100% vs. 63%, respectively; p = 0.02).

4. Discussion

This study evaluated the feasibility and initial efficacy of applying an inelastic compression garment in the operating room immediately after TKA. The effect of immediate application (ICG) on peak swelling remains unclear, but this study supports the use of an inelastic compression garment to mitigate total limb swelling in the first 3 weeks after surgery. The immediate application demonstrated promising trends toward improved early quadriceps activation and pain. Future research is warranted to conclusively evaluate efficacy as our small sample size was not designed to do so.

The ICG appears feasible after TKA. All ICG participants indicated they were completely or somewhat satisfied with the compression garment, that is, 4 – 5/5 on the Likert scale, which is consistent with the satisfaction reported in DCG [36]. Average adherence to the prescribed wear time of 12 hours per day over the intervention period was only 64% for ICG. Instead, participants recorded wearing the garment for 10.9 hours on average per day, with some indicating that they were simply not awake for 12 hours. The 12-hour wear time was chosen arbitrarily based on an estimate of the amount of time that participants would be awake each day with the surgical limb in a gravity-dependent position and potentially accumulating swelling. Our findings suggest that a 12-hour wear time may not be feasible, but also that 12 hours may not be necessary, since swelling mitigation in ICG was similar to that found in DCG. Future studies should consider a shortened daily wear time to better accommodate participants' natural daily waking hours and to improve adherence. While it is unfortunate that one participant experienced DVT while enrolled in this study, it is not appropriate to assume a causal relationship between the two. DVT after TKA occurs at a rate of 0.5% – 0.9% [50,51], suggesting that this event may be due to chance alone. Similarly, rates of MUA after TKA range from 0.6% to 4.2% [52,53]. Both of the participants in this study who wore the garment while sleeping went on to have MUA, but this does not imply causality. In addition, no DVTs or MUAs occurred in the DCG group [36]. Nevertheless, future studies should report adverse event rates with particular attention to DVT and MUA.

The ES for swelling at days 4 and 14 favored ICG, while the remaining time points favored DCG. When looking at the raw data, the ICG and DCG groups appear similar in their ability to mitigate swelling compared to a historical control cohort that only wore elastic T.E.D. hose (Figure 3) [2,36]. While it is unclear if ICG was able to mitigate peak swelling to a greater extent than DCG, our findings demonstrate the effect that an inelastic garment can have on swelling after TKA. In addition, early application would still be preferred in future studies, given the trend toward improved activation and the ease of donning the garment while the patient is still within their surgical episode of care. Applying the garment 3 – 4 days after surgery necessitates a clinic visit, which may not align with typical care pathways.

There appears to be a trend towards better WOMAC pain scores for ICG than DCG, with medium ES ranging from 0.42 to 0.57 for days 14 – 42 (Table 2). This should be interpreted with caution, as ICG had significantly higher pain scores at baseline than DCG (mean: 9.6 vs. 7.4, respectively) (Table 1), suggesting that ICG had more room for improvement. Future research should also examine narcotic pain medication usage to better assess the relationship between ICG and pain amelioration.

The ICG does not appear to have had a significant effect on quadriceps strength with small between-group mean differences

DOI: http://doi.org/10.36922/jctr.24.00026

Table 2. Effect size estimates at post-operative days 4, 7, 14, 21, and 42

Outcome	Time point	ICG			DCG			Hedges' g effect size[c] (95% CI)	Between-group mean difference (95% CI)[d]
		n	Mean difference[a]	SD	n	Mean difference[b]	SD		
Swelling (%)	Day 4	14	27.20	10.65	16	30.27	12.17	0.26 (−0.44 to 0.96)	−3.08 (−11.69 to 5.53)
	Day 7	11	22.20	10.71	16	21.71	8.98	−0.05 (−0.79 to 0.70)	0.49 (−7.34 to 8.32)
	Day 14	13	16.50	12.65	16	18.53	10.72	0.17 (−0.54 to 0.88)	−2.03 (−10.93 to 6.87)
	Day 21	11	17.03	10.84	16	14.55	7.60	−0.27 (−1.01 to 0.48)	2.48 (−4.81 to 9.77)
	Day 42	11	18.84	11.46	15	18.26	9.27	−0.06 (−0.81 to 0.70)	0.58 (−7.81 to 8.97)
Quadriceps strength (Nm/kg)	Day 21	11	−0.41	0.34	16	−0.46	0.39	0.13 (−0.61 to 0.88)	0.05 (−0.25 to 0.35)
	Day 42	11	−0.21	0.30	15	−0.24	0.40	0.07 (−0.68 to 0.83)	0.03 (−0.27 to 0.32)
Quadriceps activation (%)	Day 21	11	12.23	12.16	15	−3.24	23.20	0.77 (−0.01 to 1.56)	15.47 (0.91 to 30.03)
	Day 42	11	16.86	13.08	13	7.20	12.99	0.72 (−0.09 to 1.52)	9.66 (−1.42 to 20.73)
WOMAC pain	Day 14	10	−1.60	4.55	16	0.13	3.40	0.43 (−0.34 to 1.21)	−1.73 (−4.95 to 1.50)
	Day 21	11	−2.73	4.17	16	−0.63	3.16	0.57 (−0.19 to 1.33)	−2.10 (−5.01 to 0.80)
	Day 42	11	−3.64	4.18	16	−2.06	3.21	0.42 (−0.33 to 1.17)	−1.57 (−4.50 to 1.35)

Note: [a]mean difference=ICG post-operative day x – ICG baseline; [b]mean difference=DCG post-operative day x – DCG baseline; [c]for clarity, effect sizes have been standardized so that positive values favor ICG and negative values favor DCG; [d]between-group mean difference = (ICG mean difference) – (DCG mean difference). Abbreviations: ICG: Immediate compression garment; DCG: Delayed compression garment; SD: Standard deviation; CI: Confidence interval; WOMAC: Western Ontario and McMaster universities osteoarthritis index.

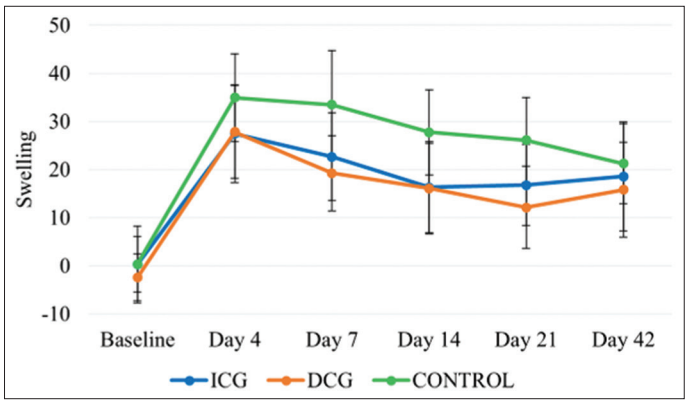

Figure 3. Changes in swelling over time for immediate compression garment, delayed compression garment, and elastic thromboembolism-deterrent garment

and ES noted at days 21 and 42 (Table 2). However, there appears to be a trend toward greater quadriceps activation for ICG at both of these time points (ES = 0.77 and 0.72, respectively). Notably, ICG had significantly lower activation compared to DCG at baseline and, thus, more room for improvement. However, this trend is possibly corroborated by the QAB data collected 4 days after surgery, revealing that 100% of ICG scored ≥ 4 compared to only 63% for DCG. Interestingly, Bade *et al.* [46] found that only 46% of participants scored ≥ 4 on the QAB 4 days after surgery when they received no specific intervention to address swelling or activation (e.g., no compression garment). This suggests that the inelastic compression garment might positively affect quadriceps activation in the acute post-operative period theoretically by minimizing swelling and quadriceps AMI. Future research is warranted to conclusively determine the impact that improved early activation may have on quadriceps strength and function.

Finally, there is a need to determine the impact of an inelastic compression garment on other outcomes that have been associated with swelling after TKA, for example, patient satisfaction [3] and early emergency department visits [4,5]. Dissatisfaction after TKA is between 8% and 19%, with actual rates possibly higher than reported in the literature [54]. In addition, in the first 90 days after TKA, the incidence of emergency department visits is between 10.8% and 13.8%, with swelling of the surgical limb being one of the most common reasons for seeking medical care [4,5]. It remains to be determined whether minimizing swelling in the early post-operative period can impact (i) long-term residual swelling and satisfaction, and (ii) the incidence of emergency department visits and healthcare costs following TKA.

Nonetheless, the study had several limitations. The primary aim of this study was to assess the feasibility of ICG among a small sample of TKA recipients. Thus, the study was not adequately designed to definitively evaluate the efficacy of ICG compared to DCG. All ESs presented should be interpreted in light of this limitation. The 95% CI for all ES includes 0, indicating that the true ES could favor either group for all outcomes. In addition, since we used a historical control (DCG), there were statistically significant baseline differences between groups for quadriceps activation and WOMAC pain. Future research should focus on randomized controlled trials with appropriate power to definitively evaluate efficacy and minimize baseline differences between groups.

5. Conclusion

The ICG appears feasible after TKA. The effect of immediate application on peak swelling remains unclear, but this study supports the use of an inelastic compression garment to mitigate total limb swelling in the first 3 weeks after surgery. The immediate application demonstrated promising trends toward improved early quadriceps activation and pain. Based on these results, a future full-scale study will be conducted with sufficient power to conclusively evaluate the efficacy of ICG on peak swelling after TKA.

DOI: http://doi.org/10.36922/jctr.24.00026

Acknowledgments

This project was facilitated by Medi USA which donated the inelastic compression garments. They provided no other contribution and were not involved in manuscript preparation.

Funding

None.

Conflicts of Interest

The authors declare that they have no conflicts of interest.

Ethics Approval and Consent to Participate

This study was registered on ClinicalTrials.Gov (NCT04841356) and was approved by Colorado Joint Replacement's institutional review board, the CommonSpirit Health Research Institute Institutional Review Board (1722208-1). All study procedures were performed in accordance with the ethical standards of the responsible committee on human experimentation and with the Helsinki Declaration. Informed written consent was obtained, and participants' rights were protected.

Consent for Publication

Consent for publication was obtained for every individual's data included in this experimental study.

Availability of Data

All data are available within this manuscript or online as supplementary material.

References

[1] Pua YH. The Time Course of Knee Swelling Post Total Knee Arthroplasty and Its Associations with Quadriceps Strength and Gait Speed. J Arthroplasty 2015;30:1215-9. doi: 10.1016/j.arth.2015.02.010

[2] Loyd BJ, Kittelson AJ, Forster J, Stackhouse S, Stevens-Lapsley J. Development of a Reference Chart to Monitor Postoperative Swelling Following Total Knee Arthroplasty. Disabil Rehabil 2020;42:1767-74. doi: 10.1080/09638288.2018.1534005

[3] Noble PC, Conditt MA, Cook KF, Mathis KB. The John Insall Award: Patient Expectations Affect Satisfaction with Total Knee Arthroplasty. Clin Orthop Relat Res 2006;452:35-43. doi: 10.1097/01.blo.0000238825.63648.1e

[4] Maldonado-Rodriguez N, Ekhtiari S, Khan MM, Ravi B, Gandhi R, Veillette C, *et al*. Emergency Department Presentation After Total Hip and Knee Arthroplasty: A Systematic Review. J Arthroplasty 2020;35:3038-45.e1. doi: 10.1016/j.arth.2020.05.022

[5] Muffly SA, An Q, Bedard NA, Brown TS, Otero JE. Early Emergency Department Visits Following Primary Hip and Knee Arthroplasty. J Arthroplasty 2021;36:1915-20. doi: 10.1016/j.arth.2021.01.058

[6] Holm B, Kristensen MT, Bencke J, Husted H, Kehlet H, Bandholm T. Loss of Knee-Extension Strength is Related to Knee Swelling after Total Knee Arthroplasty. Arch Phys Med Rehabil 2010;91:1770-6. doi: 10.1016/j.apmr.2010.07.229

[7] Loyd BJ, Stackhouse S, Dayton M, Hogan C, Bade M, Stevens-Lapsley J. The Relationship between Lower Extremity Swelling, Quadriceps Strength, and Functional Performance Following Total Knee Arthroplasty. Knee 2019;26:382-91. doi: 10.1016/j.knee.2019.01.012

[8] Stevens JE, Mizner RL, Snyder-Mackler L. Quadriceps Strength and Volitional Activation before and after Total Knee Arthroplasty for Osteoarthritis. J Orthop Res 2003;21:775-9. doi: 10.1016/s0736-0266(03)00052-4

[9] Mizner RL, Petterson SC, Snyder-Mackler L. Quadriceps Strength and the Time Course of Functional Recovery after Total Knee Arthroplasty. J Orthop Sports Phys Ther 2005;35:424-36. doi: 10.2519/jospt.2005.35.7.424

[10] Bade MJ, Kohrt WM, Stevens-Lapsley JE. Outcomes before and after Total Knee Arthroplasty Compared to Healthy Adults. J Orthop Sports Phys Ther 2010;40:559-67. doi: 10.2519/jospt.2010.3317

[11] Silva M, Shepherd EF, Jackson WO, Pratt JA, McClung CD, Schmalzried TP. Knee Strength after Total Knee Arthroplasty. J Arthroplasty 2003;18:605-11. doi: 10.1016/s0883-5403(03)00191-8

[12] Rossi MD, Hasson S. Lower-limb Force Production in Individuals after Unilateral Total Knee Arthroplasty. Arch Phys Med Rehabil 2004;85:1279-84. doi: 10.1016/j.apmr.2003.11.034

[13] Yoshida Y, Mizner RL, Ramsey DK, Snyder-Mackler L. Examining Outcomes from Total Knee Arthroplasty and the Relationship between Quadriceps Strength and Knee Function Over Time. Clin Biomech (Bristol, Avon) 2008;23:320-8. doi: 10.1016/j.clinbiomech.2007.10.008

[14] Berth A, Urbach D, Awiszus F. Improvement of Voluntary Quadriceps Muscle Activation after Total Knee Arthroplasty. Arch Phys Med Rehabil 2002;83:1432-6. doi: 10.1053/apmr.2002.34829

[15] Schache MB, McClelland JA, Webster KE. Lower Limb Strength Following Total Knee Arthroplasty: A Systematic Review. Knee 2014;21:12-20. doi: 10.1016/j.knee.2013.08.002

[16] Mizner RL, Petterson SC, Stevens JE, Vandenborne K, Snyder-Mackler L. Early Quadriceps Strength Loss after Total Knee Arthroplasty. The Contributions of Muscle

Atrophy and Failure of Voluntary Muscle Activation. J Bone Joint Surg Am 2005;87:1047-53.
doi: 10.2106/jbjs.D.01992

[17] Mizner RL, Stevens JE, Snyder-Mackler L. Voluntary Activation and Decreased Force Production of the Quadriceps Femoris Muscle after Total Knee Arthroplasty. Phys Ther 2003;83:359-65.

[18] Bade MJ, Struessel T, Dayton M, Foran J, Kim RH, Miner T, *et al*. Early High-Intensity Versus Low-Intensity Rehabilitation after Total Knee Arthroplasty: A Randomized Controlled Trial. Arthritis Care Res (Hoboken) 2017;69:1360-8.
doi: 10.1002/acr.23139

[19] Jakobsen TL, Kehlet H, Husted H, Petersen J, Bandholm T. Early Progressive Strength Training to Enhance Recovery after Fast-track Total Knee Arthroplasty: A Randomized Controlled Trial. Arthritis Care Res (Hoboken) 2014;66:1856-66.
doi: 10.1002/acr.22405

[20] Loyd BJ, Stackhouse SK, Hogan C, Dayton MR, Stevens-Lapsley JE, Kittelson AJ. Peripheral Nociception Is Associated with Voluntary Activation Deficits and Quadriceps Weakness Following Total Knee Arthroplasty. J Bone Joint Surg Am 2019;101:1539-45.
doi: 10.2106/jbjs.18.01457

[21] Rice DA, McNair PJ. Quadriceps Arthrogenic Muscle Inhibition: Neural Mechanisms and Treatment Perspectives. Semin Arthritis Rheum 2010;40:250-66.
doi: 10.1016/j.semarthrit.2009.10.001

[22] Palmieri-Smith RM, Kreinbrink J, Ashton-Miller JA, Wojtys EM. Quadriceps Inhibition Induced by an Experimental Knee Joint Effusion Affects Knee Joint Mechanics During A Single-legged Drop Landing. Am J Sports Med 2007;35:1269-75.
doi: 10.1177/0363546506296417

[23] Palmieri-Smith RM, Villwock M, Downie B, Hecht G, Zernicke R. Pain and Effusion and Quadriceps Activation and Strength. J Athl Train 2013;48:186-91.
doi: 10.4085/1062-6050-48.2.10

[24] Rice D, McNair PJ, Dalbeth N. Effects of Cryotherapy on Arthrogenic Muscle Inhibition Using An Experimental Model of Knee Swelling. Arthritis Rheum 2009;61:78-83.
doi: 10.1002/art.24168

[25] Thacoor A, Sandiford NA. Cryotherapy Following Total Knee Arthroplasty: What is the Evidence? J Orthop Surg (Hong Kong) 2019;27:2309499019832752.
doi: 10.1177/2309499019832752

[26] Thijs E, Schotanus MG, Bemelmans YF, Kort NP. Reduced Opiate Use after Total Knee Arthroplasty Using Computer-assisted Cryotherapy. Knee Surg Sports Traumatol Arthrosc 2019;27:1204-12.
doi: 10.1007/s00167-018-4962-y

[27] Zhong Y, Zheng C, Du W, Zheng J, Xu S, Tong P. Mirabilite with Ice Pack after Total Knee Arthroplasty: A Randomized Controlled Trial Study. Evid Based Complement Alternat Med 2021;2021:6611614.
doi: 10.1155/2021/6611614

[28] Brouwers HFG, de Vries AJ, van Zuilen M, van Kouswijk HW, Brouwer RW. The Role of Computer-assisted Cryotherapy in the Postoperative Treatment after Total Knee Arthroplasty: Positive Effects on Pain and Opioid Consumption. Knee Surg Sports Traumatol Arthrosc 2022;30:2698-706.
doi: 10.1007/s00167-021-06568-x

[29] Yuksel E, Unver B, Karatosun V. Comparison of Kinesio Taping and Cold Therapy in patients with Total Knee Arthroplasty: A Randomized Controlled Trial. Clin Rehabil 2022;36:359-68.
doi: 10.1177/02692155211049152

[30] Donec V, Kriščiūnas A. The Effectiveness of Kinesio Taping® after Total Knee Replacement in Early Postoperative Rehabilitation Period. A Randomized Controlled Trial. Eur J Phys Rehabil Med 2014;50:363-71.

[31] Jarecki J, Sobiech M, Turżańska K, Tomczyk-Warunek A, Jabłoński M. A Kinesio Taping Method Applied in the Treatment of Postsurgical Knee Swelling after Primary Total Knee Arthroplasty. J Clin Med 2021;10:2992.
doi: 10.3390/jcm10132992

[32] Sobiech M, Czępińska A, Zieliński G, Zawadka M, Gawda P. Does Application of Lymphatic Drainage with Kinesiology Taping Have Any Effect on the Extent of Edema and Range of Motion in Early Postoperative Recovery following Primary Endoprosthetics of the Knee Joint? J Clin Med 2022;11:3456.
doi: 10.3390/jcm11123456

[33] Guney-Deniz H, Kinikli GI, Aykar S, Sevinc C, Caglar O, Atilla B, *et al*. Manual Lymphatic Drainage and Kinesio Taping Applications Reduce Early-stage Lower Extremity Edema and Pain Following Total Knee Arthroplasty. Physiother Theory Pract 2022;39:1582-90.
doi: 10.1080/09593985.2022.2044422

[34] Ebert JR, Joss B, Jardine B, Wood DJ. Randomized Trial Investigating the Efficacy of Manual Lymphatic Drainage to Improve Early Outcome after Total Knee Arthroplasty. Arch Phys Med Rehabil 2013;94:2103-11.
doi: 10.1016/j.apmr.2013.06.009

[35] Pichonnaz C, Bassin JP, Lécureux E, Christe G, Currat D, Aminian K, *et al*. Effect of Manual Lymphatic Drainage after Total Knee Arthroplasty: A Randomized Controlled Trial. Arch Phys Med Rehabil 2016;97:674-82.
doi: 10.1016/j.apmr.2016.01.006

[36] Carmichael J, Dennis D, Jennings J, Stevens-Lapsley J, Bade M. Feasibility and Initial Efficacy of a Multimodal Swelling Intervention after Total Knee Arthroplasty: A Prospective Pilot Study with Historical Controls. Knee

2022;35:25-33.
doi: 10.1016/j.knee.2022.01.008

[37] Tornatore L, De Luca ML, Ciccarello M, Benedetti MG. Effects of Combining Manual Lymphatic Drainage and Kinesiotaping on Pain, Edema, and Range of Motion in Patients with Total Knee Replacement: A Randomized Clinical Trial. Int J Rehabil Res 2020;43:240-6.
doi: 10.1097/mrr.0000000000000417

[38] Feng X, Zhao G, Yan Q. The Efficacy and Safety of Modified Robert Jones Bandage in Total Knee Arthroplasty: A Meta-analysis of Randomized-controlled Trials. Int J Surg 2019;63:22-33.
doi: 10.1016/j.ijsu.2019.01.015

[39] Munk S, Jensen NJ, Andersen I, Kehlet H, Hansen TB. Effect of Compression Therapy on Knee Swelling and Pain after Total Knee Arthroplasty. Knee Surg Sports Traumatol Arthrosc 2013;21:388-92.
doi: 10.1007/s00167-012-1963-0

[40] Kayamori S, Tsukada S, Sato M, Komata K, Isida Y, Wakui M. Impact of Postoperative Compression Dressing Using Polyethylene Foam Pad on the Multimodal Protocol for Swelling Control Following Total Knee Arthroplasty: A Randomized Controlled Trial. Arthroplast Today 2016;2:199-204.
doi: 10.1016/j.artd.2016.05.004

[41] Matthews CN, Chen AF, Daryoush T, Rothman RH, Maltenfort MG, Hozack WJ. Does an Elastic Compression Bandage Provide Any Benefit After Primary TKA? Clin Orthop Relat Res 2019;477:134-44.
doi: 10.1097/CORR.0000000000000459

[42] Christensen LMR, Arnesen CE, Möller S, Hyldig N. The Effect of Compression Therapy on Post-surgical Swelling and Pain after Total Knee Arthroplasty. Int J Orthop Trauma Nurs 2021;41:100815.
doi: 10.1016/j.ijotn.2020.100815

[43] Hendrickx AA, Krijnen WP, Bimmel R, van der Schans CP, Damstra RJ. Effect of Nonelastic Compression With an Adjustable Wrap After Total Knee Arthroplasty. Orthop Nurs 2020;39:377-83.
doi: 10.1097/NOR.0000000000000709

[44] Loyd BJ, Burrows K, Forster JE, Stackhouse SK, Hogan C, Stevens-Lapsley JE. Reliability and Precision of Single Frequency Bioelectrical Impedance Assessment of Lower Extremity Swelling Following Total Knee Arthroplasty. Physiother Theory Pract 2019;37:197-203.
doi: 10.1080/09593985.2019.1619886

[45] Stevens-Lapsley JE, Balter JE, Wolfe P, Eckhoff DG, Kohrt WM. Early Neuromuscular Electrical Stimulation to Improve Quadriceps Muscle Strength after Total Knee Arthroplasty: A Randomized Controlled Trial. Phys Ther 2012;92:210-26.
doi: 10.2522/ptj.20110124

[46] Bade M, Struessel T, Paxton R, Winters J, Baym C, Stevens-Lapsley J. Performance on a Clinical Quadriceps Activation Battery is Related to a Laboratory Measure of Activation and Recovery after Total Knee Arthroplasty. Arch Phys Med Rehabil 2018;99:99-106.
doi: 10.1016/j.apmr.2017.07.013

[47] Clement ND, Bardgett M, Weir D, Holland J, Gerrand C, Deehan DJ. What is the Minimum Clinically Important Difference for the WOMAC Index After TKA? Clin Orthop Relat Res 2018;476:2005-14.
doi: 10.1097/corr.0000000000000444

[48] Whitehead AL, Julious SA, Cooper CL, Campbell MJ. Estimating the Sample Size for a Pilot Randomised Trial to Minimise the Overall Trial Sample Size for the External Pilot and Main Trial for a Continuous Outcome Variable. Stat Methods Med Res 2016;25:1057-73.
doi: 10.1177/0962280215588241

[49] Cohen J. Statistical Power Analysis for the Behavioral Sciences. 2nd ed. United States: L. Erlbaum Associates; 1988.

[50] Lee DK, Kim HJ, Lee DH. Incidence of Deep Vein Thrombosis and Venous Thromboembolism Following TKA in Rheumatoid Arthritis Versus Osteoarthritis: A Meta-analysis. PLoS One 2016;11:e0166844.
doi: 10.1371/journal.pone.0166844

[51] Warren JA, Sundaram K, Anis HK, Kamath AF, Higuera CA, Piuzzi NS. Have Venous Thromboembolism Rates Decreased in Total Hip and Knee Arthroplasty? J Arthroplasty 2020;35:259-64.
doi: 10.1016/j.arth.2019.08.049

[52] Zachwieja E, Perez J, Hardaker WM, Levine B, Sheth N. Manipulation Under Anesthesia and Stiffness after Total Knee Arthroplasty. JBJS Rev 2018;6:e2.
doi: 10.2106/jbjs.Rvw.17.00113

[53] Brigati DP, Huddleston J, Lewallen D, Illgen R, Jaffri H, Ziegenhorn D, *et al*. Manipulation Under Anesthesia after Total Knee: Who Still Requires A Revision Arthroplasty? J Arthroplasty 2020;35:S348-51.
doi: 10.1016/j.arth.2020.03.009

[54] Wylde V, Dieppe P, Hewlett S, Learmonth ID. Total Knee Replacement: Is It Really an Effective Procedure For All? Knee 2007;14:417-23.
doi: 10.1016/j.knee.2007.06.001

Publisher's note

Journal of Clinical and Translational Research 2024; 10(5): 296-306

Journal of Clinical and Translational Research

Journal homepage: http://www.jctres.com/en/home

ORIGINAL ARTICLE

Immediate inelastic compression garment for swelling management after total knee arthroplasty: a feasibility study

Supplementary File

Table S1. Home exercise program

Exercise	Demonstration
Ankle pumps: Perform for 1 min; 5+times per day	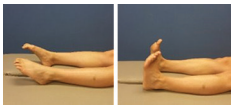
Knee flexion exercise (choose any): Perform 10 repetitions; 5+times per day Heel slides	
Floor scrubs	
Stair stretch	

DOI: http://doi.org/10.36922/jctr.24.00026

Table S2. Statistics at all time points

Time point	Statistic	Swelling (%)		Quadriceps strength (Nm/kg)		Quadriceps activation (%)		WOMAC pain	
		ICG	DCG	ICG	DCG	ICG	DCG	ICG	DCG
Baseline	n	14	16	14	16	14	16	14	16
	Mean	0.3	−2.5	1.1	1.2	61.3	79.6	9.6	7.4
	SD	8.0	4.9	0.5	0.5	18.4	16.4	3.7	2.6
Day 4	n	14	16	-	-	-	-	-	-
	Mean	27.5	27.8	-	-	-	-	-	-
	SD	10.1	9.7	-	-	-	-	-	-
Day 7	n	11	16	-	-	-	-	-	-
	Mean	22.6	19.3	-	-	-	-	-	-
	SD	9.1	7.8	-	-	-	-	-	-
Day 14	n	13	16	-	-	-	-	12	16
	Mean	16.3	16.1	-	-	-	-	7.0	7.5
	SD	9.5	9.4	-	-	-	-	2.0	2.6
Day 21	n	11	16	11	16	11	15	11	16
	Mean	16.8	12.1	0.6	0.7	72.3	76.3	5.8	6.8
	SD	8.5	8.6	0.3	0.3	14.1	15.8	2.6	2.5
Day 42	n	11	15	11	15	11	13	11	16
	Mean	18.6	15.8	0.8	0.9	77.0	88.0	4.9	5.3
	SD	11.3	9.9	0.3	0.4	10.5	6.7	2.2	2.7

Abbreviations: WOMAC: Western Ontario and McMaster universities osteoarthritis index; ICG: Immediate compression garment; DCG: Delayed compression garment; SD: Standard deviation.

DOI: http://doi.org/10.36922/jctr.24.00026

Journal of Clinical and Translational Research 2024; 10(5): 307-316

Journal of Clinical and Translational Research

Journal homepage: http://www.jctres.com/en/home

ORIGINAL ARTICLE

Processed microvascular tissue improves healing in a case series of challenging wounds

Jonathan F. Arnold[1]*, Douglas M. Arm[2]

[1]*The Healing Center at Mercy Medical Center, Cedar Rapids, Iowa, United States of America,* [2]*MicroVascular Tissues, Inc., San Diego, California, United States of America*

(This article belongs to the Special Issue: Innovations in Wound Healing)

ARTICLE INFO

Article history:
Received: August 31, 2024
Accepted: November 2, 2024
Published Online: November 22, 2024

Keywords:
Microvascular tissue
Wound healing
Diabetic foot ulcer
Charcot foot
Venous leg ulcer
Mohs defect
Advanced wound care
Case series

**Corresponding author:*
Jonathan F. Arnold, M.D.
Medical Director, The Healing Center,
Mercy Medical Center, Cedar Rapids, Iowa,
United States of America.
Email: jarnold@mercycare.org

ABSTRACT

Background: Healthy microvasculature provides nutrient and oxygen delivery and removes waste metabolites critical for sustained tissue viability and function after wound healing. Processed microvascular tissue (PMVT), a novel allograft, aims to directly address the compromised microvasculature found in chronic and complex wounds.

Aim: Building on a Level 1 randomized controlled trial demonstrating improved healing and lower extremity sensation with PMVT in neuropathic diabetic foot ulcers, along with a sub-study demonstrating increased wound area blood flow, this article details the authors' clinical experience with PMVT in a case series of challenging wounds, including diabetic foot ulcer, Charcot foot ulcer, venous leg ulcer, and Mohs surgical wound cases.

Methods: Patients received weekly or semi-weekly topical PMVT treatment until wound sites demonstrated active healing with evidence of good microcirculation and progressing re-epithelialization. In all cases, PMVT was covered with a non-adherent dressing and left untouched between visits. Patients were directed not to change the wound dressing, to comply with standard care guidance appropriate for each of their wounds, and to return weekly for assessment of the wound and (if needed) reapplication of the PMVT product. Wound size was measured using a ruler at each visit.

Results: Closure criteria were 100% epithelialization with no maceration, exudate, or signs of infection. The topical application of PMVT successfully healed all challenging or at-risk wounds evaluated in this clinical case series.

Conclusion: By repairing the deficient local microvasculature within and around the wounds, PMVT was able to facilitate the delivery of oxygen and nutrients to the ulcer and enable healing.

Relevance for Patients: PMVT demonstrates the potential to be a strong advanced wound care technology for the treatment of chronic and complex wounds that are refractory to standard care.

1. Introduction

Normal wound healing involves several sequential yet overlapping steps: hemostasis; inflammation; migration, attachment, and proliferation of responding cells; angiogenesis; re-epithelialization; and tissue remodeling [1-3]. Chronic non-healing wounds generally fail to progress through the normal stages of healing, remaining stuck in the inflammation stage. These affect about 3 – 6 million people in the United States of America (USA), resulting in healthcare expenditures exceeding $3 billion/year [4].

Patients with a compromised blood supply are prone to developing ischemic tissue, especially in the lower extremities furthest from the heart that also bear the burden of supporting the body's weight, creating a dangerous combination that leaves patients susceptible to chronic skin wounds. The lack of vascularity in this tissue limits

DOI: http://doi.org/10.36922/jctr.24.00059

migration of responding cells to the wound site, hindering repair. In addition, the oxygen-deprived environment impairs the healing ability of the cells that do arrive [5]. As in all wounds, a functioning microcirculation that provides adequate tissue oxygenation is essential for healing. Wound healing, microvascular ingrowth into a non-healing site, and general tissue repair all require an effective extracellular matrix (ECM) scaffold.

During normal wound healing, angiogenesis leads to tissue revascularization and the establishment of a functioning microcirculation to deliver oxygen and nutrients required for proper tissue repair, along with the removal of waste metabolites and combating microbial burden [5]. The microvasculature, composed of small blood vessels (arterioles, capillaries, and venules), ECM proteins that form the basement membrane and vessel structure, and inherent cells (multipotent cells, endothelial cells, pericytes, fibroblasts, and smooth muscle cells), serves as the foundation for granulation and remodeling during wound healing [6-8]. Microvascular ECM proteins form the basic structure of blood vessels and provide physical scaffolding, mechanical stability, and biochemical cues necessary for tissue to form and maintain stability [9,10]. The ECM is capable of modulating a whole host of processes, including cell migration, attachment, differentiation, and repair [11].

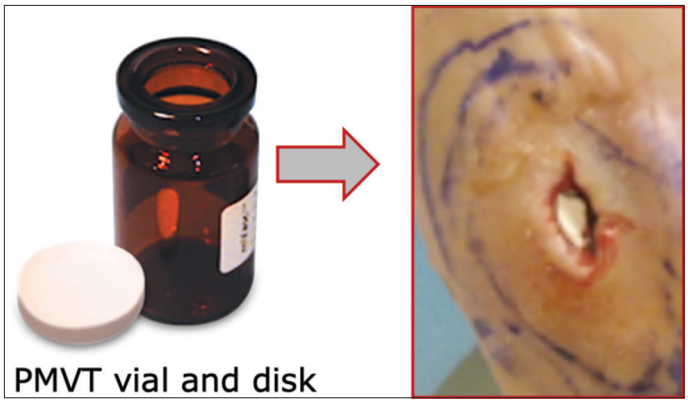

Figure 1. Application of processed microvascular tissue (PMVT). The sterile, lyophilized PMVT disk can be removed from the vial, broken into pieces if desired, and applied topically in dry form to a surface wound site.

Repair of damaged microvascular structure and restoration of adequate blood flow to provide oxygen and nutrients to the site is essential to promote healing and minimize tissue breakdown in the newly epithelialized wound. Formation of a new neurovascular network after tissue injury is critical for wound resolution and maintaining tissue viability and function. Advanced age, diabetes, and radiation treatments are all conditions that manifest in deficient or dysfunctional microvasculature, which can compromise the healing process, leading to poor tissue quality and impaired healing in these patient populations.

Processed microvascular tissue (PMVT) is a microvascular tissue structural allograft (mVASC®; MicroVascular Tissues, Inc., USA) consisting of lyophilized and terminally sterilized allogeneic microvascular tissue ECM harvested from the hypodermal tissue of cadaveric human donors. It is packaged as a lyophilized disk in a sealed glass vial for single-patient

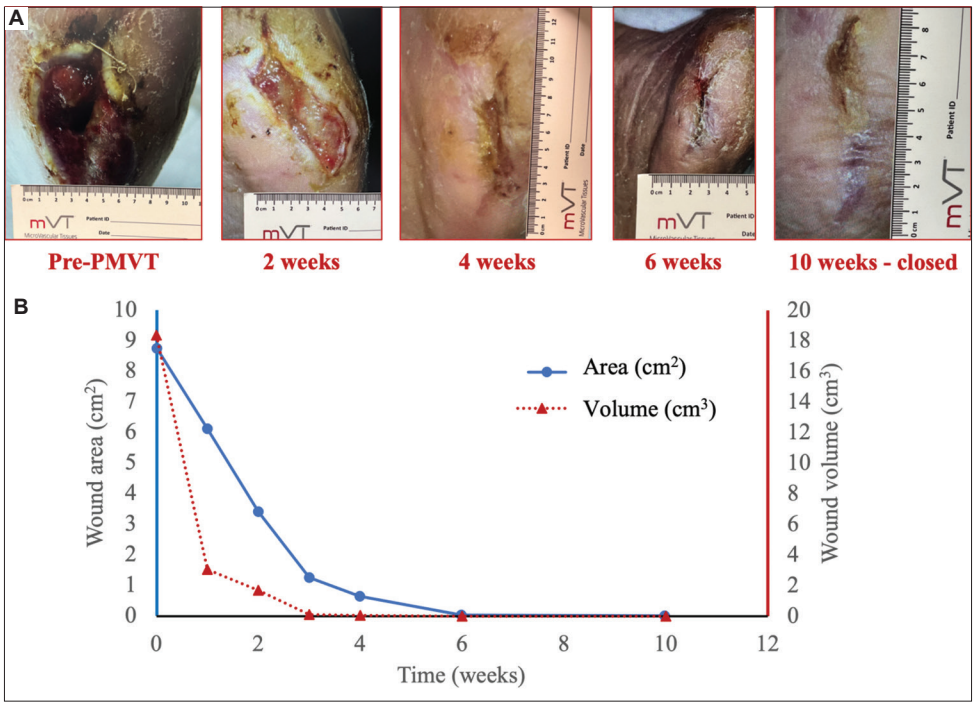

Figure 2. Progression of metatarsal diabetic foot ulcer. (A) Images demonstrating that weekly topical application of processed microvascular tissue through week 6 rapidly healed the ulcer, leading to complete closure by week 10. (B) Graph detailing the healing rate of the closing ulcer by area and volume.

DOI: http://doi.org/10.36922/jctr.24.00059

use and can be topically applied in a dry form to the surface of the wound (Figure 1). PMVT is isolated through a proprietary process that involves cutting, cleaning, isolation, lyophilization, and sterilization of the harvested tissue, and is intended to improve blood flow through the repair and reconstruction of microvascular tissue, by serving as a scaffold for cellular invasion and capillary growth. The benefits of improved microcirculatory blood flow may be particularly impactful on patients with compromised microvasculature.

Preclinical studies of PMVT demonstrated angiogenesis support and significantly increased healing rates in rodent models of pressure injury and ischemia [12,13]. In a robust Level 1, prospective, randomized, controlled, and multicenter clinical trial involving 100 diabetic patients with non-healing Wagner Grades 1 and 2 neuropathic foot ulcers (the "HIFLO Trial"), the weekly topical application of PMVT resulted in significantly increased complete wound closure at 12 weeks compared to the standard-of-care group (74% vs. 38%; P = 0.00029, with a nine-fold increased odds of healing). Sub-studies also demonstrated improved wound area perfusion and increased levels of sensation and tissue quality in this neuropathic patient population [14,15]. Here, we report on real-world clinical experiences with PMVT in a case series of five challenging non-healing wounds.

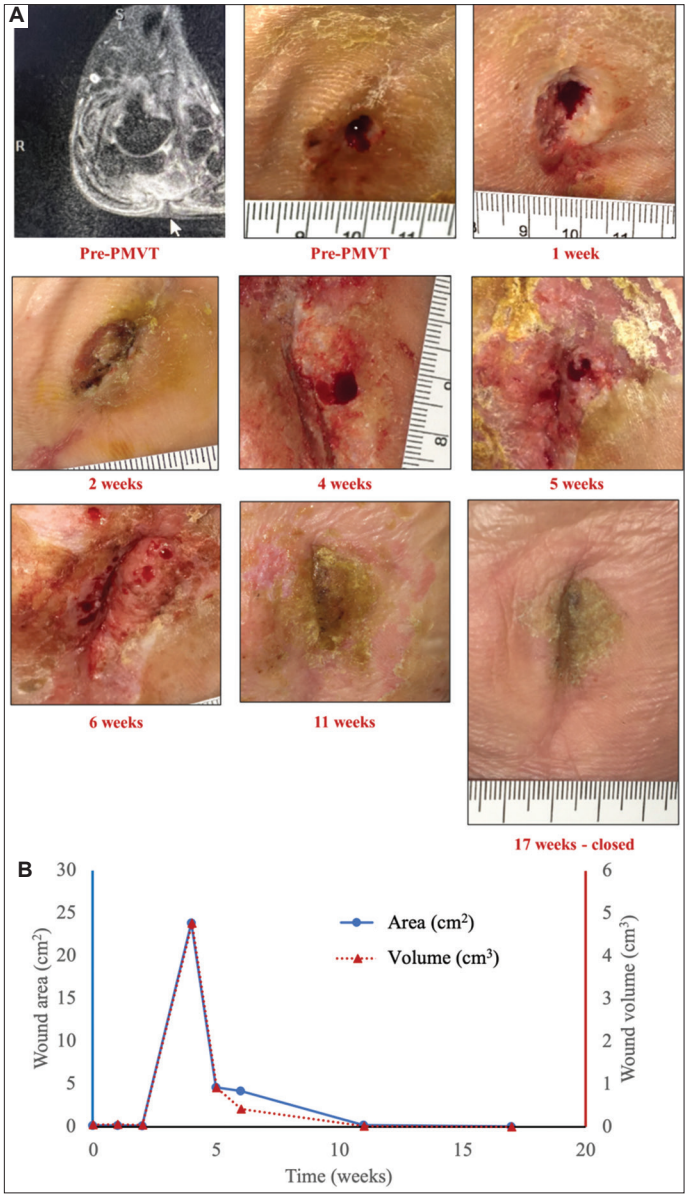

Figure 3. Progression of Charcot diabetic foot ulcer. (A) Images of the defect on initial presentation and progression with topical processed microvascular tissue (PMVT) application, which healed the ulcer, despite off-loading non-compliance during treatment and re-emergence of infection; this led to 99% epithelialization by 11 weeks (seven PMVT applications) and complete closure by 17 weeks. (B) Graph detailing the healing rate of the closing ulcer by area and volume.

2. Methods

All patients received weekly or semi-weekly topical PMVT treatment until wound sites closed or demonstrated active healing with evidence of good microcirculation and progressing re-epithelialization. In all cases within this series, PMVT was covered with a non-adherent dressing and left untouched between visits. Patients were directed not to change the wound dressing, to comply with standard care guidance appropriate for each of their wounds, and to return weekly for assessment of the wound and (if needed) reapplication of the PMVT product. Wound size was measured using a ruler at each visit, and, when appropriate, wound depth was determined using a DM Stick foam-tipped measuring device (Puritan, USA). Closure criteria were 100% epithelialization with no maceration, exudate, or signs of infection.

As this case series was conducted under the standard practice of medicine with a commercial human tissue product for each respective application, no additional ethical regulations or formal research protocol were required, nor were the cases added to a public database. All facility procedures for obtaining patient consent for treatment were followed, and release forms to allow data and image publication were obtained from each patient.

3. Results

3.1. Case 1: Stimulation of perfusion and healing using PMVT in a refractory metatarsal diabetic foot ulcer

Despite growing efforts to adopt a "limb preservation" approach in wound clinics, amputations are an increasingly unwanted complication of non-healing foot ulcers in diabetic patients and are known to have a 50% mortality rate within 5 years [16]. When amputation is necessary, a transmetatarsal amputation (TMA) (as opposed to a below-the-knee amputation) may be justified when macrovascular blood flow to the foot is sufficient. However, patients with TMA are at high risk of skin breakdown or higher amputation, especially when vascular deficiency is present [17,18].

In this case, the patient, a 57-year-old male with poorly controlled type 2 diabetes who had a prior right foot TMA, presented with a DFU on his fifth metatarsal at the TMA site. Following 6 months of unsuccessful treatment with

DOI: http://doi.org/10.36922/jctr.24.00059

standard dressings, collagen, offloading, hyperbaric oxygen, and intravenous (IV) antibiotics, the patient presented with a refractory wound of 7 cm^2 in area and 2 cm deep, with exposed bone and chronic osteomyelitis. He was treated with weekly applications of topical PMVT along with additional IV antibiotics. High-resolution photos of the wound progression and a graph depicting wound area and volume reduction are displayed in Figure 2A and B. After just one treatment with PMVT, over 80% of the wound volume had been replaced with new tissue. After six applications, the wound size had reduced by more than 99%, so PMVT treatment was discontinued. The ulcer fully closed after four additional weeks with standard care and remained healed at his most recent visit 9 months following closure.

3.2. Case 2: Stimulation of perfusion and healing using PMVT in a non-healing Charcot diabetic foot ulcer

Diabetic neuropathy is one of the most frequent complications of diabetes, experienced by 50 – 60% of the 389 million diabetic patients worldwide [19,20]. The most common form is peripheral neuropathy, where peripheral nerves are damaged or destroyed, resulting in loss of feeling and/or sensations of pain or paresthesia, primarily in the extremities [21,22]. While the cause of diabetic neuropathy is not fully understood, the combination of vascular and neural components is recognized as important elements in its pathophysiology. Diabetic neuropathy is a progressive disease, in which tissue-level structural changes occur in the patient's peripheral microvascular system [23-25]. The first pathological changes observed are the narrowing of the microvascular vessels and alteration of the normal local microvascular tissue network. As diabetic neuropathy progresses, neuronal dysfunction and reduction in peripheral nerve function have been demonstrated to correlate with the development of blood vessel abnormalities. Neuronal ischemia is a well-established characteristic of diabetic neuropathy [26]. Charcot foot, a severe complication of peripheral neuropathy that can damage the bones, joints, and soft tissue in the foot, is known to result in the formation of non-healing ulcers [27].

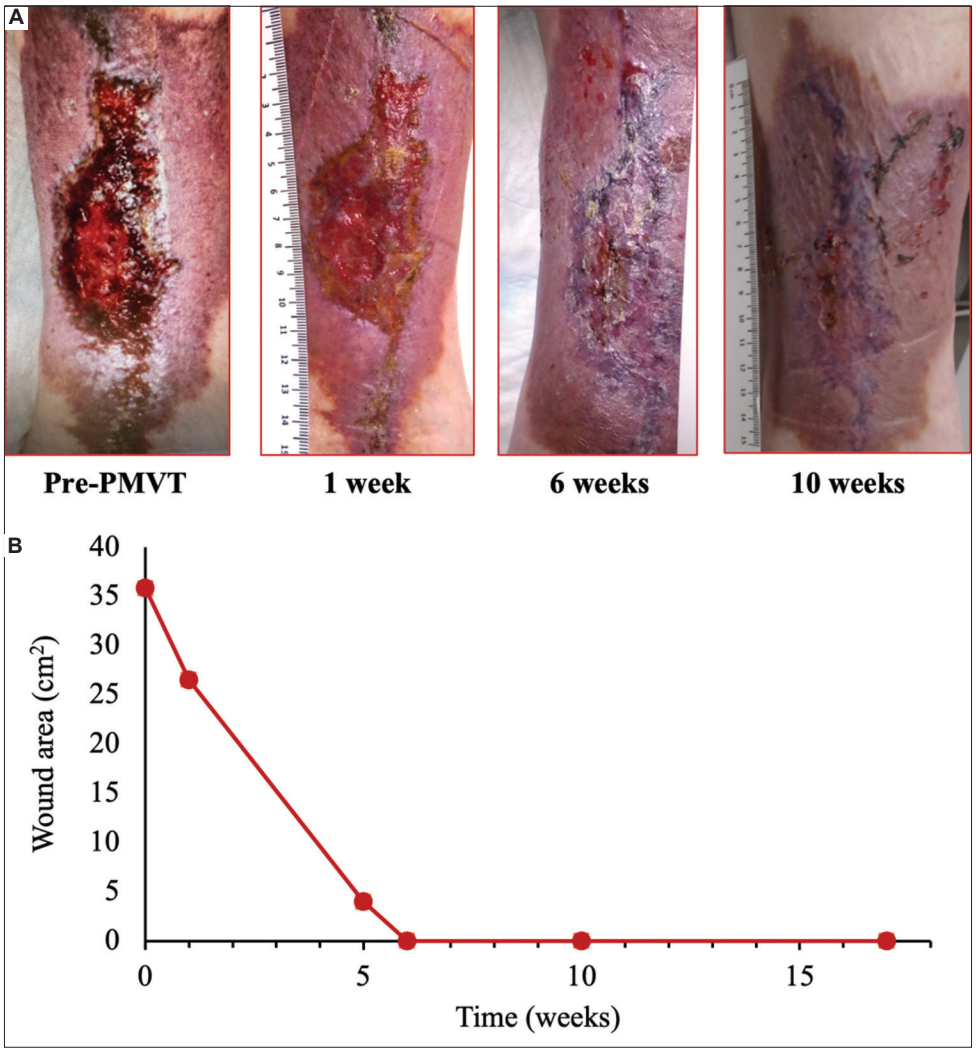

Figure 4. Progression of a venous leg ulcer (VLU). (A) Case images (from left to right): VLU before initial processed microvascular tissue (PMVT) treatment; 1 week after initial treatment; closed 6 weeks after initial treatment (three PMVT applications); healing confirmed 10 and 17 weeks after initial treatment. (B) Graph detailing the healing rate of the closing ulcer by area.

DOI: http://doi.org/10.36922/jctr.24.00059

In this case, a 65-year-old male presented with a poorly granulated 1 cm^2 left plantar Charcot DFU. The wound had been open for more than 1 year despite standard care, including serial debridement, negative pressure wound therapy (NPWT), and total contact casting. The lesion extended 0.4 cm deep to devitalized bone, and the patient was being treated concurrently for chronic osteomyelitis on presentation and initiation of PMVT treatment. Between 2 and 4 weeks, offloading non-compliance led to re-emergence of infection, requiring significant debridement and initiation of antibiotics. Following this, the wound area was now 24 cm^2. Despite this setback, after three additional PMVT applications, the wound had become 99% epithelialized, and PMVT treatment was discontinued. The ulcer went on to fully close within 6 additional weeks with standard care and has remained healed 6 months to date following closure. Images of the ulcer progression and the wound area/volume graph are displayed in Figure 3A and B.

3.3. Case 3: Increasing blood flow using PMVT to treat a chronic venous leg ulcer

Venous leg ulcers (VLUs), among the most common types of lower extremity wounds, are open ulcers that frequently occur on the inside of the leg above the ankle. VLUs comprise about

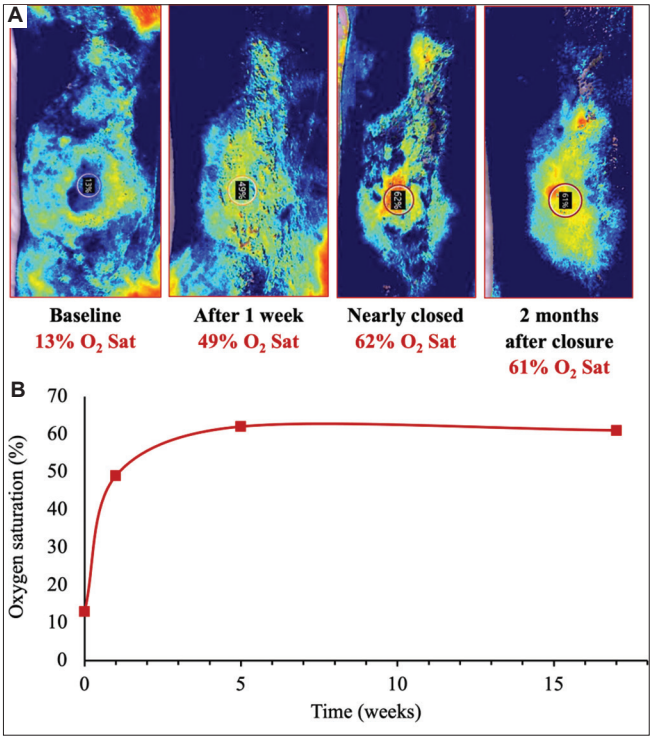

Figure 5. Tissue oxygenation changes within a healing venous leg ulcer. (A) Tissue oxygenation saturation images from historical baseline through processed microvascular tissue treatment and closure. Near-infrared imaging allows for visualization and quantification of oxygen saturation from very low (black/dark blue) to high (yellow and red) levels. Note the relative change in oxygen saturation from the periphery of the wound bed to within the wound bed, indicative of increased local blood flow. (B) Graph detailing the oxygen saturation increase of the closing ulcer over time.

28% of global chronic wounds that require treatment, accounting for nearly $2 billion in annual expenditures, representing an enormous and growing global problem [28]. Up to 60% of VLUs are considered chronic because they persist for more than 6 weeks, usually as a result of blood circulation problems. Obesity, smoking, deep vein thrombosis (DVT), varicose veins, previous leg injury or surgery, age, and diabetes are all risk factors that can contribute to the development of a VLU [28]. As PMVT is intended to improve blood flow through the repair and reconstruction of microvascular tissue by serving as a scaffold for cellular invasion and capillary growth, the benefits of improved microcirculatory blood flow may be particularly impactful on patients with compromised microvasculature, such as patients with increased risk for non-healing VLUs.

The 64-year-old male with a history of chronic kidney disease (Stage 3b), hypertension, chronic DVT, Leiden Factor V, and asthma, who presented with a left VLU in August 2021, is an example of such a patient. The ulcer worsened following DVT in April 2022. No thrombectomy interventions were advisable due to an unacceptably high risk of complications. Multiple topical wound management products, including silver alginate, foam, hydroconductive and other composite dressings, cadexomer iodine, topical antibiotics, and an ECM xenograft, along with compression wraps (the patient's job requires standing 8 h a day), all failed to close the VLU.

In January 2024, after nearly 2.5 years of not healing, the patient received his first treatment of PMVT. The PMVT disk was removed from the vial and applied directly onto the surface of the ulcer after very minimal selective debridement. On contact with blood at the wound site, the PMVT graft was quickly absorbed into the surrounding tissue. Two additional PMVT applications were made at weeks 1 and 5 after the initial treatment. A non-adherent dressing (Mepitel; Mölnlycke Health Care, USA) was used to cover 1 – 2 cm beyond the ulcer's edges after each PMVT application. The VLU was covered further by a compression bandage (initially an alginate-based absorbent compress for the first two treatments, then Coban 2 Lite [3M Healthcare, USA] for the final application). The patient suffered a right hip fracture requiring surgery and hospitalization 2 weeks after initial treatment and had limited transportation means for further follow-up visits until week 6, resulting in a gap between the second and third PMVT applications. As with the other cases, the VLU was visually examined and photographed at each visit, and the wound size was measured using a ruler. In addition, tissue oxygenation was assessed using a point-of-care near-infrared (NIR) imaging device (Snapshot NIR; Kent Imaging, Canada).

The ulcer closed after just three applications of PMVT. Images of the VLU's progression are displayed in Figure 4A, with evident wound closure at the 6-week visit. Wound size over time is presented in Figure 4B. A confirmation visit at 10 weeks demonstrated the wound had remained healed and the surrounding erythema had noticeably subsided, and remained so at 17 weeks, even after the patient had returned to work with significant time on his feet.

The sequential oxygenation saturation images (Figure 5A) and corresponding graph (Figure 5B) depict increased tissue

DOI: http://doi.org/10.36922/jctr.24.00059

oxygenation within the center region of the wound area from the historical baseline (13%), after initial PMVT treatment (49%), through healing just before closure (62%), and maintained following closure (61%). Although these numbers are relative, the increased oxygen saturation represents improved blood flow and is indicative of the transition to the proliferative and remodeling phases of healing within the wound area.

By repairing the deficient local microvasculature around the VLU, PMVT was able to assist with the delivery of oxygen and nutrients to the ulcer. With just three topical applications, it successfully healed a challenging ulcer that had not closed after over 2.5 years of conventional wound management.

3.4. Cases 4 and 5: Stimulation of healing using PMVT in a challenging at-risk Mohs surgical defect

Mohs surgery is the gold standard technique to remove cancerous lesions from the skin [29]. Risk factors, such as ongoing chemotherapy and/or radiation treatment, diabetes, or peripheral vascular disease, may lead to a dysfunctional local microcirculation, which, along with the size and depth of the defect, patient age, and other factors, may cause the post-surgical skin defect to be at greater risk for not healing. In such cases, proactive use of an advanced wound care treatment may be warranted.

The first Mohs patient, a 51-year-old male with coronary artery disease, hypertension, nicotine dependence, and post-COVID pulmonary issues, had undergone Mohs excision of a basal cell carcinoma on his right scapula. Initial attempts to close the defect using standard treatment and negative pressure wound therapy were unsuccessful, and he presented 5 weeks post-excision with a defect 13 cm^2 in area and 0.4 cm deep. After just one treatment of topical PMVT, over 50% of the wound volume had been replaced with new tissue. After 5 weekly applications, the defect had closed, and PMVT treatment was discontinued. Wound progression during PMVT treatment is presented in the images and graph in Figure 6A and B.

The second Mohs patient was a non-compliant 84-year-old female former smoker with prior breast cancer who presented with a 6 cm^2 defect on her left leg following squamous cell carcinoma excision. Despite the patient's non-compliance in maintaining compression on her leg, as evidenced by the staggered progress in the wound size graph on the right, after

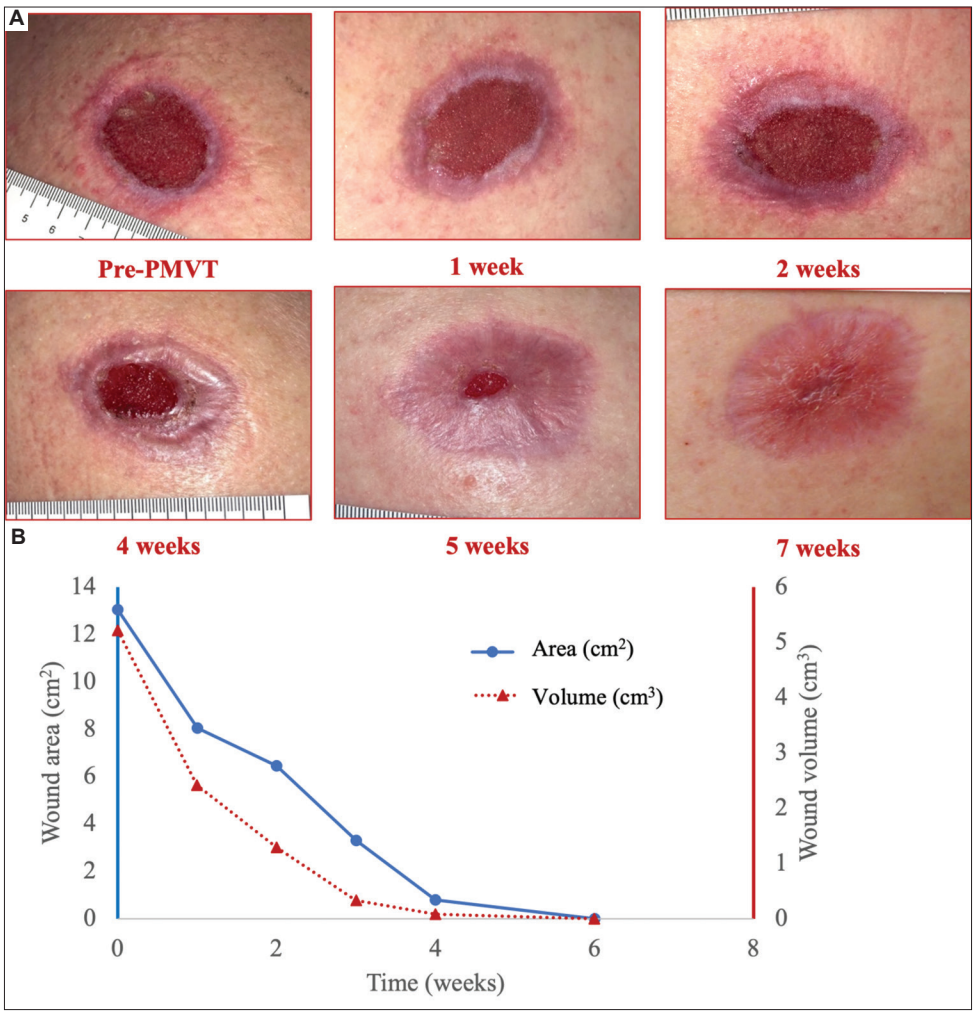

Figure 6. Progression of at-risk Mohs surgical defect. (A) Images demonstrating that weekly topical application of processed microvascular tissue healed the wound in 7 weeks. (B) Graph detailing the healing rate of the closing defect by area and volume.

DOI: http://doi.org/10.36922/jctr.24.00059

8 weeks of weekly topical PMVT treatments, the defect was completely filled and 99% epithelialized. After 10 weeks, the defect was closed, and PMVT treatment was discontinued. Wound progression during PMVT treatment is presented in the images and graph in Figure 7A and B.

4. Discussion

Repairing damaged microvascular structures and restoring blood flow to provide oxygen and nutrients to the site and remove waste metabolites is essential to promote healing and minimize tissue breakdown in a newly epithelialized wound. Reversing the stalled wound environment, restoring blood flow, and changing the trajectory of healing toward wound resolution have been previously reported as hallmarks of PMVT treatment, including within a Level 1 randomized controlled trial (RCT) on diabetic patients with neuropathic DFUs [12,14,30,31]. PMVT's microvascular ECM composition drives host cell attachment and supports angiogenesis, important modes of action in the treatment of wounds with deficient microvascular tissue.

Two of the most common complications of diabetes that lead to ulceration are microvascular dysfunction and peripheral neuropathy. Vascular changes, including endothelial dysfunction, hyperpermeability, decreased blood flow, and tissue hypoxia, can directly result from hyperglycemia. Vascular defects involving the vasa nervorum contribute to diabetic neuropathy [23,26,32-35], which can lead to undetected ulcers at greater risk of delayed healing [36-39]. Formation of a new vascular and neural network beneath complete epithelialization of the skin enables the functionality of the healed tissue. Microvascular tissue therapy, with documented evidence of improved perfusion and improvement in neuropathy, can be effective in healing chronic wounds and achieving complete wound closure in diabetic ulcers, Charcot foot ulcers, VLU, and at-risk surgical wounds, as demonstrated in the PMVT case series reported here. No other advanced wound care technologies have been reported to directly address the microcirculatory defects or neuropathy present in chronic or refractory wounds.

The structure of PMVT serves as an ECM scaffold for revascularization, positioning it as a viable option to address conditions of compromised vascularity. The increase in local tissue perfusion documented by the increased tissue oxygen

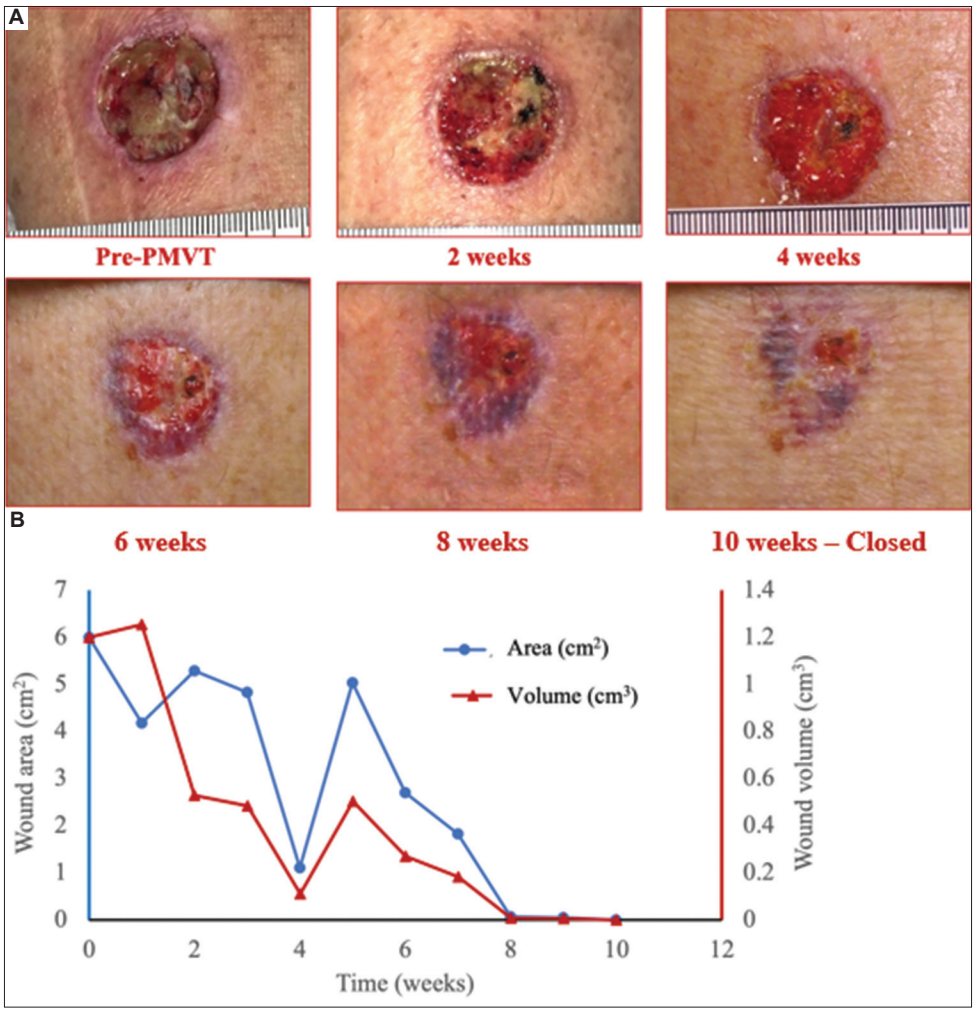

Figure 7. Progression of Mohs surgical defect in a non-compliant patient. (A) Images demonstrating weekly topical application of processed microvascular tissue healed the wound in 10 weeks. (B) Graph detailing the healing rate of the closing defect by area and volume.

DOI: http://doi.org/10.36922/jctr.24.00059

saturation with NIR imaging in the VLU case presented here supports the use of PMVT and addresses a key risk factor for non-healing. The restoration of the microcirculation enables increased oxygen and nutrient delivery to the wound, which promotes granulation and wound epithelialization [40].

This case series demonstrates the breadth of potential applications for PMVT in real-world clinical experience, beyond the previously published Level 1 RCT data neuropathic DFUs. Podiatrists, plastic and reconstructive surgeons, and wound care practitioners may all benefit from learning about the outcomes in this series for their own hard-to-heal wounds and skin defects in patients with damaged or deficient microvasculature. The authors recognize that the number of patients treated within each wound category reported here is limited, and that ideally a more formal protocol-driven case series or clinical trial would provide additional insight into PMVT's effectiveness in these different types of wounds. PMVT is limited to local applications only; intravascular or other systemic delivery is contraindicated.

5. Conclusion

While the broad conclusions that can be drawn from this series of challenging wound cases are limited, it is evident that the use of PMVT can benefit patients with non-healing or at-risk tissue defects of different types caused by microvascular insufficiencies. All defects fully healed in the five cases presented in this series, with patients requiring 3 – 8 topical PMVT applications before closure. Tissue in the healing defect sites became progressively more granulated during PMVT treatment, as assessed through visual observation and NIR spectroscopy images of tissue oxygenation. This is indicative of PMVT's ability to support the repair and reconstruction of microvascular tissue, which, in turn, drove complete wound healing. Successful closure of these refractory and challenging cases across the spectrum of non-healing and at-risk wounds demonstrates both the broad importance of repairing and reconstructing damaged or deficient microvascular tissue and the use of PMVT to improve healing in multiple complex wound environments.

Acknowledgments

The PMVT product used in this case series was provided by MicroVascular Tissues, Inc.

Funding

None.

Conflict of Interest

J.F.A. reports no conflict of interest. D.M.A. is an employee of MicroVascular Tissues, Inc., the company that provided the product for this case series.

Ethics Approval and Consent to Participate

As this case series was conducted under standard practice of medicine with a commercial human tissue product for each respective application, no additional ethical regulations or formal research protocol were required, nor were the cases added to a public database. All facility procedures for obtaining patient consent for treatment were followed, and release forms to allow data and image publication were obtained from each patient.

Consent for Publication

As this case series was conducted under standard practice of medicine with a commercial human tissue product for each respective application, no additional ethical regulations or formal research protocol were required, nor were the cases added to a public database. All facility procedures for obtaining patient consent for treatment were followed, and release forms to allow data and image publication were obtained from each patient.

Availability of Data

Due to commercial reasons, access to the data that support the findings of this case series is restricted.

References

[1] Gosain A, DiPietro LA. Aging and Wound Healing. World J Surg 2004;28:321-6. doi: 10.1007/s00268-003-7397-6

[2] Guo S, DiPietro LA. Factors Affecting Wound Healing. J Dent Res 2010;89:219-29. doi: 10.1177/0022034509359125

[3] Mathieu D, Linke JC, Wattel F. Non-Healing Wounds. In: Mathieu DE, editor. Handbook on Hyperbaric Medicine. Ch. 2.2.9. Amsterdam: Springer; 2006. p. 401-27.

[4] Menke NB, Ward KR, Witten TM, Bonchev DG, Diegelmann RF. Impaired Wound Healing. Clin Dermatol 2007;25:19-25. doi: 10.1016/j.clindermatol.2006.12.005

[5] Shaw TJ, Martin P. Wound Repair at a Glance. J Cell Sci 2009;122(18):3209-13. doi: 10.1242/jcs.031187

[6] Dulmovits BM, Herman IM. Microvascular Remodeling and Wound Healing: A Role for Pericytes. Int J Biochem Cell Biol 2012;44:1800-12. doi: 10.1016/j.biocel.2012.06.031

[7] Pham HT, Economides PA, Veves A. The Role of Endothelial Function on the Foot. Microcirculation and Wound Healing in Patients with Diabetes. Clin Podiatr Med Surg 1998;15:85-93.

[8] Yuan SY, Rigor RR. Structure and Function of Exchange Microvessels. In: Regulation of Endothelial Barrier Function. Ch. 2. San Rafael, CA: Morgan and Claypool Life Sciences; 2010.

[9] Kim Y, Ko H, Kwon IK, Shin K. Extracellular Matrix Revisited: Roles in Tissue Engineering. Int Neurourol J 2016;20:S23-9. doi: 10.5213/inj.1632600.318

[10] Xu J, Shi GP. Vascular Wall Extracellular Matrix

Proteins and Vascular Diseases. Biochim Biophys Acta 2014;1842:2106-19.
doi: 10.1016/j.bbadis.2014.07.008

[11] Hayden MR, Sowers JR, Tyagi SC. The Central Role of Vascular Extracellular Matrix and Basement Membrane Remodeling in Metabolic Syndrome and Type 2 Diabetes: The Matrix Preloaded. Cardiovasc Diabetol 2005;4:9.
doi: 10.1186/1475-2840-4-9

[12] Dobke M, Peterson DR, Mattern RH, Arm DM, Li WW. Microvascular Tissue as a Platform Technology to Modify the Local Microenvironment and Influence the Healing Cascade. Regen Med 2020;15(2):1313-28.
doi: 10.2217/rme-2019-0139

[13] Gimble JM, Frazier T, Wu X, Uquillas AA, Llamas C, Brown T, *et al*. A Novel, Sterilized Microvascular Tissue Product Improves Healing in a Murine Pressure Ulcer Model. Plast Reconstr Surg Glob Open 2018;6:e2010.
doi: 10.1097/GOX.0000000000002010

[14] Gould LJ, Orgill DP, Armstrong DG, Galiano RD, Glat PM, Zelen CM, *et al*. Improved Healing of Chronic Diabetic Foot Wounds in a Prospective Randomized Controlled Multi-centre Clinical Trial with a Microvascular Tissue Allograft. Int Wound J 2022;19:811-25.
doi: 10.1111/iwj.13679

[15] Glat P, Gould L, Pickett LJ, Arm DM. Minimizing Bias in a Diabetic Foot Ulcer Clinical Evaluation: Analysis of the HIFLO Trial. Wounds 2023;35:36-40.
doi: 10.25270/wnds/22062

[16] Armstrong DG, Swerdlow MA, Armstrong AA, Conte MS, Padula WV, Bus SA. Five Year Mortality and Direct Costs of Care for People with Diabetic Foot Complications Are Comparable to Cancer. J Foot Ankle Res 2020;13:16.
doi: 10.1186/s13047-020-00383-2

[17] Mueller MJ, Allen BT, Sinacore DR. Incidence of Skin Breakdown and Higher Amputation after Transmetatarsal Amputation: Implications for Rehabilitation. Arch Phys Med Rehabil 1995;76:50-4.
doi: 10.1016/s0003-9993(95)80042-5

[18] Truong DH, Ngoo AK, Tsai S, Yang AK, Wukich DK, Lavery LA. Success of Transmetatarsal Amputation for Limb Salvage in Patients with Peripheral Artery Disease. Int Wound J 2024;21:e14360.
doi: 10.1111/iwj.14360

[19] Dyck PJ, Kratz KM, Karnes JL, Litchy WJ, Klein R, Pach JM, *et al*. The Prevalence by Staged Severity of Various Types of Diabetic Neuropathy, Retinopathy, and Nephropathy in a Population-based Cohort: The Rochester Diabetic Neuropathy Study. Neurology 1993;43:817-24.
doi: 10.1212/wnl.43.4.817

[20] Driver VR, Lavery LA, Reyzelman AM, Dutra TG, Dove CR, Kotsis SV, *et al*. A Clinical Trial of Integra Template for Diabetic Foot Ulcer Treatment. Wound Repair Regen 2015;23:891-900.
doi: 10.1111/wrr.12357

[21] Yagihashi S, Mizukami H, Sugimoto K. Mechanism of Diabetic Neuropathy: Where Are We Now and Where to Go? J Diabetes Investig 2011;2:18-32.
doi: 10.1111/j.2040-1124.2010.00070.x

[22] Boulton AJ, Vinik AI, Arezzo JC, Bril V, Feldman EL, Freeman R, *et al*. Diabetic Neuropathies: A Statement by the American Diabetes Association. Diabetes Care 2005;28:956-62.
doi: 10.2337/diacare.28.4.956

[23] Fang F, Wang J, Wang YF, Peng YD. Microangiopathy in Diabetic Polyneuropathy Revisited. Eur Rev Med Pharmacol Sci 2018;22:6456-62.
doi: 10.26355/eurrev_201810_16058

[24] Malik RA, Tesfaye S, Thompson SD, Veves A, Hunter A, Sharma AK, *et al*. Transperineurial Capillary Abnormalities in the Sural Nerve of Patients with Diabetic Neuropathy. Microvasc Res 1994;48:236-45.
doi: 10.1006/mvre.1994.1051

[25] Akbari C, LoGerfo FW. Diabetes and Peripheral Vascular Disease. J Vasc Surg 1999;30:373-84.
doi: 10.1016/s0741-5214(99)70154-0

[26] Nukada H. Ischemia and diabetic neuropathy. Handb Clin Neurol 2014;126:469-87.
doi: 10.1016/B978-0-444-53480-4.00023-0

[27] Marmolejo VS, Arnold JF, Ponticello M, Anderson CA. Charcot Foot: Clinical Clues, Diagnostic Strategies, and Treatment Principles. Am Fam Phys 2018;97:594-9.

[28] BCC Research. Markets for Advanced Wound Management Technologies. Boston, MA: BCC Publishing; 2021.

[29] Bowen GM, White GL, Gerwels JW. Mohs Micrographic Surgery. Am Fam Physician 2005;72:845-8.

[30] Dobke MK. Case Report: Treatment of a Lower Leg Defect in the Course of Sarcoma with Microvascular Tissue. Wounds 2023;35:E154-9.
doi: 10.25270/wnds/22073

[31] Dobke M, Kolb FJ, Arm DM. Leveraging the Outcome of a Frontal Bone Tumor Facial Reconstruction Case by a Multimodal Approach. Case Reports Plast Surg Hand Surg 2024;11:2365174.
doi: 10.1080/23320885.2024.2365174

[32] Rohkamm R. In: Taub E, trans/editor. Color Atlas of Neurology. 2nd ed. Stuttgart, Germany: Georg Thieme Verlag; 2004. p. 90.

[33] Moore KL, Agur AM, Dalley AF. Clinically Oriented Anatomy. 6th ed. Philadelphia, PA: Lippincott Williams & Wilkins, Wolters Kluwer; 2010. p. 50.

[34] Cameron NE, Eaton SEM, Cotter MA, Tesfaye S.

Vascular Factors and Metabolic Interactions in the Pathogenesis of Diabetic Neuropathy. Diabetologia 2001;44:1973-88.
doi: 10.1007/s001250100001

[35] Thrainsdottir S, Malik RA, Dahlin LB, Wiksell P, Eriksson KF, Rosén I, *et al*. Endoneurial Capillary Abnormalities Presage Deterioration of Glucose Tolerance and Accompany Peripheral Neuropathy in Man. Diabetes 2003;52:2615-22.
doi: 10.2337/diabetes.52.10.2615

[36] Boulton AJ. The Pathway to Foot Ulceration in Diabetes. Med Clin North Am 2013;97:775-90.
doi: 10.1016/j.mcna.2013.03.007

[37] Boulton AJ. Diabetic Neuropathy and Foot Complications. Handb Clin Neurol 2014;126:97-107.
doi: 10.1016/B978-0-444-53480-4.00008-4

[38] Tomita M, Kabeya Y, Okisugi M, Katsuki T, Oikawa Y, Atsumi Y, *et al*. Diabetic Microangiopathy is an Independent Predictor of Incident Diabetic Foot Ulcer. J Diabetes Res 2016;2016:5938540.
doi: 10.1155/2016/5938540

[39] Armstrong DG, Boulton AJM, Bus SA. Diabetic Foot Ulcers and Their Recurrence. N Engl J Med 2017;376:2367-75.
doi: 10.1056/NEJMra1615439

[40] Gottrup F. Oxygen in Wound Healing and Infection. World J Surg 2004;28:312-5.
doi: 10.1007/s00268-003-7398-5

DOI: http://doi.org/10.36922/jctr.24.00059

Journal of Clinical and Translational Research

Journal of Clinical and Translational Research (JCTR) welcomes submissions from various research topics that are centered on solving clinically-driven issues to ultimately benefit patients.

You will benefit from the following key features of JCTR as our author:

- Open access
- Author-friendly guidelines: 'your paper, your way'
- Reputable editorial board
- No word count or reference restrictions
- Double-blind review process to minimize bias
- Rapid production and publication
- Broad scope, interdisciplinary research exchange platform

The research areas that JCTR covers include, but are not limited to:

Internal medicine (all branches)	Gastroenterology and hepatology
Vascular medicine and phlebology	Surgery and transplantation
Oncology	Hematology
Cardiology	Nephrology
Intensive care medicine	Dermatology
Ophthalmology	Endocrinology and metabolism
Neurology and neurosciences	Anesthesiology
Anatomy, physiology, and embryology	Radiology and nuclear medicine
Pathology	Clinical chemistry
Clinical physics	Genetics and epigenetics
Epidemiology	Global health
Medical devices	Nutrition
Pharmacology	Immunology
Microbiology	Virology
Parasitology	Biomedical engineering

Biomedical spectroscopy and spectrometry

Thanks for considering the Journal of Clinical and Translational Research.

Editorial team JCTR

Journal of Clinical and Translational Research is an independent open access journal published by ACCSCIENCE PUBLISHING

Contact: info@jctres.com · Tel: +65 8182 1586
www.jctres.com

ACCSCIENCE PUBLISHING

ACCSCIENCE PUBLISHING
8 Burn Road, #15-03 Trivex, Singapore 369977.
Tel: +65 8182 1586